

UNIVERSITY OF KWAZULU-NATAL

**ON FREE CONVECTION AND HEAT TRANSFER IN A MICROPOLAR
FLUID FLOW PAST A MOVING SEMI-INFINITE PLATE**

2012

KASSAHUN MENGIST TESSEMA

**ON FREE CONVECTION AND HEAT TRANSFER IN A MICROPOLAR
FLUID FLOW PAST A MOVING SEMI-INFINITE PLATE**

**A DISSERTATION SUBMITTED IN FULFILMENT OF THE ACADEMIC
REQUIREMENTS FOR THE DEGREE OF
MASTER OF SCIENCE**



By

Kassahun Mengist Tessema

School of Mathematics, Statistics and Computer Science

University of KwaZulu-Natal

April 2012

Dedication

To God Almighty for his mercy that endures forever. To my wife, Firehyiwet Engida, my brother Aynalem Engida and his family.

Declaration

The work described in this dissertation was carried out under the supervision and direction of Professor P. Sibanda, School of Mathematics, Statistics and Computer Science, University of KwaZulu Natal, Pietermaritzburg.

I, Kassahun Mengist Tessema, declare that this thesis is my own work. It has not been submitted in any form for any degree or diploma to any other University. Where use has been made of the work of others, it is duly acknowledged..

.....

Signature (Kassahun Mengist Tessama)

.....

Date

.....

Signature (Prof. Precious Sibanda)

.....

Date

Acknowledgements

Before everything, I would like to give thanks to Almighty God, who makes everything possible.

I would like to thank my supervisor, Prof. P. Sibanda for his direction, advice, patience and encouragement throughout the research work. My deep appreciation goes to Prof. Temesgen Zewotir, Prof. S.S. Motsa, Dawit Getnet, Ahmed Khidir, F.G. Awad, Ayoub Basheer and Asinake Worku for their advice and direction during my MSc studies. I would like to thank the staff and postgraduate students in the School of Mathematics, Statistics and Computer Science, Pietermaritzburg, for the help and encouragement they provided during my study.

I thank, with deep appreciation, Mr Aynalem Engida and his family for sponsoring my studies. I want to take this opportunity to thank my wife Mrs Firehiwot Engida, for the support and love she has given me.

Finally, I would like to thank to my brothers Birhanu mengistu and Dessalegn Mengistu and to my sister Abebech Mengistu. They have always been a pillar of strength, this is an opportunity to thank them for their sacrifices in ensuring my earlier studies.

Abstract

In this dissertation we investigate free convective heat and mass transfer in micropolar fluid flow past a moving semi-infinite vertical porous plate in the presence of a magnetic field. The aim of this study was to use recent semi-numerical methods such as the successive linearisation method and the spectral-homotopy analysis method to study the effects of viscous heating and the effects of different fluid parameters.

The governing boundary layer equations for linear momentum, angular momentum (microrotation), temperature and concentration profiles are transformed to a system of ordinary differential equations and solved using the successive linearisation method and the spectral-homotopy analysis method.

The accuracy of the solutions was determined by comparison with numerical approximations obtained using the Matlab `bvp4c` solver. The influences of the micropolar parameter, Darcy number, Prandtl number, Schmidt number, magnetic parameter, heat absorption parameter, Soret and Dufour numbers, local Reynolds number and Grashof number on velocity, microrotation, temperature and concentration profiles were determined. The results obtained are presented graphically and in tabular form.

Table of Contents

Declaration	ii
Table of Contents	v
List of Figures	x
List of Tables	xiii
1 Introduction	1
1.1 Heat and mass transfer	10
1.2 Free, forced and mixed convection	11
1.3 Review of the homotopy analysis method	13
1.4 Review of the spectral-homotopy analysis method	16
1.5 The successive linearisation method	21

1.6	Objective of the study	26
1.7	Outline of dissertation	26
2	Steady MHD convection in a micropolar fluid	28
2.1	Introduction	28
2.2	The governing equations	29
2.3	The skin friction coefficient and the local Nusselt number	32
2.4	Successive Linearisation Method	32
2.5	Results and Discussions	38
2.6	Summary	53
3	Steady MHD convection in a micropolar fluid with Dufour and Soret effects	55
3.1	Introduction	55
3.2	The governing equations	56
3.3	The skin friction coefficient, the local Nusselt and the local sherwood numbers	59
3.4	The spectral-homotopy analysis method	60
3.5	Results and Discussions	71

3.6 Summary	88
4 Conclusion	90

List of Figures

2.1	Velocity, micropolar and temperature plots with respect to K with parameters; $M = 0.3$, $Da = 1$, $Fr = 0.1$, $Gr = 1.2$, $Pr = 0.71$, $Q = 0.01$, $Ec = 0.04$, $Re = 2$	47
2.2	Velocity, micropolar and temperature plots with respect to Da with parameters; $Pr = 0.71$, $M = 0.3$, $K = 1$, $Fr = 0.5$, $Gr = 2.2$, $Q = 0.01$, $Ec = 0.04$, $Re = 2$	48
2.3	Velocity and temperature plots with respect to Fr with parameters; $K = 0.01$, $M = 0.3$, $Da = 2$, $Gr = 0.5$, $Pr = 0.71$, $Q = 0.08$, $Ec = 0.03$, $Re = 1$	49
2.4	Velocity, microrotation and temperature plots with respect to M with parameters; $Pr = 0.71$, $K = 1$, $Da = 1$, $Fr = 0.5$, $Gr = 2.2$, $Q = 0.01$, $Ec = 0.04$, $Re = 2$	50
2.5	Effect of Grashof number (Gr) on velocity and temperature profiles; $K = 1$, $M = 0.3$, $Da = 1$, $Fr = 0.5$, $Pr = 0.71$, $Q = 0.01$, $Ec = 0.04$, $Re = 2$. . .	51

2.6	Effect of heat absorption on velocity and temperature profiles with parameters; $Pr = 0.71$, $M = 0.5$, $Re = 0.1$, $K = 0.1$, $Da = 1$, $Fr = 0.5$, $Gr = 2.4$, $Ec = 0.4$	52
2.7	Effect of local Reynolds number (Re) on velocity and temperature profiles; $K = 6$, $M = 0.3$, $Da = 0.8$, $Fr = 0.5$, $Gr = 2.2$, $Pr = 0.71$, $Q = 0.01$, $Ec = 0.04$	52
2.8	Effect of Eckert number on temperature profile; $K = 0.1$, $M = 0.5$, $Da = 1$, $Fr = 0.5$, $Pr = 0.71$, $Gr = 2.4$, $Q = 0.01$, $Re = 0.1$	53
3.1	The h -curves for $f'(0)$, $\omega(0)$, $\theta(0)$ and $\phi(0)$ when; $K = 10$, $M = 0.3$, $Da = 3$, $Fr = 2$, $Gr = 0.85$, $Pr = 0.71$, $Q = 0.35$, $Ec = 0.03$, $Du = 0.75$, $Sc = 0.75$, $Sr = 0.2$, $Gm = 0.2$, $Re = 2$, $L = 15$	72
3.2	Velocity, microrotation, temperature and concentration plots with respect to K with parameters; $M = 0.3$, $Da = 3$, $Fr = 1$, $Gr = 1$, $Pr = 0.71$, $Q = 0.01$, $Ec = 0.1$, $Du = 0.6$; $Sc = 0.1$, $Sr = 0.1$, $Gm = 0.3$, $Re = 1$	83
3.3	Velocity and Temperature plots with respect to Da with parameters; $K = 15$, $Da = 2$, $M = 0.3$, $Fr = 1$, $Gr = 1$, $Pr = 0.71$, $Q = 0.1$, $Ec = 0.01$, $Du = 0.6$, $Sc = 0.1$, $Sr = 0.1$, $Gm = 0.5$, $Re = 1$	84
3.4	Velocity and temperature plots with respect to Fr with parameters; $K = 1$, $M = 0.3$, $Da = 1.5$, $Gr = 2$, $Pr = 0.71$, $Q = 0.01$, $Ec = 0.03$, $Du = 0.6$, $Sc = 0.5$, $Sr = 0.1$, $Gm = 3$, $Re = 2$	85

-
- 3.5 Velocity plot with respect to M with parameters; $K = 2$, $Da = 2$, $Fr = 1$,
 $Gr = 1$, $Pr = 0.71$, $Q = 0.01$, $Ec = 0.01$, $Du = 0.6$, $Sc = 0.1$, $Sr = 0.1$,
 $Gm = 0.5$, $Re = 0.1$ 86
- 3.6 Effect of Grashof number on velocity and temperature profiles with param-
eters; $K = 18$, $M = 0.3$, $Da = 1$, $Fr = 1$, $Pr = 0.71$, $Q = 0.1$, $Ec = 0.01$,
 $Du = 0.6$, $Sc = 0.1$, $Sr = 0.1$, $Gm = 0.5$, $Re = 1$ 86
- 3.7 Effect of heat absorption on the velocity and temperature profiles with
parameters; $K = 1$, $Da = 2$, $M = 0.3$, $Fr = 1$, $Gr = 1$, $Pr = 0.71$,
 $Q = 0.1$, $Ec = 0.01$, $Du = 0.6$, $Sc = 0.1$, $Sr = 0.1$, $Gm = 0.5$, $Re = 1$ 87
- 3.8 The effect of Dufour and Sorer numbers on temperature and concentration
profiles with parameters; $K = 1$, $M = 0.3$, $Da = 1$, $Fr = 2$, $Gr = 5$,
 $Pr = 0.71$, $Q = 0.1$, $Ec = 0.3$, $Sc = 0.5$, $Gm = 3$, $Re = 0.1$ 88

List of Tables

2.1	Comparison of the bvp4c results against the SLM approximate solutions with $N = 50$ and different values of K when $M = 0.6$, $Da = 2$, $Fr = 0.8$, $Gr = 0.01$, $Pr = 0.71$, $Q = 0.001$, $Ec = 0.01$, $Re = 0.1$	39
2.2	Comparison of the bvp4c results against the SLM approximate solutions with $N = 50$ and different values of Fr when $K = 20$, $M = 0.8$, $Da = 2$, $Gr = 0.01$, $Pr = 0.71$, $Q = 0.001$, $Ec = 0.001$, $Re = 0.1$	40
2.3	Comparison of the bvp4c results against the SLM approximate solutions with $N = 60$ and different values of M when $K = 15$, $Fr = 1$, $Da = 2$, $Gr = 0.01$, $Pr = 0.71$, $Q = 0.001$, $Ec = 0.001$, $Re = 0.1$	41
2.4	Comparison of the bvp4c results against the SLM approximate solutions with $N = 50$ and different values of Da when $K = 20$, $M = 0.8$, $Fr = 0.1$, $Gr = 0.01$, $Pr = 0.71$, $Q = 0.001$, $Ec = 0.001$, $Re = 0.2$	42
2.5	Comparison of the bvp4c results against the SLM approximate solutions with $N = 50$ and different values of Gr when $K = 15$, $Da = 6$, $Fr = 1$, $M = 0.7$, $Pr = 0.71$, $Q = 0.001$, $Ec = 0.01$, $Re = 0.1$	43

- 2.6 Comparison of the **bvp4c** results against the SLM approximate solutions with $N = 50$ and different values of Ec when $K = 15$, $Da = 2$, $Fr = 0.1$, $M = 0.5$, $Pr = 0.71$, $Q = 0.001$, $Gr = 0.01$, $Re = 0.1$ 44
- 2.7 Comparison of the **bvp4c** results against the SLM approximate solutions with $N = 50$ and different values of Re when $K = 18$, $Da = 10$, $Fr = 1$, $M = 0.7$, $Pr = 0.71$, $Q = 0.001$, $Gr = 0.01$, $Ec = 0.01$ 45
- 2.8 Effects of heat absorbtion coefficient on the skin friction $f''(0)$ and the rate of heat transfer $-\theta'(0)$ with parameters $K = 1$, $Da = 1$, $M = 0.3$, $Fr = 0.5$, $Gr = 2.2$, $Pr = 0.71$, $Ec = 0.04$, $Re = 2$ 46
- 3.1 Comparison of the **bvp4c** results against the **SHAM** and **SLM** approximate solutions with $N = 100$ and different values of K with parameters; $M = 0.4$, $Da = 2$, $Fr = 1$, $Gr = 0.001$, $Pr = 0.71$, $Q = 0.0001$, $Ec = 0.001$, $Du = 0.6$, $Sc = 0.1$, $Sr = 0.1$, $Gm = 0.1$, $Re = 0.1$ 74
- 3.2 Comparison of the **bvp4c** results against the **SHAM** and **SLM** approximate solutions with $N = 120$ and different values of M with parameters; $K = 20$, $Da = 2$, $Fr = 1$, $Gr = 0.001$, $Pr = 0.71$, $Q = 0.0001$, $Ec = 0.001$, $Du = 0.6$, $Sc = 0.1$, $Sr = 0.1$, $Gm = 0.01$, $Re = 0.1$ 75
- 3.3 Comparison of the **bvp4c** results against the **SHAM** and **SLM** approximate solutions with $N = 120$ and different values of Da with parameters; $K = 20$, $M = 0.3$, $Fr = 1$, $Gr = 0.001$, $Pr = 0.71$, $Q = 0.0001$, $Ec = 0.001$, $Du = 0.6$, $Sc = 0.1$, $Sr = 0.1$, $Gm = 0.01$, $Re = 0.1$ 77

- 3.4 Comparison of the **bvp4c** results against the **SHAM** and **SLM** approximate solutions with $N = 100$ and different values of Fr with parameters; $K = 20$, $Da = 2$, $M = 0.3$, $Gr = 0.01$, $Pr = 0.71$, $Q = 0.0001$, $Ec = 0.001$, $Du = 0.6$, $Sc = 0.1$, $Sr = 0.1$, $Gm = 0.01$, $Re = 1$ 78
- 3.5 Comparison of the **bvp4c** results against the **SHAM** and **SLM** approximate solutions with $N = 100$ and different values of Gr with parameters; $K = 20$, $M = 0.3$, $Da = 2$, $Fr = 1$, $Pr = 0.71$, $Q = 0.0001$, $Ec = 0.001$, $Du = 0.6$, $Sc = 0.1$, $Sr = 0.1$, $Gm = 0.01$, $Re = 0.1$ 79
- 3.6 Comparison of the **bvp4c** results against the **SHAM** and **SLM** approximate solutions with $N = 60$ and different values of Re with parameters; $K = 20$, $Da = 2$, $M = 0.3$, $Fr = 1$, $Gr = 0.01$, $Pr = 0.71$, $Q = 0.0001$, $Ec = 0.001$, $Du = 0.6$, $Sc = 0.1$, $Sr = 0.1$, $Gm = 0.01$ 80
- 3.7 Effects of Soret and Dofour parameters on the skin friction $f''(0)$, the rate of heat transfer $-\theta'(0)$ and the rate of mass transfer $-\phi'(0)$ with parameters; $K = 1$, $Da = 1$, $Fr = 0.5$, $M = 0.3$, $Pr = 0.71$, $Gr = 2.2$, $Ec = 0.03$, $Q = 0.5$, $Sc = 0.2$, $Gm = 0.4$, $Re = 2$ 81
- 3.8 Effects of heat absorbtion coefficient on skin friction $f''(0)$, the rate of heat transfer $-\theta'(0)$ and the rate of mass transfer $-\phi'(0)$ with parameters; $K = 5$, $M = 0.3$, $Da = 2$, $Fr = 2$, $Gr = 5$, $Pr = 0.71$, $Ec = 0.03$, $Du = 0.6$, $Sr = 0.1$, $Sc = 0.05$, $Gm = 3$, $Re = 1$ 82

1

Introduction

Micropolar fluids are fluids which contain suspensions of rigid particles such as liquid crystals, blood, oil, colloidal suspensions, polymeric fluids, etc (see Eringen [19]). The theory of micropolar fluids was first formulated by Eringen [19] in 1964 as an alternative to the Navier-Stokes equations of classical hydrodynamics. Eringen [20] developed the theory of micropolar fluids to include microrotation inertia effects and extended this to include thermomicropolar fluids (Eringen [21]) by incorporating thermal effects such as heat conduction, convection and dissipation. The theory is useful for modeling non-Newtonian fluids with microstructure. The limitation of the Navier-Stokes model is that it does not take into account the microstructure of the fluid and constituents. The theory of micropolar fluids takes into account both the linear and rotational motion of the fluid and any suspended microparticles (Pažanin [41]).

Micropolar fluids were studied by Peddieson and McNitt [40] who investigated the boundary layer due to a micropolar fluid. They solved the governing equations numerically using a finite difference scheme. A review of micro continuum fluid mechanics and the general flow of micropolar fluids was investigated by Ariman et al. [5] and Ariman et al. [6]

respectively. The flow of incompressible micropolar fluids over a semi- infinite plate using numerical methods was investigated by Ahmadi et al. [2].

The flow of micropolar fluids has been investigated by different researchers, such as Soundalgekar and Takhar [53]. They examined the flow of micropolar fluids over a continuous moving plate. They solved the problem numerically and studied the effects of the coupling parameter and the micro-rotation parameter. Mixed convection in boundary layer flow over a solid sphere with Newtonian heating was studied by Salleh et al. [48]. They solved the governing equations numerically using the Keller-box method. Moreover, they showed that, near the lower stagnation point of a sphere, when the micropolar parameter increases the velocity profile decreases while the temperature profile increases. They also showed that near the lower stagnation point of the sphere both the velocity and temperature profiles decrease when the Prandtl number increases.

Gorla [22] studied micropolar fluid flow along a vertical surface with constant heat flux using numerical methods. Rees and Pop [46] also examined boundary layer flow of micropolar fluid along the vertical flat plate. They solved the governing equations numerically using the Keller-box method. Nazar et al. [38] studied unsteady boundary layer flow over a stretching sheet in a micropolar fluid. They solved the governing equations using the Keller-box method and investigated the effect of the microrotation and micropolar parameters.

Micropolar fluid flow past a moving plate with heat radiation was also investigated by Raptis [44]. El-Arabawy [17] studied the effect of suction or injection in micropolar fluids. From this study the main finding was that the suction parameter increased whereas the skin friction and the couple stress decreased . He also showed that the Darcy number and inertia effect reduced the skin friction, the Nusselt number and the couple stress. However,

the micropolar parameter enhanced the skin friction and reduced the heat transfer rate.

Hassanien et al. [23] studied the flow of a micropolar fluid from a permeable surface with uniform heat flux in porous medium numerically by the well-known Shooting method with Runge Kutta method. In their study they found that the heat transfer rate decreased with an increase in wall injection, Prandtl numbers and the radiation parameter. However, the values of the skin friction coefficient and the local couple stress decreased as the suction parameter increases. They also showed that the Darcy number and the inertia effect tended to reduce the skin friction, the Nusselt number and the couple stress. The micropolar parameter enhanced the skin friction and reduced the heat transfer rate.

Flow of a micropolar fluid driven by injection between two porous disks has been investigated by Kamal et al. [26]. They used Richardson's extrapolation method and showed that the skin friction marginally changes for large negative values of the Reynolds number. Moreover, for positive Richardson numbers, a significant change was observed in relation to small changes in the Reynolds numbers.

Heat and mass transfer in a micropolar fluid along a vertical channel has been investigated by Cheng [15]. The main findings of this study indicated that the volume flow rate, the total heat transfer rate and the mass transfer in a micropolar fluid are lower than those in Newtonian fluids.

The flow of a micropolar fluid on a continuous moving surface was investigated by Ishak et al. [25]. They solved the governing equations numerically using the Keller-box method. They found that the skin friction decreases but the local heat transfer rate increases with an increase in the value of the coupling parameter. Moreover, the study showed that the velocity increases whereas the temperature decreases with the material parameter. In

addition, they found that, near the wall, as the material parameter increases the angular velocity decreases, although the opposite trend was observed far away from the wall. On the other hand, the Prandtl and Eckert numbers had no influence on the skin friction in addition to the velocity and angular velocity or microrotation profiles.

Eldabe and Ouaf [18] studied the flow of a micropolar fluid past a stretching surface with ohmic heating and viscous dissipation. They investigated the problem numerically using the Chebyshev finite difference method. The numerical results showed that an increase in the magnetic parameter reduces the velocities, the Nusselt number and the Sherwood number. However, an increase in the magnetic parameter increases the shear stress, the couple stress at the surface, temperature and concentration fields. The material parameter has the opposite effect to the magnetic field parameter. Furthermore, the temperature decreases as the Prandtl number increases, or increases as the Eckert number increases.

Abdel [1] studied the flow of a micropolar fluid subject to a magnetic field. They solved the problem numerically and the results showed that, as the material parameter increases, the velocity distribution becomes less broad and the microrotation field intensity diminishes in value. The boundary layer thickness decreased with increasing values of Reynolds number.

Mohamed and Abo-Dahab [32] investigated the influence of a chemical reaction and thermal radiation on the heat and mass transfer in micropolar flows on a vertical moving plate. Aouadi [4] studied micropolar flow over a stretching sheet using a numerical approach. Due to the nonlinear nature of the governing equations, many studies in this field have used the finite element method or the Chebyshev finite difference method. Both numerical methods have been employed in the study of the flow of an incompressible micropolar fluid flow past a horizontal stretching sheet.

Rawat et al. [45] examined the problem of transport phenomena in magnetohydrodynamic (MHD) micropolar flow in a Darcy-Forchheimer porous medium. They solved the governing equation using the finite element method. Kim and Kim [28] studied the flow of micropolar fluid past an impulsively started infinite vertical plate. In their study, they used the Laplace transform method. The study indicated that the boundary layer in the case of micropolar fluids is reduced for smaller Prandtl numbers. They however considered only the simple form of the angular momentum equation to avoid the highly nonlinear cases. Due to this, their results require further validation.

The flow of a micropolar fluid in a porous channel with heat and mass transfer has been investigated by Ziabakhsh and Domairry [56]. They used the homotopy analysis method to solve the governing equations. The homotopy analysis method results were found to be in agreement with the numerical solution.

Rahman and Sultana [43] studied the flow of micropolar fluids with variable heat flux and radiative heat transfer numerically using the Nachtsheim-Swigert shooting iteration technique. From the study, they concluded that the skin friction coefficient increases with the increase in the suction, buoyancy parameter, coupling, microrotation and the spin gradient viscosity parameters. The skin friction coefficient also decreased with the increase in the Darcy parameter. Furthermore, plate couple stress increases with the increase in the suction, buoyancy, coupling, and microrotation parameters. The rate of heat transfer increases with the increase in the suction, buoyancy, coupling and microrotation parameters. Large Darcy parameter leads to a decrease in the velocity profile, microrotation as well as temperature profiles.

Shu and Lee [51] investigated the fundamental solutions of micropolar fluids using the boundary-integral method and the singularity method. They however found that these

fundamental solutions can be used to calculate the drag coefficients for a translating solid sphere and a circular cylinder in a micropolar fluid at low Reynolds numbers. Bachok and Ishak [9] investigated the flow of a micropolar fluid with prescribed wall heat flux near a stagnation-point. The governing equations were solved numerically using the Keller-box method. In the study, they found that for micropolar fluids, drag reduction characteristics were reduced as compared those for the classical Newtonian fluids.

Magnetohydrodynamic effects on the flow from a sphere in a non-Darcian porous medium with heat generation were studied by Beg et al.[10]. For the study, the network simulation methodology (NSM) technique was used. Their investigation indicated that an increase in the magnetic field parameter reduces the velocity and increases the temperature. In addition to this an increase in the Darcy number increases the velocity and reduces the temperature profiles. Moreover, increasing the Grashof number induced a decrease in velocity and surface temperature gradients but considerably increased the temperature in the porous regime.

Khedr et al. [27] studied the magnetohydrodynamic effects on the flow of a micropolar fluid on a stretched permeable surface with heat generation or absorption. In the study, an implicit, iterative, finite-difference scheme was used. The results showed that the local skin-friction coefficient increased as either the wall suction or the injection parameter or the Hartmann number increased. However, the local skin-friction coefficient decreased as the microrotation coupling constant increased. Furthermore, the local skin friction coefficient increased due to increases in either of the suction or injection parameter, Prandtl number or the radiation parameter while it decreased with the Hartmann number. When either the absorption coefficient or the microrotation coupling constant increased, the local heat transfer coefficient was also predicted to increase.

Rahman et al. [42] studied the flow of a thermo-micropolar fluid with variable heat flux in a porous medium with radiative heat transfer along a vertical permeable plate. They solved the governing equations numerically using a sixth order Runge-Kutta method along with a shooting iteration technique. From the study they concluded that the plate couple stress is directly proportional to suction, buoyancy, coupling and non-zero microrotation parameters. The rate of heat transfer was also found to be directly proportional to suction, buoyancy, coupling and microrotation parameters. Moreover, large Darcy numbers lead to a decrease in the velocity and temperature profiles and an increase in the microrotation vector. Finally, radiation was found to reduce the velocity and temperature fields, while enhancing the angular velocity.

Sajid et al. [47] studied micropolar fluid flow through a porous channel using the homotopy analysis method. Their investigation showed that increasing the Reynolds number leads to an increase in microrotation. Similarly, Sharma et al. [49] studied magnetohydrodynamic convection, heat and mass transfer in a micropolar fluid past a semi-infinite vertical porous plate. They used the element free Galerkin method to solve the governing equations. In their study, they found that the velocity increases with the increasing of the Grashof number and permeability parameter. Furthermore, the velocity profile decreased as the magnetic field and the Schmidt number increased. The temperature profile decreased with increasing of the Grashof number. However, the concentration profile increased as the heat absorption parameter increased but decreased as the Schmidt number increased. Moreover, the concentration profile increased as Soret and Dufour numbers increased.

Sharma et al. [50] investigated the combined effect of a magnetic field and heat absorption on a micropolar fluid. They used a meshless element free Galerkin method (EFGM) to solve the the governing equations. In this study, they showed that the velocity is directly

proportional to the plate velocity or Darcy number. However, the velocity profile decreased with each of the magnetic parameter, the Forchhimer number and the micropolar parameter increases. The temperature was also found to be inversely proportional to the plate velocity and the Darcy number. But the temperature profile increased with each of the magnetic parameter, the Forchhimer number and the micropolar parameter increases. They concluded that the magnetic field may be used to control the rate of heat transfer, which is a useful attribute in applications such as in MHD generators and nuclear reactors.

The flow of a micropolar fluid driven by injection or suction between a porous and a non-porous disk was studied by Motsa et al. [33]. They used the Spectral homotopic analysis method to solve the governing equations. Their findings showed that the normal velocity profile is only marginally affected by the micropolar structure of fluids. Moreover, the stream wise velocity distributions and the microrotation profiles were significantly influenced by the micropolar structure of fluids.

Similarly, Sibanda and Awad [52] studied micropolar fluid flow in a channel with heat and mass transfer using the homotopy analysis method. Their investigation showed that when the Peclet number increased the temperature also increased with the maximum temperature occurring in the middle of the channel. However, the Peclet number was found to have no effect on the velocity and the microrotation vectors. Moreover, an increase in the Reynolds number led to a decrease in the velocity and the microrotation vector but had a marginal effect on the temperature and concentration fields.

Pažanin [41] investigated the flow of a micropolar fluid through a thin and long pipe using an asymptotic approximation. From this investigation he estimated the velocity and pressure from the Poincare's inequality and studied the effects of microstructure on the flow.

Alam et al. [3] investigated the effects of Soret and Dufour on steady free convection and mass transfer flow past on continuous moving semi-infinite vertical porous plate in a porous medium. They solved the governing equations numerically using a shooting method and a Runge-Kutta sixth-order integration scheme. Their investigation showed that the temperature and concentration fields are influenced by the presence of Dufour and Soret effects.

Chemically-reacting magneto-hydrodynamic (MHD) free convection heat and mass transfer in porous medium with Soret and Dufour effects was investigated by Bhargava et al. [12]. They solved the governing equations numerically using the finite element method (FEM). Their investigation showed that increasing the Dufour and reducing the Soret effects simultaneously increases the temperature in the porous medium. However, increasing the Soret and reducing the Dufour numbers simultaneously increased the concentration values in the porous medium. Furthermore, increasing the magnetic parameter reduced the velocity. Likewise increasing the Eckert number heated the porous regime, that is increasing the temperature. Moreover, increasing the Schmidt number reduced both the temperature and concentration values in the porous regime. In addition to this, a decrease in Soret number and an increase in Dufour number simultaneously leads to decrease the skin friction coefficient.

The effects of Soret and Dufour parameters on free convection along a vertical wavy surface were studied by Narayana and Sibanda [37] numerically using the fourth order Runge-Kutta method. They investigated the effects of the size of the amplitude of the wavy surface along with the diffusivity and the buoyancy ratio parameter on heat and mass transfer coefficients. Their findings were that increasing the amplitude of the wavy surface tended to increase the amplitude of the local heat and mass transfer coefficients

in the medium in both the aiding and opposing buoyancy cases. Moreover, a reduction in the axial mass transfer coefficient occurred with increasing Soret parameter values.

The effects of Soret and Dufour parameters on mixed convection in a non-Darcy porous medium saturated with a micropolar fluid was studied numerically using the Keller-box method by Srinivascharya and RamReddy [54]. They suggested that the microrotation increased at the wall with a rise in Prandtl numbers but decreased away from the wall. The investigation also showed that the Dufour and Soret effects have a significant influence on the flow structure.

Another study on the effects of Dufour and Soret parameters on heat and mass transfer in a micropolar fluid flow along a horizontal channel was carried out by Awad and Sibanda [8]. For this study, they used the homotopy analysis method to solve the governing equations. One of their findings was that increasing the Reynolds numbers reduced the velocity and micro-rotation profiles. Mixed convective heat and mass transfer on a stretching surface in a porous medium under the influence of the Soret and Dufour parameters were numerically investigated by Pal and Chatterjee [39]. In this study they showed that the temperature profile increases as the Dufour parameter increases and higher values of the Soret parameter increases the concentration distribution.

1.1. Heat and mass transfer

Heat transfer is defined as energy movement due to a temperature gradient. A fundamental law of physics is that energy can neither be created nor destroyed, but can only be changed from one form in to another (Incropera and De Witt [24]). The transfer of heat is normally from a region of higher temperature to low temperature zones. In heat

transfer problems, temperature represents the amount of thermal energy available while heat flow represents the movement of thermal energy from one point to another.

Heat transfer mechanisms can be grouped into three broad categories. These are conduction, convection and radiation, which may be defined as follows (Incropera and De Witt [24]).

- (a) Conduction. This is the movement of thermal energy from regions of greater molecular kinetic energy to regions of less molecular energy.
- (b) Convection. This is the state in which fluid motion is responsible for the transfer of heat from one region to another. The heated fluid becomes buoyant and displaces cooler fluid through convection rolls or through translation from one region to another.
- (c) Radiation. This is observed when temperatures are not uniform and thermal energy is transported from surfaces at a higher temperature to surfaces at a lower temperature. Radiation requires neither the presence of a solid medium through which thermal energy may be transmitted nor the movement of the fluid.

1.2. Free, forced and mixed convection

Convective heat transfer mechanisms can be grouped according to the nature of the flow. They are forced, free (natural) and combined (mixed) convection. When the flow is caused by external means, such as a pump, a fan, atmospheric winds etc, this type of convective heat transfer is called forced convection. When the flow is induced by buoyancy forces which arise from density differences caused by temperature variations in the fluid, this

gives rise to free or natural convection. Mixed convection results from fluid motions caused by both external sources and internal temperature gradients (see Incropera and De Witt [24]).

Free and mixed convection in boundary-layer flows along vertical moving surfaces has been studied by many researchers including Gorla [22], Rees [46] and Sharma et al. [50]. Awad et al. [7] investigated convection for an inverted cone in a porous medium with the effects cross-diffusion using the successive linearisation method. Their investigation showed that increasing the Dufour parameter decreases of the thermal thickness of the boundary layer thus increasing the heat transfer rate at the wall and increasing the Soret number leads to increase in concentration thickness of the boundary layer. Chamkha and Nakhi [14] studied mixed convection and radiative heat transfer along a permeable surface in the presence of Soret and Dufour effects numerically using the finite-difference method. They concluded that both the local Nusselt and Sherwood numbers decreased due to the presence of a magnetic field. They concluded that in the absence of blowing or injection, the local Nusselt number decreased as the Dufour number increased, but that it increased in the presence of injection or blowing. Increasing the Soret effect was found to enhance the local Nusselt number for all suction or injection conditions while it caused the local Sherwood number to decrease in the presence of suction and to increase in the presence of injection etc.

The spectral homotopy analysis method was developed by Motsa et al. [35], for solving nonlinear boundary value problems. The method is based on the blending of the Chebyshev pseudospectral methods [16] and the homotopy analysis method (HAM) [29]. Motsa et al. [34] used this method to solve the MHD Jeffery-Hamel flow problem. They showed that, the spectral homotopy analysis method is more converged than the homotopy analy-

sis method. Their results showed that the fluid velocity increases with increasing Hartman numbers.

In the present work we used the spectral homotopy analysis method to study the combined effects of a magnetic field and heat absorption on steady free convection and heat transfer flow in a micropolar fluid. The accuracy of the spectral homotopy analysis method solutions was determined by comparing the series solutions with the numerical approximations obtained using the Matlab **bvp4c** solver and the successive linearisation method.

1.3. Review of the homotopy analysis method

The homotopy analysis method is based on the concept of homotopy in topology. The homotopy analysis method is a semi-analytical technique for solving nonlinear ordinary and partial differential equations. This method was developed by Shi-Jun Liao in 1992 [29]. The method is superior to traditional perturbation methods in that it leads to convergent series solutions of strongly nonlinear problems. The method uses auxiliary functions and parameters which can be controlled to improve the convergence and accuracy of the solution. The accuracy and convergence of the homotopy analysis solution series depends on the careful selection of an auxiliary parameter \hbar . Moreover, the method gives an explicit series solution for nonlinear equations. This solution is generally uniformly valid for all governing parameters.

The basic idea of the homotopy analysis method (HAM) (see Liao [29]) is as follows.

We consider the nonlinear differential equation,

$$\mathcal{N}[f(t, q)] = 0, \tag{1.1}$$

where \mathcal{N} is a nonlinear operator, $q \in [0, 1]$ is an embedding parameter and $f(t, q)$ is a function of t and the embedding parameter q .

We construct the homotopy or the *zeroth order* deformation equation,

$$(1 - q)\mathcal{L}[F(t, q) - f_0(t)] = q\hbar H(t, q)\mathcal{N}[F(t, q)], \quad (1.2)$$

where $\hbar \neq 0$ is an auxiliary parameter, $H(t, q)$ and $\mathcal{L}(t, q)$ represents an auxiliary function and a linear operator respectively, $f_0(t)$ is an initial approximation. The HAM has the flexibility of allowing us to choose any suitable values of \hbar , H and \mathcal{L} .

For $q = 0$ and $q = 1$, we have

$$F(t, 0) = f_0(t) \quad \text{and} \quad F(t, 1) = f(t, q). \quad (1.3)$$

This tells us the solution of the non linear equation varies from the initial guess to the exact solution as q varies from 0 to 1. Expanding the function $f(t, q)$ using Taylor's series with respect to the embedding parameters q , we get

$$F(t, q) = F(t, 0) + \sum_{m=1}^{+\infty} f_m(t, q)q^m, \quad (1.4)$$

where

$$f_m(t, q) = \frac{1}{m!} \frac{\partial^m F(t, q)}{\partial q^m} \Big|_{q=0}. \quad (1.5)$$

The auxiliary functions \hbar and $H(t, q)$ are carefully selected so that the series (1.4) converges at $q = 1$, yielding the homotopy-series solution

$$f(t, q) = f_0(t) + \sum_{m=1}^{+\infty} f_m(t, q)q^m. \quad (1.6)$$

Differentiating equations (1.2) m times with respect to the embedding parameter q and then setting $q = 0$ and finally, dividing the resulting equations by $m!$, gives the so-called

m^{th} order deformation equations

$$\mathcal{L}[f_m(t, q) - \chi f_{m-1}(t, q)] = \hbar H(t, q) R_m(\vec{f}_{m-1}), \quad (1.7)$$

subject to the initial conditions

$$f_m(0) = 0, \quad (1.8)$$

where

$$R_m(\vec{f}_{m-1}(t)) = \frac{1}{(m-1)!} \frac{\partial^{m-1} \mathcal{N}[f(t, q)]}{\partial q^{m-1}} \Big|_{q=0}, \quad (1.9)$$

and

$$\chi_m = \begin{cases} 0, & m \leq 1 \\ 1, & m > 1, \end{cases} \quad (1.10)$$

The value of $f_m(t, q)$ for $m \geq 1$ can be found from equation (1.7) which form uncoupled linear first order differential equations when solved subject to the boundary conditions (1.8).

The homotopy analysis method has many limitations compared to the spectral homotopy analysis method. In the homotopy analysis method one is restricted to choosing a simple initial approximation whereas in the spectral-homotopy analysis method any form of initial guess may be used as long as it satisfies the boundary conditions. The homotopy analysis method is less flexible compared to the SHAM. In this method one is not restricted to using the method of higher order differential mapping. In using the homotopy analysis method the range of \hbar values is narrow as compared to the spectral-homotopy analysis method and the method is slow to converge in comparison with the spectral-homotopy analysis method (see [35]).

1.4. Review of the spectral-homotopy analysis method

Motsa et al. [35] presented the spectral-homotopy analysis method for solving non-linear second order boundary value problems. The main advantage of the spectral-homotopy analysis method is that it removes certain limitations associated with the use of the standard homotopy analysis method, such as the requirement that the solution sought should satisfy the rule of solution expression and rule of coefficient ergodicity. The spectral homotopy analysis method algorithm presented by Motsa et al. ([35], [34]) is as follows.

Consider the following non-linear differential equation;

$$Y''(x) + B_1(x)Y(x) + B_2(x)Y'(x) + Y^T(x)B_3(x)Y(x) + Y^T(x)B_4(x)Y'(x) = \mathbf{M}(x), \quad (1.11)$$

subject to the boundary conditions

$$Y(-1) = Y(1) = 0, \quad (1.12)$$

where the superscript T denotes the transpose and

$$Y = \begin{bmatrix} u(x) \\ v(x) \end{bmatrix}, \quad \mathbf{M} = \begin{bmatrix} g(x) \\ h(x) \end{bmatrix}, \quad (1.13)$$

$$B_l = \begin{bmatrix} b_{11}^{(l)}(x) & b_{12}^{(l)}(x) \\ b_{21}^{(l)}(x) & b_{22}^{(l)}(x) \end{bmatrix}, \quad l=1,2,3,4. \quad (1.14)$$

where $g(x)$ and $h(x)$ are source terms and $b_{ij}^{(l)}(x)$, ($i, j = 1, 2$) are known functions of x .

We define the following linear operators based on the homogeneous linear part of the governing equation (1.11),

$$\mathcal{L}[G(x, q)] = \frac{\partial^2 G}{\partial x^2}(x, q) + B_1(x)G(x, q) + B_2(x)\frac{\partial G}{\partial x}(x, q), \quad (1.15)$$

where $q = [0, 1]$ is the embedding parameter, and $G(x, q) = [U(x, q), V(x, q)]^T$ are unknown functions. The linear operators in the above equations depend on more than one unknown function. We take the initial approximation to be the solution of the nonhomogeneous linear part of the governing equation (1.11).

$$Y_0''(x) + B_1(x)Y_0(x) + B_2(x)Y_0'(x) = \mathbf{M}(x), \quad (1.16)$$

We can solve the above equation subject to the boundary condition (1.12). The unknown function $g(x)$ and $h(x)$ are approximated as truncated series of Chebyshev polynomials of the form

$$u_0(x) \approx u_0^N(x_j) = \sum_{k=0}^N \tilde{u}_k T_k(x_j), v_0(x) \approx v_0^N(x_j) = \sum_{k=0}^N \tilde{v}_k T_k(x_j), j = 0, 1, \dots, N \quad (1.17)$$

where T_k is the k^{th} Chebyshev polynomial, \tilde{u}, \tilde{v} are Chebyshev coefficients and x_0, x_1, \dots, x_N are the Gauss-Lobatto collocation points, see Motsa et al.([35]).

$$x_j = \cos \frac{\pi j}{N}, \quad j = 0, 1, 2, \dots, N. \quad (1.18)$$

\mathcal{D} is the Chebyshev spectral differentiation matrix whose entries see [16] are given by

$$\begin{aligned} \mathcal{D}_{kj} &= -\frac{1}{2} \frac{c_k}{c_j} \frac{(-1)^{k+j}}{\sin \frac{\pi}{2N}(j+k) \sin \frac{\pi}{2N}(j-k)}, \quad j \neq k, \\ \mathcal{D}_{kj} &= -\frac{1}{2} \frac{\cos \frac{\pi k}{N}}{\sin^2 \frac{\pi k}{N}}, \quad k \neq 0 \\ \mathcal{D}_{00} &= -\mathcal{D}_{NN} = \frac{2N^2+1}{6} \\ \mathcal{D}_{kj} &= -\mathcal{D}_{N-k, N-j}, \quad k = \frac{N}{2} + 1, \dots, N. \end{aligned} \quad (1.19)$$

Here $c_0 = c_N = 2$ and $c_j = 1$ with $1 \leq j \leq N - 1$.

We substitute equations (1.17) and (1.19) in (1.16) to obtain the system of equations of the form

$$BY = \mathbf{M} \tag{1.20}$$

where B , \mathbf{M} and Y are defined as

$$B = \begin{bmatrix} \mathcal{D}^2 + b_{11}^{(2)}\mathcal{D} + b_{11}^{(1)} & b_{12}^{(2)}\mathcal{D} \\ b_{21}^{(2)}\mathcal{D} + b_{21}^{(1)} & \mathcal{D}^2 + b_{22}^{(2)}\mathcal{D} + b_{22}^{(1)} \end{bmatrix}, \tag{1.21}$$

$$Y = \begin{bmatrix} u_0(x_0) \\ u_0(x_1) \\ \vdots \\ u_0(x_N) \\ v_0(x_0) \\ v_0(x_1) \\ \vdots \\ v_0(x_N) \end{bmatrix}, \quad \mathbf{M} = \begin{bmatrix} g(x_0) \\ g(x_1) \\ \vdots \\ g(x_N) \\ h(x_0) \\ h(x_1) \\ \vdots \\ h(x_N) \end{bmatrix}, \tag{1.22}$$

$$b_{rs}^{(l)} = \begin{bmatrix} b_{rs}^{(l)}(x_0) & 0 & 0 & \cdots & 0 & 0 \\ 0 & b_{rs}^{(l)}(x_1) & 0 & \cdots & 0 & 0 \\ 0 & 0 & b_{rs}^{(l)}(x_2) & \cdots & 0 & 0 \\ 0 & 0 & 0 & b_{rs}^{(l)}(x_3) & \cdots & 0 \\ \vdots & \vdots & \vdots & \ddots & \vdots & \vdots \\ 0 & 0 & 0 & \cdots & b_{rs}^{(l)}(x_{N-1}) & 0 \\ 0 & 0 & 0 & \cdots & 0 & b_{rs}^{(l)}(x_N) \end{bmatrix} \tag{1.23}$$

with $r, s, l = 1, 2$. The boundary conditions are given by

$$u_0(x_0) = u_0(x_N) = v_0(x_0) = v_0(x_N) = 0. \quad (1.24)$$

The matrix B has dimensions $2(N+1) \times 2(N+1)$ while matrices Y and M have dimensions $2(N+1)$. To implement the boundary conditions (1.36) we delete the first, $N+1$, $N+2$ and the last rows of B , Y , M . The first, $N+1$, $N+2$ and last columns of B are also deleted. This reduces the dimensions of B to $2(N-1) \times 2(N-1)$ and those of Y and M to $2(N-1) \times 1$.

The values of $[u_o(x_1), u_o(x_2), \dots, u_o(x_{N-1}), v_o(x_1), v_o(x_2), \dots, v_o(x_{N-1})]$ are determined from the solution of the coupled linear system (1.16)

$$Y = B^{-1}\mathbf{M}. \quad (1.25)$$

We now construct the zeroth order deformation equations as

$$(1-q)\mathcal{L}[F(x, q) - Y_0(x)] = q\hbar(\mathcal{N}[F(t, q)] - M(x)), \quad (1.26)$$

where \mathcal{N} is the nonlinear operator defined as

$$\begin{aligned} \mathcal{N}[F(t, q)] = & \frac{\partial^2 F}{\partial x^2}(x, q) + B_1(x)F(x, q) + B_2(x)\frac{\partial F}{\partial x}(x, q) \\ & + F(x, q)B_3(x)F(x, q) + F(x, q)B_4(x)\frac{\partial F}{\partial x}(x, q). \end{aligned} \quad (1.27)$$

Differentiating (1.26) m times with respect to q and then setting $q = 0$ and finally dividing the resulting equations by $m!$ yields the higher order deformation equations

$$\mathcal{L}([u_m(x), v_m(x)] - \chi_m[u_{m-1}(x), v_{m-1}(x)]) = \hbar\mathbf{R}_m, \quad (1.28)$$

subject to the boundary conditions

$$u_m(-1) = u_m(1) = v_m(-1) = v_m(1) = 0, \quad (1.29)$$

where

$$\mathbf{R}_m = \begin{bmatrix} R_{m,1}(x) \\ R_{m,2}(x) \end{bmatrix}, \quad (1.30)$$

with

$$\begin{aligned} R_{m,1}(x) &= u''_{m-1} + b_{11}^{(2)} u'_{m-1} + b_{11}^{(1)} u_{m-1} + b_{12}^{(2)} v'_{m-1} + b_{12}^{(1)} v_{m-1} \\ &\quad \sum_{n=0}^{m-1} \left(b_{11}^{(3)} u_n u_{m-1-n} + b_{12}^{(3)} u_n v_{m-1-n} \right) + \\ &\quad \sum_{n=0}^{m-1} \left(b_{11}^{(4)} u_n u'_{m-1-n} + b_{12}^{(4)} u_n v'_{m-1-n} \right), \end{aligned} \quad (1.31)$$

$$\begin{aligned} R_{m,2}(x) &= v''_{m-1} + b_{22}^{(2)} v'_{m-1} + b_{22}^{(1)} v_{m-1} + b_{21}^{(2)} u'_{m-1} + b_{21}^{(1)} u_{m-1} \\ &\quad \sum_{n=0}^{m-1} \left(b_{22}^{(3)} v_n v_{m-1-n} + b_{21}^{(3)} v_n u_{m-1-n} \right) + \\ &\quad \sum_{n=0}^{m-1} \left(b_{22}^{(4)} v_n v'_{m-1-n} + b_{21}^{(4)} v_n u'_{m-1-n} \right). \end{aligned} \quad (1.32)$$

When we apply the Chebyshev pseudospectral transformation to equations (1.28)- (1.32) we get

$$\begin{bmatrix} \mathcal{D}^2 + b_{11}^{(2)} \mathcal{D} + b_{11}^{(1)} & b_{12}^{(2)} \mathcal{D} \\ b_{21}^{(2)} \mathcal{D} + b_{21}^{(1)} & \mathcal{D}^2 + b_{22}^{(2)} \mathcal{D} + b_{22}^{(1)} \end{bmatrix} \begin{bmatrix} u_m \\ v_m \end{bmatrix} = -\hbar(1 - \chi_m) B, \quad (1.33)$$

$$(\chi_m + \hbar) \begin{bmatrix} \mathcal{D}^2 + b_{11}^{(2)} \mathcal{D} + b_{11}^{(1)} & b_{12}^{(2)} \mathcal{D} \\ b_{21}^{(2)} \mathcal{D} + b_{21}^{(1)} & \mathcal{D}^2 + b_{22}^{(2)} \mathcal{D} + b_{22}^{(1)} \end{bmatrix} \begin{bmatrix} u_{m-1} \\ v_{m-1} \end{bmatrix} + \begin{bmatrix} P_{m-1} \\ Q_{m-1} \end{bmatrix}. \quad (1.34)$$

We can express the above as

$$BY_m = (\chi + \hbar)BY_{m-1} - \hbar(1 - \chi_m)\mathbf{M} + \hbar B_{m-1}, \quad (1.35)$$

subject to the boundary conditions

$$u_m(x_0) = u_m(x_N) = v_m(x_0) = v_m(x_N) = 0, \quad (1.36)$$

where $Y_m = [u_m(x_j), v_m(x_j)^T]$ for $j = 1, 2, \dots, N - 1$ and

$$\mathbf{A}_{m-1} = \begin{bmatrix} P_{m-1} \\ Q_{m-1} \end{bmatrix} \quad (1.37)$$

with

$$P_{m-1} = \sum_{n=0}^{m-1} (b_{11}^3 u_n u_{m-1-n} + b_{12}^3 u_n v_{m-1-n} + b_{11}^4 \mathcal{D}u_{m-1-n} + b_{12}^4 \mathcal{D}v_{m-1-n}), \quad (1.38)$$

$$Q_{m-1} = \sum_{n=0}^{m-1} (b_{22}^3 v_n v_{m-1-n} + b_{21}^3 v_n u_{m-1-n} + b_{22}^4 \mathcal{D}v_{m-1-n} + b_{21}^4 \mathcal{D}u_{m-1-n}). \quad (1.39)$$

The value of $\mathbf{Y}_m (m \geq 1)$ is then determined from the following recursive scheme;

$$\mathbf{Y}_m = (\chi_m + \hbar)Y_{m-1} + \hbar B^{-1} [\mathbf{A}_{m-1} - (1 - \chi_m)\mathbf{M}]. \quad (1.40)$$

Therefore, starting from the initial guess we can calculate the m^{th} order approximations successively using the formula (1.40).

1.5. The successive linearisation method

The successive linearisation method is a recent method which has been used to solve non-linear boundary value problems (see Makukula et al.[30, 31]). Makukula et al.[30, 31] investigated the steady two-dimensional flow of a viscous incompressible fluid which is bounded by two permeable surfaces using the successive linearisation method. Awad et al. [7] investigated convection for an inverted cone in a porous medium with the effects cross-diffusion using the successive linearisation method. The method is based on the assumptions that the governing nonlinear equations can be reduced to a linear system of equations which can be solved using spectral methods.

The successive linearisation method has been shown to give accurate results, comparable to numerical methods such as the Runge-Kutta, shooting methods and the Keller-box based implicit finite difference schemes.

Consider the following a general n-order non-linear ordinary differential equation

$$\mathcal{L}([y(x), y'(x), y''(x), y'''(x), \dots, y^{(n)}]) + \mathcal{N}([y(x), y'(x), y''(x), y'''(x), \dots, y^{(n)}]) = 0 \quad (1.41)$$

we solve this equation for $x \in [a, b]$ subject to the boundary conditions

$$y(a) = y_a, \quad y(b) = y_b, \quad (1.42)$$

where $y(x)$ is an unknown function, x is an independent variable and the primes denote ordinary differentiation with respect to x . The functions \mathcal{L} and \mathcal{N} represent the linear and non-linear components of the governing equation respectively and y_a and y_b are given constants. For the initial guess of the solution of equation (1.41) we choose a function, $y_0(x)$, that satisfies the boundary conditions (1.42).

Define a function $Y_1(x)$ to represent the vertical difference between $y(x)$ and the initial guess y_0 , that is

$$Y_1(x) = y(x) - y_0(x), \quad (1.43)$$

Substituting equation (1.43) in (1.41) gives

$$\begin{aligned} & \mathcal{L}([Y_1, Y_1', Y_1'', Y_1''', \dots, Y_1^{(n)}]) + \mathcal{N}([y_0 + Y_1, y_0' + Y_1', y_0'' + Y_1'', \dots, y_0^{(n)} + Y_1^{(n)}]) \\ & = -\mathcal{L}([y_0, y_0', y_0'', y_0''', \dots, y_0^{(n)}]). \end{aligned} \quad (1.44)$$

Since $y_0(x)$ is given, we can solve equation (1.44) to obtain an exact solution for $Y_1(x)$. We look for an approximate solution which is obtained by solving the linear part of the equation assuming that $Y_1(x)$ and its derivatives are small. If $Y_1(x)$ is the solution of the

full equation (1.44) we let $y_1(x)$ denote the solution of the linearised version of (1.44).

Expanding (1.44) using Taylor series and neglecting higher order terms gives

$$\begin{aligned} & \mathcal{L}[y_1, y_1', y_1'', \dots, y_1^{(n)}] + y_1 \frac{\partial N}{\partial y_1} \Big|_{(y_0, y_0', y_0'', \dots, y_0^{(n)})} + y_1' \frac{\partial N}{\partial y_1'} \Big|_{(y_0, y_0', y_0'', \dots, y_0^{(n)})} \\ & + y_1'' \frac{\partial N}{\partial y_1''} \Big|_{(y_0, y_0', y_0'', \dots, y_0^{(n)})} + \dots + y_1^{(n)} \frac{\partial N}{\partial y_1^{(n)}} \Big|_{(y_0, y_0', y_0'', \dots, y_0^{(n)})} \\ & = -\mathcal{L}[y_0, y_0', y_0'', \dots, y_0^{(n)}] - \mathcal{N}[y_0, y_0', y_0'', \dots, y_0^{(n)}]. \end{aligned} \quad (1.45)$$

Equation (1.45) can be written in compact form as

$$\begin{aligned} & \mathcal{L}[y_1, y_1', y_1'', \dots, y_1^{(n)}] + a_{0,0} y_1^{(n)} + a_{1,0} y_1^{(n-1)} + \dots \\ & + a_{n-1,0} y_1' + a_{n,0} y_1 = r_0(x), \end{aligned} \quad (1.46)$$

subject to the boundary conditions

$$y_1(a) = 0, \quad y_1(b) = 0, \quad (1.47)$$

where

$$a_{0,0}(x) = \frac{\partial \mathcal{N}}{\partial y_1^{(n)}} \left(y_0, y_0', y_0'', \dots, y_0^{(n)} \right), \quad (1.48)$$

$$a_{1,0}(x) = \frac{\partial \mathcal{N}}{\partial y_1^{(n-1)}} \left(y_0, y_0', y_0'', \dots, y_0^{(n)} \right), \quad (1.49)$$

$$\vdots \quad (1.50)$$

$$a_{n-1,0}(x) = \frac{\partial \mathcal{N}}{\partial y_1'} \left(y_0, y_0', y_0'', \dots, y_0^{(n)} \right), \quad (1.51)$$

$$a_{n,0}(x) = \frac{\partial \mathcal{N}}{\partial y_1} \left(y_0, y_0', y_0'', \dots, y_0^{(n)} \right), \quad (1.52)$$

$$r_0(x) = -\mathcal{L}[y_0, y_0', y_0'', \dots, y_0^{(n)}] - \mathcal{N} \left(y_0, y_0', y_0'', \dots, y_0^{(n)} \right). \quad (1.53)$$

The right hand side of equation (1.46) is known and the left hand side is linear then the equation is solved for $y_1(x)$ by assuming the solution of the linear part of equation (1.46)

is close to the solution of the equation (1.44). The solution is $Y_1(x) \approx y_1(x)$ and from this the first order estimate $y(x)$ is

$$y(x) \approx y_0(x) + y_1(x), \quad (1.54)$$

To improve this solution we find the solution of $Y_2(x)$ by adding $Y_1(x)$ to $y_1(x)$ that is

$$Y_1(x) = Y_2(x) + y_1(x), \quad (1.55)$$

Since $y_1(x)$ is now known, we substitute equation (1.55) in equation (1.44) to obtain

$$\begin{aligned} \mathcal{L}[Y_2, Y_2', Y_2'', Y_2''', \dots, Y_2^{(n)}] + \mathcal{N}[y_0 + y_1 + Y_2, y_0' + y_1' + Y_2', \dots, y_0^{(n)} + y_1^{(n)} + Y_2^{(n)}] \\ = -\mathcal{L}[y_0 + y_1, y_0' + y_1', y_0'' + y_1'', \dots, y_0^{(n)} + y_1^{(n)}], \end{aligned} \quad (1.56)$$

Solving equation (1.56) would result in an exact solution for $Y_2(x)$. The solution of the new linear equation is $y_2(x)$, such that $Y_2(x) \approx y_2(x)$.

This process is repeated for $m = 3, 4, 5, \dots, i$. In general, we have

$$Y_i(x) = Y_{i+1}(x) + y_i(x), \quad (1.57)$$

So that $y(x)$ is obtained as,

$$y(x) = Y_1(x) + y_0(x), \quad (1.58)$$

$$= Y_2(x) + y_1(x) + y_0(x), \quad (1.59)$$

$$= Y_3(x) + y_2(x) + y_1(x) + y_0(x), \quad (1.60)$$

⋮

$$= Y_{i+1} + y_i(x) + \dots y_3(x) + y_2(x) + y_1(x) + y_0(x), \quad (1.61)$$

$$= Y_{i+1} + \sum_{m=0}^i y_m(x). \quad (1.62)$$

The value of $Y_i(x)$ for $i = 2, 3, \dots$ becomes increasingly smaller, when i becomes large.

Thus, for large i , the i^{th} order solution of $y(x)$ is approximated by

$$y(x) = \sum_{m=0}^i y_m = y_i(x) + \sum_{m=0}^{i-1} y_m(x). \quad (1.63)$$

Starting from a known initial guess $y_0(x)$, the solutions for $y_i(x)$ can be obtained by successively linearizing the governing equation (1.41) and solving the resulting linear equation for $y_i(x)$ given that the previous guess $y_{i-1}(x)$ is known.

The general form of the linearised equation to be solved for $y_i(x)$ is given by

$$\begin{aligned} \mathcal{L}[y_i, y_i', y_i'', \dots, y_i^n] + a_{0,i-1}y_i^{(n)} + a_{1,i-1}y_i^{(n-1)} + \dots \\ + a_{n-1,i-1}y_i' + a_{n,i-1}y_i = r_{i-1}(x), \end{aligned} \quad (1.64)$$

subject to the boundary conditions

$$y_i(a) = 0, \quad y_i(b) = 0, \quad (1.65)$$

where

$$a_{0,i-1}(x) = \frac{\partial \mathcal{N}}{\partial y_i^{(n)}} \left(\sum_{m=0}^{i-1} y_m(x), \sum_{m=0}^{i-1} y_m'(x), \sum_{m=0}^{i-1} y_m''(x) \dots \sum_{m=0}^{i-1} y_m^{(n)}(x) \right), \quad (1.66)$$

$$a_{1,i-1}(x) = \frac{\partial \mathcal{N}}{\partial y_i^{(n-1)}} \left(\sum_{m=0}^{i-1} y_m(x), \sum_{m=0}^{i-1} y_m'(x), \sum_{m=0}^{i-1} y_m''(x) \dots \sum_{m=0}^{i-1} y_m^{(n)}(x) \right), \quad (1.67)$$

$$a_{n-1,i-1}(x) = \frac{\partial \mathcal{N}}{\partial y_i'} \left(\sum_{m=0}^{i-1} y_m(x), \sum_{m=0}^{i-1} y_m'(x), \sum_{m=0}^{i-1} y_m''(x) \dots \sum_{m=0}^{i-1} y_m^{(n)}(x) \right), \quad (1.68)$$

$$a_{n,i-1}(x) = \frac{\partial \mathcal{N}}{\partial y_i} \left(\sum_{m=0}^{i-1} y_m(x), \sum_{m=0}^{i-1} y_m'(x), \sum_{m=0}^{i-1} y_m''(x) \dots \sum_{m=0}^{i-1} y_m^{(n)}(x) \right), \quad (1.69)$$

$$\begin{aligned} r_{i-1}(x) = -\mathcal{L} \left(\sum_{m=0}^{i-1} y_m(x), \sum_{m=0}^{i-1} y_m'(x), \sum_{m=0}^{i-1} y_m''(x) \dots \sum_{m=0}^{i-1} y_m^{(n)}(x) \right) \\ - \mathcal{N} \left(\sum_{m=0}^{i-1} y_m(x), \sum_{m=0}^{i-1} y_m'(x), \sum_{m=0}^{i-1} y_m''(x) \dots \sum_{m=0}^{i-1} y_m^{(n)}(x) \right). \end{aligned} \quad (1.70)$$

1.6. Objective of the study

The objectives of this study may be summarised as follows. We sought to;

1. investigate the effects of micro-rotation, inertia and a magnetic field on the flow of a micropolar fluid.
2. determine the effects of heat absorption on steady free convection in a micropolar fluid.
3. study convection and heat transfer in a micropolar fluid flow past a semi-infinite moving plate with viscous dissipation subject to Dufour and Soret effects.

The mathematical equations for the flow of a micropolar fluid are highly nonlinear and analytical solutions are hard to find. We used the successive linearisation method [31] and the spectral-homotopy analysis method to solve the governing flow and microrotation equations. The partial differential equations were first transformed to ordinary differential equations using a similarity transformation.

1.7. Outline of dissertation

This dissertation is divided into four chapters. In this chapter we presented the research background on micropolar fluid flows. We also presented a review of heat and mass transfer studies in micropolar fluids.

In Chapter 2 we present the Successive linearisation method (see Makukula et al. [31], Makukula et al. [30], Motsa et al. [33]) for solving the nonlinear equations for free

convection and heat transfer in steady micropolar fluids subject to a magnetic field.

Chapter 3 is concerned with the solution and discussion of steady free convection and heat transfer flow in micropolar fluids subject to Dufour and Soret effects. We use the spectral homotopy analysis method to solve the governing equations.

Chapter 4 provides a summary of the main findings of this study.

2

Steady MHD convection in a micropolar fluid

2.1. Introduction

The steady MHD flow and convection in micropolar fluids has been investigated by different researchers, such as Rahman and Sultana [43] who investigated the effect of variable heat flux and radiative heat transfer using a numerical method.

Khedr et al. [27] studied steady MHD convection in a micropolar fluid along a stretched semi-infinite vertical plate in the presence of heat generation or absorption, thermal radiation and viscous dissipation effects.

Beg et al.[10] studied steady MHD convection in a micropolar fluid flow about a sphere with heat generation. Rahman et al. [42] studied the flow of a thermo-micropolar fluid with variable heat flux in a porous medium using a sixth order Runge-Kutta method.

Sharma et al. [50] investigated unsteady MHD convection in a micropolar fluid with the presence of a magnetic field and heat absorption on a micropolar fluid using a meshless element free Galerkin method (EFGM).

The present model is an extension of the earlier study by Sharma et al. [50] to include steady magnetohydrodynamic flow and convection in a micropolar fluid. We use the successive linearisation method (see Makukula et al. [31]) to solve the governing nonlinear differential equations.

2.2. The governing equations

We consider steady magnetohydrodynamic (MHD) convection in a micropolar fluid through a porous medium in the presence of viscous dissipation and variable suction. The x -axis is along the vertical plate and the y -axis is in the horizontal direction. A magnetic field of uniform strength B_0 is applied transversely to the direction of the flow. The plate moves impulsively in its own plane with constant velocity u_0 and the fluid temperature in the ambient fluid is T_∞ .

A heat source is placed within the flow to allow for possible heat absorption effect. With the usual boundary layer and Boussinesq approximations, the problem is governed by the following set of equations (see Sharma et al.[50]).

$$\frac{\partial u}{\partial x} + \frac{\partial v}{\partial y} = 0, \quad (2.1)$$

$$\rho \left(u \frac{\partial u}{\partial x} + v \frac{\partial u}{\partial y} \right) = (\mu + k) \frac{\partial^2 u}{\partial y^2} + k \frac{\partial \mathbf{N}}{\partial y} - \left(\sigma B_0^2 + \frac{(\mu + k)}{k_p} \varepsilon + \frac{F \rho \varepsilon^2}{k_p^{1/2}} u \right) u + g \beta \rho (T - T_\infty), \quad (2.2)$$

$$\rho j \left(u \frac{\partial \mathbf{N}}{\partial x} + v \frac{\partial \mathbf{N}}{\partial y} \right) = \gamma \frac{\partial^2 \mathbf{N}}{\partial y^2} - k \left(2\mathbf{N} + \frac{\partial u}{\partial y} \right), \quad (2.3)$$

$$u \frac{\partial T}{\partial x} + v \frac{\partial T}{\partial y} = \frac{k_f}{\rho c_p} \frac{\partial^2 T}{\partial y^2} + \frac{1}{\rho c_p} \left(\frac{(\mu + k) \varepsilon}{k_p} u^2 + \frac{F \rho \varepsilon^2}{k_p^{1/2}} u^3 + (\mu + k) \left(\frac{\partial u}{\partial y} \right)^2 \right) - \frac{Q_0}{\rho c_p} (T - T_\infty). \quad (2.4)$$

The boundary conditions on the vertical surface and in the free stream are as follows;

$$y = 0 : u = u_0, \quad v = 0, \quad \mathbf{N} = -n \frac{\partial u}{\partial y}, \quad T = T_w,$$

$$y \rightarrow \infty : u \rightarrow 0, \quad \mathbf{N} \rightarrow 0, \quad T = T_\infty,$$

where u and v are the velocity components along the x and y -axes, \mathbf{N} is the component of the microrotation vector normal to the x y - plane, T is the fluid temperature, g is the magnitude of the acceleration due to gravity, ρ is the fluid density, μ is the absolute viscosity, k is the vortex viscosity, γ is the spin-gradient viscosity, ν is the kinematic viscosity, j is the microinertia density, β is thermal expansion coefficients, and n is a constant such that $0 \leq n \leq 1$. Here $n = \frac{1}{2}$ indicates a weak concentration of microelements and the vanishing of the anti-symmetric component of the stress tensor, $n = 1$ indicates turbulent boundary-layer flow and $n = 0$ indicates a strong concentration case in which the microelements close to the wall are unable to rotate, (see Rahman and Sultana [43]). The other variables which are mentioned in the above equations are defined on pages 93 and 94 in this dissertation. In equation (2.4), the middle terms are the viscous dissipation terms in the Darcy-Forchheimer media and the last term is the heat source term.

We introduce the following dimensionless variables (see Rahman and Sultana [43]):

$$\eta = y\sqrt{\frac{U_0}{2\nu x}}, \quad \psi = \sqrt{2\nu U_0 x}f(\eta), \quad \theta(\eta) = \frac{T - T_\infty}{T_w - T_\infty},$$

$$\mathbf{N} = \sqrt{\frac{U_0^3}{2\nu x}}\omega(\eta), \quad \gamma = \left(\mu + \frac{k}{2}\right)j = \mu j\left(1 + \frac{K}{2}\right), \quad j = \frac{2\nu x}{U_0}.$$

Substituting the above dimensionless variables into equations (2.1)-(2.4), these reduce to the local similarity forms;

$$\kappa f'''' + ff'' + K\omega' - 2Re \left(M + \frac{\kappa}{Da} + \frac{Fr}{Da}f' \right) f' + 2ReGr\theta = 0, \quad (2.5)$$

$$\left(1 + \frac{K}{2}\right)\omega'' - K(2\omega + f'') + f\omega' + f'\omega = 0, \quad (2.6)$$

$$\frac{1}{Pr}\theta'' + f\theta' + 2ReEc \left(\kappa \frac{1}{Da}(f')^2 + \frac{Fr}{Da}(f')^3 \right) + Ec\kappa(f'')^2 - 2ReQ\theta = 0, \quad (2.7)$$

where $K + 1 = \kappa$, with boundary conditions

$$f(0) = 0, \quad f'(0) = 1, \quad \omega(0) = -nf''(0) = 0, \quad \theta(0) = 1, \quad (2.8)$$

$$f'(\infty) \rightarrow 0, \quad \omega(\infty) \rightarrow 0, \quad \theta(\infty) \rightarrow 0, \quad (2.9)$$

In the above equations, a prime denotes differentiation with respect to η . The physical parameters appearing in equations (2.5)-(2.7) are γ the microrotation viscosity or spin-gradient, K is the coupling constant parameter, Ec is the Eckert number, Pr is the Prandtl number, M is the magnetic field parameter, Da is the Darcy parameter, Fr is a Forcheimmer parameter, Gr is the Grashof number, Q is the heat absorption parameter, ν is the kinematic viscosity, Re is the local Reynolds number and assume that $n = 0$ we use this assumption throughout the dissertation.

These parameters are defined as follows;

$$\gamma = \left(\mu + \frac{k}{2}\right)j = \mu j\left(1 + \frac{K}{2}\right), \quad K = \frac{k}{\rho\nu}, \quad Ec = \frac{U_o^2}{c_p(T_w - T_\infty)}, \quad Pr = \frac{\rho\nu c_p}{k_f}, \quad M = \frac{\sigma B_o^2\nu}{\rho U_o^2},$$

$$Da = \frac{k_p U_o^2}{\varepsilon\nu^2}, \quad Fr = \frac{F\varepsilon U_o k_p^{1/2}}{\nu}, \quad Gr = \frac{\nu g\beta(T_w - T_\infty)}{U_o^3}, \quad Q = \frac{Q_o\nu}{\rho c_p U_o^2}, \quad \nu = \frac{\mu}{\rho} \quad \text{and} \quad Re = \frac{U_o x}{\nu}.$$

2.3. The skin friction coefficient and the local Nusselt number

The physical properties of engineering interest are the skin friction coefficient and the rate of heat transfer or Nusselt number. The skin friction coefficient at the surface of plate is given by:

$$c_f = \frac{\tau_w}{\rho u_w^2} \quad \text{where} \quad \tau_w = -[(\mu + k)\frac{\partial u}{\partial y} + k\mathbf{N}]_{y=0}. \quad (2.10)$$

Hence, in dimensionless form:

$$c_f/\sqrt{Re} = -(1 + k)\frac{\partial U}{\partial Y}|_{Y=0}. \quad (2.11)$$

The heat transfer coefficient at the wall of the plate in terms of the local Nusselt number is calculated as follows:

$$N_u(x) = \frac{-x}{(T_W - T_\infty)} \frac{\partial T}{\partial y} \Big|_{y=0}. \quad (2.12)$$

Hence, in dimensionless form:

$$N_u(x) = -\sqrt{\frac{Re}{2}} \frac{\partial \theta}{\partial Y} \Big|_{Y=0}. \quad (2.13)$$

We use the successive linearisation method to find numerical solutions of equations (2.5)-(2.7).

2.4. Successive Linearisation Method

The successive linearisation method (SLM) is used to solve the non-linear ordinary differential equations (2.5)-(2.7). The SLM assumes that the unknown functions $F(\eta)$, $H(\eta)$

and $G(\eta)$ may be expanded as

$$\left. \begin{aligned} F(\eta) &= F_i(\eta) + \sum_{m=0}^{i-1} f_m(\eta), \\ H(\eta) &= H_i(\eta) + \sum_{m=0}^{i-1} h_m(\eta), \\ G(\eta) &= G_i(\eta) + \sum_{m=0}^{i-1} g_m(\eta), \end{aligned} \right\}_{,i=1,2,3,\dots} \quad (2.14)$$

where $F_i(\eta)$, $H_i(\eta)$ and $G_i(\eta)$ are unknown functions and f_m , h_m and g_m ($m \geq 1$) are approximations which are obtained by recursive solving the linear part of the system that results from substituting (2.14) into (2.5)-(2.7). This gives

$$F_i'''' + a_{1,i-1}F_i'' + a_{2,i-1}F_i' + a_{3,i-1}F_i + a_{4,i-1}H_i' + a_{5,i-1}G_i = r_{1,i-1}, \quad (2.15)$$

$$H_i'' + b_{1,i-1}H_i' + b_{2,i-1}H_i + b_{3,i-1}F_i'' + b_{4,i-1}F_i' + b_{5,i-1}F_i = r_{2,i-1}, \quad (2.16)$$

$$G_i'' + c_{1,i-1}G_i' + c_{2,i-1}G_i + b_{3,i-1}F_i'' + c_{4,i-1}F_i' + c_{5,i-1}F_i = r_{3,i-1}. \quad (2.17)$$

where the coefficient parameters $a_{k,i-1}$, $b_{k,i-1}$, $c_{k,i-1}$, $r_{1,i-1}$, $r_{2,i-1}$ and $r_{3,i-1}$ ($k = 1, \dots, 5$) are defined as

$$\left. \begin{aligned} a_{1,i-1} &= \frac{1}{\kappa} \sum_{m=0}^{i-1} f_m, & a_{2,i-1} &= \frac{-2Re}{\kappa} \left(M + \frac{\kappa}{Da} + 2 \frac{Fr}{Da} \sum_{m=0}^{i-1} f_m' \right), \\ a_{3,i-1} &= \frac{1}{\kappa} \sum_{m=0}^{i-1} f_m'', & a_{4,i-1} &= \frac{K}{\kappa}, & a_{5,i-1} &= \frac{2ReGr}{\kappa}, \\ b_{1,i-1} &= \frac{2}{(K+2)} \sum_{m=0}^{i-1} f_m, & b_{2,i-1} &= \frac{2}{(K+2)} (-4K + \sum_{m=0}^{i-1} f_m), & b_{3,i-1} &= \frac{-4K}{K+2}, \\ b_{4,i-1} &= \frac{2}{(K+2)} \sum_{m=0}^{i-1} h_m, & b_{5,i-1} &= \frac{2}{(K+2)} \sum_{m=0}^{i-1} h_m', & c_{1,i-1} &= \sum_{m=0}^{i-1} f_m, \\ c_{2,i-1} &= -2ReQPr, & c_{3,i-1} &= 2Pr\kappa Ec \sum_{m=0}^{i-1} f_m'', \\ c_{4,i-1} &= 4RePrEc \frac{\kappa}{Da} \sum_{m=0}^{i-1} f_m' + 6RePrEc \frac{Fr}{Da} \left(\sum_{m=0}^{i-1} f_m' \right)^2, & c_{5,i-1} &= Pr \left(\sum_{m=0}^{i-1} g_m' \right) \end{aligned} \right\}_{,i=1,2,3,\dots} \quad (2.18)$$

$$\left. \begin{aligned}
 r_{1,i-1} &= - \sum_{m=0}^{i-1} f_m'' - \frac{1}{\kappa} \sum_{m=0}^{i-1} f_m \sum_{m=0}^{i-1} f_m'' - \frac{K}{\kappa} \sum_{m=0}^{i-1} h_m' - \frac{2ReGr}{\kappa} \sum_{m=0}^{i-1} g_m \\
 &\quad + \frac{2ReM}{\kappa} \sum_{m=0}^{i-1} f_m' + \frac{2Re}{Da} \sum_{m=0}^{i-1} f_m' - \frac{Fr}{Da\kappa} \left(\sum_{m=0}^{i-1} f_m' \right)^2, \\
 r_{2,i-1} &= - \sum_{m=0}^{i-1} h_m'' + \frac{8K}{K+2} \sum_{m=0}^{i-1} h_m - \frac{2}{K+2} \sum_{m=0}^{i-1} h_m' \sum_{m=0}^{i-1} f_m \\
 &\quad - \frac{2}{K+2} \sum_{m=0}^{i-1} h_m \sum_{m=0}^{i-1} f_m' + \frac{4K}{K+2} \sum_{m=0}^{i-1} f_m'', \\
 r_{3,i-1} &= - \sum_{m=0}^{i-1} g_m'' - Pr - \sum_{m=0}^{i-1} f_m \sum_{m=0}^{i-1} h_m' - 2RePrEc \frac{\kappa}{Da} \left(\sum_{m=0}^{i-1} f_m' \right)^2 \\
 &\quad - 2RePrEc \frac{Fr}{Da} \left(\sum_{m=0}^{i-1} f_m' \right)^3 - Pr\kappa Ec \left(\sum_{m=0}^{i-1} f_m'' \right)^2 + 2ReQPr \sum_{m=0}^{i-1} g_m.
 \end{aligned} \right\}_{,i=1,2,3,\dots} \quad (2.19)$$

The SLM algorithm starts from the initial approximations

$$f_0(\eta) = 1 - e^{-\eta}, \quad \omega_0(\eta) = \eta e^{-\eta}, \quad \theta_0(\eta) = e^{-\eta}, \quad (2.20)$$

which are chosen to satisfy the boundary conditions (2.9). The solutions f_m , h_m and g_m ($m \geq 1$) are obtained successively by solving the linear form of equations (2.22)-(2.23) which are given as

$$f_i''' + a_{1,i-1} f_i'' + a_{2,i-1} f_i' + a_{3,i-1} f_i + a_{4,i-1} h_i' + a_{5,i-1} g_i = r_{1,i-1}, \quad (2.21)$$

$$h_i'' + b_{1,i-1} h_i' + b_{2,i-1} h_i + b_{3,i-1} f_i'' + b_{4,i-1} f_i' + b_{5,i-1} f_i = r_{2,i-1}, \quad (2.22)$$

$$g_i'' + c_{1,i-1} g_i' + c_{2,i-1} g_i + c_{3,i-1} f_i'' + c_{4,i-1} f_i' + c_{5,i-1} f_i = r_{3,i-1}. \quad (2.23)$$

subject to the boundary conditions in which the microelements close to the wall are unable to rotate in such a way that, $n = 0$ so:

$$f_i(0) = f_i'(0) = f_i'(\infty) = h_i(0) = h_i(\infty) = g_i(0) = g_i(\infty). \quad (2.24)$$

Once each solution f_i , h_i , g_i ($i \geq 1$) has been found from iteratively solving equations

(2.22)-(2.23) for each i , the approximate solutions $F(\eta)$, $H(\eta)$ and $G(\eta)$ are obtained as

$$F(\eta) \approx \sum_{m=0}^M f_m(\eta), \quad H(\eta) \approx \sum_{m=0}^M h_m(\eta), \quad G(\eta) \approx \sum_{m=0}^M g_m(\eta), \quad (2.25)$$

where M is the order of successive linearisation method (SLM) approximation. In coming up with (2.24), it is assumed that F_i , H_i and G_i become increasingly small when i becomes large, that is

$$\lim_{i \rightarrow \infty} F_i = \lim_{i \rightarrow \infty} H_i = \lim_{i \rightarrow \infty} G_i = 0. \quad (2.26)$$

Since the coefficient parameters and the right hand side of equations (2.22)-(2.23), for $i = 1, 2, 3, \dots$, are known, the system (2.22)-(2.24) can easily be solved using any numerical method such as finite differences, finite elements, shooting methods or collocation methods.

In this work, equations (2.22)-(2.24) were solved using the Chebyshev spectral collocation method. The method approximates the unknown functions by the Chebyshev interpolating polynomials in such a way that they are collocated at the Gauss-Lobatto points defined as

$$\xi_j = \cos \frac{\pi j}{N}, \quad j = 0, 1, 2, \dots, N. \quad (2.27)$$

where N is the number of collocation points used (see for example [13], [55]). In order to implement the method, the physical region $[0, \infty)$ is transformed into the region $[-1, 1]$ using the domain truncation technique in which the problem is solved on the interval $[0, L]$ instead of $[0, \infty)$. This leads to the mapping

$$\frac{\eta}{L} = \frac{\xi + 1}{2}, \quad -1 \leq \xi \leq 1. \quad (2.28)$$

where L is a scaling parameter used to invoke the boundary condition at infinity. The

unknown functions f_i, h_i and g_i are approximated at the collocation points by

$$\begin{aligned} f_i(\xi) &\approx \sum_{k=0}^N f_i(\xi_k) T_i(\xi_k), & h_i(\xi) &\approx \sum_{k=0}^N h_i(\xi_k) T_i(\xi_k), \\ g_i(\xi) &\approx \sum_{k=0}^N g_i(\xi_k) T_i(\xi_k), & j &= 0, 1, 2, \dots, N. \end{aligned} \quad (2.29)$$

where T_k is the k^{th} Chebyshev polynomial defined by

$$T_i(\xi) = \cos[k \cos^{-1}(\xi)]. \quad (2.30)$$

The derivatives of the variables at the collocation points are represented as

$$\begin{aligned} \frac{d^a f_i}{d\eta^a} &= \sum_{k=0}^N \mathbf{D}_{kj}^a f_i(\xi_k), & \frac{d^a h_i}{d\eta^a} &= \sum_{k=0}^N \mathbf{D}_{kj}^a h_i(\xi_k), \\ \frac{d^a g_i}{d\eta^a} &= \sum_{k=0}^N \mathbf{D}_{kj}^a g_i(\xi_k), & j &= 0, 1, 2, \dots, N. \end{aligned} \quad (2.31)$$

where a is the order of differentiation and $\mathbf{D} = \frac{2}{L} \mathcal{D}$ with \mathcal{D} being the Chebyshev spectral differentiation matrix (see for example [13], [55]). Substituting equations (2.28 - 2.31) in (2.22) - (2.23) leads to the matrix equation given by

$$\mathbf{A} \mathbf{Y}_i = \mathbf{R}_{i-1}, \quad (2.32)$$

and the boundary conditions transform to ,

$$\left. \begin{aligned} f_i(\xi_N) &= \sum_{k=0}^N \mathbf{D}_{kj} f_i(\xi_k) = \sum_{k=0}^N \mathbf{D}_{0k}^a f_i(\xi_k) = h_i(x_0) = g_i(x_0) = 0, \\ \sum_{k=0}^N \mathbf{D}_{Nk} f_i(\xi_k) &= h_i(x_N) = g_i(x_N) = 0 \end{aligned} \right\} \quad (2.33)$$

in which \mathbf{A} is a $3(N+1) \times 3(N+1)$ square matrix and \mathbf{Y} and \mathbf{R} are $4(N+1) \times 1$ column vectors defined by

$$\mathbf{A} = \begin{bmatrix} A_{11} & A_{12} & A_{13} \\ A_{21} & A_{22} & A_{23} \\ A_{31} & A_{32} & A_{33} \end{bmatrix}, \quad \mathbf{Y}_i = \begin{bmatrix} F_i \\ H_i \\ G_i \end{bmatrix}, \quad \mathbf{R}_{i-1} = \begin{bmatrix} r_{1,i-1} \\ r_{2,i-1} \\ r_{3,i-1} \end{bmatrix}, \quad (2.34)$$

with

$$\left. \begin{aligned}
 F_i &= [f_i(\xi_0), f_i(\xi_1), f_i(\xi_2), f_i(\xi_3), \dots, f_i(\xi_{N-1}), f_i(\xi_N)]^T, \\
 H_i &= [h_i(\xi_0), h_i(\xi_1), h_i(\xi_2), h_i(\xi_3), \dots, h_i(\xi_{N-1}), h_i(\xi_N)]^T, \\
 G_i &= [g_i(\xi_0), g_i(\xi_1), g_i(\xi_2), g_i(\xi_3), \dots, g_i(\xi_{N-1}), g_i(\xi_N)]^T, \\
 r_{1,i-1} &= [r_{1,i-1}(\xi_0), r_{1,i-1}(\xi_1), r_{1,i-1}(\xi_2), r_{1,i-1}(\xi_3), \dots, r_{1,i-1}(\xi_{N-1}), r_{1,i-1}(\xi_N)]^T, \\
 r_{2,i-1} &= [r_{2,i-1}(\xi_0), r_{2,i-1}(\xi_1), r_{2,i-1}(\xi_2), r_{2,i-1}(\xi_3), \dots, r_{2,i-1}(\xi_{N-1}), r_{2,i-1}(\xi_N)]^T, \\
 r_{3,i-1} &= [r_{3,i-1}(\xi_0), r_{3,i-1}(\xi_1), r_{3,i-1}(\xi_2), r_{3,i-1}(\xi_3), \dots, r_{3,i-1}(\xi_N)]^T,
 \end{aligned} \right\} \quad (2.35)$$

$$\left. \begin{aligned}
 A11 &= \mathbf{D}^3 + a_{1,i-1}\mathbf{D}^2 + a_{2,i-1}\mathbf{D} + a_{3,i-1}, \\
 A12 &= a_{4,i-1}\mathbf{D} + a_{5,i-1}, \\
 A13 &= a_{6,i-1}, \\
 A21 &= b_{3,i-1}\mathbf{D}^2 + b_{4,i-1}\mathbf{D} + b_{5,i-1}, \\
 A22 &= \mathbf{D}^2 + b_{1,i-1}\mathbf{D} + b_{2,i-1}, \quad A23 = 0, \\
 A31 &= c_{3,i-1}\mathbf{D}^2 + c_{4,i-1}\mathbf{D} + c_{5,i-1}, \quad A32 = 0, \\
 A33 &= \mathbf{D}^2 + c_{1,i-1}\mathbf{D} + c_{5,i-1},
 \end{aligned} \right\} \quad (2.36)$$

In the above definitions, $A23$ and $A32$ are zero square matrices of size $(N+1) \times (N+1)$ and also $a_{k,i-1}$, $b_{k,i-1}$, $c_{k,i-1}$ ($k = 1, 2, \dots, 5$) are diagonal matrices of size $(N+1) \times (N+1)$.

2.5. Results and Discussions

In this section, we discuss the convergence of the successive linearisation method when $N = 150$ and $L = 25$. To validate the SLM solutions, the equations were further solved using the Matlab **bvp4c** solver. The comparison between the SLM results and the numerical solutions is shown in Table 2.1 - Table 2.7. These show that the SLM solutions converge to the numerical solution.

The functions $f''(0)$, $\omega'(0)$ and $-\theta'(0)$ which are respectively proportional to the local skin friction coefficient, the plate couple stress and the heat transfer coefficient have been determined in Table 2.1 - Table 2.7. In this study we have used $Pr = 0.71$ which corresponds to air (see Awad et al. [7], Alam et al. [3]). From Table 2.1 we observe that $f''(0)$ and $-\theta'(0)$ increase as K increases but the plate couple stress $\omega'(0)$ decreases as K increases. These results are in agreement with Sharma et al. [50], Bachok and Ishak [9] and El- Arabawy [17].

From Table 2.2 we observe that the local skin friction coefficient $f''(0)$ and the heat transfer coefficient $-\theta'(0)$ decrease and the plate couple stress $\omega'(0)$ increases as Fr increases. These results are also in agreement with Sharma et al. [50], El- Arabawy [17].

From Table 2.3 we observe that the local skin friction coefficient $f''(0)$ and the heat transfer coefficient $-\theta'(0)$ decrease and the plate couple stress $\omega'(0)$ increases as M increases.

From Table 2.4 we observe that the local skin friction coefficient $f''(0)$ and the heat transfer coefficient $-\theta'(0)$ increase and the plate couple stress $\omega'(0)$ decreases as Da increases. The results in Table 2.3 and Table 2.4 are in agreement with the results obtained by Cheng [15], Beg et al. [10], El- Arabawy [17] and Sharma et al. [50].

Table 2.1: Comparison of the **bvp4c** results against the SLM approximate solutions with $N = 50$ and different values of K when $M = 0.6$, $Da = 2$, $Fr = 0.8$, $Gr = 0.01$, $Pr = 0.71$, $Q = 0.001$, $Ec = 0.01$, $Re = 0.1$.

	SLM results				bvp4c
	K	2nd order	4rd order	6th order	
$f''(0)$	5.0	-0.37476112	-0.37478010	-0.37478010	-0.37478010
	6.0	-0.35811621	-0.35813183	-0.35813183	-0.35813183
	7.0	-0.34539943	-0.34541211	-0.34541211	-0.34541211
	8.0	-0.33536556	-0.33537581	-0.33537581	-0.33537581
$\omega'(0)$	5.0	0.32600148	0.32602504	0.32602504	0.32602504
	6.0	0.32264087	0.32266088	0.32266088	0.32266088
	7.0	0.31932144	0.31933807	0.31933807	0.31933806
	8.0	0.31623515	0.31624885	0.31624885	0.31624885
$-\theta'(0)$	5.0	0.55276080	0.55321168	0.55321231	0.55321231
	6.0	0.55569453	0.55611927	0.55611980	0.55611980
	7.0	0.55767000	0.55806657	0.55806702	0.55806702
	8.0	0.55896879	0.55933794	0.55933834	0.55933834

Table 2.2: Comparison of the **bvp4c** results against the SLM approximate solutions with $N = 50$ and different values of Fr when $K = 20$, $M = 0.8$, $Da = 2$, $Gr = 0.01$, $Pr = 0.71$, $Q = 0.001$, $Ec = 0.001$, $Re = 0.1$.

	SLM results				bvp4c
	Fr	2nd order	4rd order	6th order	
$f''(0)$	2.0	-0.29497044	-0.29497268	-0.29497268	-0.29497268
	4.0	-0.30282974	-0.30283429	-0.30283429	-0.30283429
	6.0	-0.31053381	-0.31054119	-0.31054119	-0.31054119
	8.0	-0.31809168	-0.31810234	-0.31810234	-0.31810234
$\omega'(0)$	2.0	0.30061661	0.30061977	0.30061977	0.30061977
	4.0	0.30544510	0.30545134	0.30545134	0.30545134
	6.0	0.31013400	0.31014399	0.31014399	0.31014399
	8.0	0.31469213	0.31470643	0.31470643	0.31470643
$-\theta'(0)$	2.0	0.58386142	0.58406944	0.58406960	0.58406960
	4.0	0.58215569	0.58238510	0.58238527	0.58238527
	6.0	0.58049204	0.58074091	0.58074110	0.58074110
	8.0	0.57886791	0.57913453	0.57913473	0.57913473

Table 2.3: Comparison of the **bvp4c** results against the SLM approximate solutions with $N = 60$ and different values of M when $K = 15$, $Fr = 1$, $Da = 2$, $Gr = 0.01$, $Pr = 0.71$, $Q = 0.001$, $Ec = 0.001$, $Re = 0.1$.

	SLM results				bvp4c
	M	2nd order	4rd order	6th order	
$f''(0)$	0.2	-0.57290226	-0.57290229	-0.57290229	-0.57290229
	0.4	-0.57466601	-0.57466604	-0.57466604	-0.57466604
	0.6	-0.57642528	-0.57642531	-0.57642531	-0.57642531
	0.8	-0.57818010	-0.57818013	-0.57818013	-0.57818013
$\omega'(0)$	0.2	0.47085171	0.47085175	0.47085175	0.47085175
	0.4	0.47180089	0.47180093	0.47180093	0.47180093
	0.6	0.47274603	0.47274607	0.47274607	0.47274607
	0.8	0.47368716	0.47368720	0.47368720	0.47368720
$-\theta'(0)$	0.2	0.51172269	0.51190888	0.51190965	0.51190965
	0.4	0.51129548	0.51147914	0.51147990	0.51147990
	0.6	0.51086965	0.51105076	0.51105152	0.51105152
	0.8	0.51044518	0.51062374	0.51062449	0.51062449

Table 2.4: Comparison of the **bvp4c** results against the SLM approximate solutions with $N = 50$ and different values of Da when $K = 20$, $M = 0.8$, $Fr = 0.1$, $Gr = 0.01$, $Pr = 0.71$, $Q = 0.001$, $Ec = 0.001$, $Re = 0.2$.

	SLM results				bvp4c
	Da	2nd order	4rd order	6th order	
$f''(0)$	2.0	-0.29097950	-0.29098080	-0.29098080	-0.29098080
	4.0	-0.22088143	-0.22089613	-0.22089613	-0.22089613
	6.0	-0.19317947	-0.19322712	-0.19322712	-0.19322712
	8.0	-0.17806197	-0.17815831	-0.17815831	-0.17815831
$\omega'(0)$	2.0	0.29814702	0.29814890	0.29814890	0.29814890
	4.0	0.24281216	0.24283252	0.24283252	0.24283251
	6.0	0.21938652	0.21945140	0.21945140	0.21945140
	8.0	0.20618518	0.20631529	0.20631529	0.20631529
$-\theta'(0)$	2.0	0.58473092	0.58492748	0.58492763	0.58492763
	4.0	0.60465731	0.60444897	0.60444859	0.60444859
	6.0	0.61282666	0.61222442	0.61222371	0.61222371
	8.0	0.61741577	0.61647282	0.61647185	0.61647185

From Table 2.5 we observe that the local skin friction coefficient $f''(0)$ and the heat transfer coefficient $-\theta'(0)$ increase and the plate couple stress $\omega'(0)$ decreases as Gr increases. These results are agreement with Sharma et al. [49], Cheng [15] and El- Arabawy [17].

Table 2.5: Comparison of the **bvp4c** results against the SLM approximate solutions with $N = 50$ and different values of Gr when $K = 15$, $Da = 6$, $Fr = 1$, $M = 0.7$, $Pr = 0.71$, $Q = 0.001$, $Ec = 0.01$, $Re = 0.1$.

	SLM results				bvp4c
	Gr	2nd order	4rd order	6th order	
$f''(0)$	2.0	-0.18468106	-0.18468922	-0.18468914	-0.18468914
	4.0	-0.16310052	-0.16301244	-0.16301227	-0.16301227
	6.0	-0.14179579	-0.14159933	-0.14159909	-0.14159909
	8.0	-0.12074054	-0.12042898	-0.12042867	-0.12042867
$\omega'(0)$	2.0	0.21689216	0.21691414	0.21691404	0.21691403
	4.0	0.20387410	0.20378115	0.20378095	0.20378095
	6.0	0.19113632	0.19091352	0.19091323	0.19091323
	8.0	0.17865038	0.17828922	0.17828886	0.17828886
$-\theta'(0)$	2.0	0.59944548	0.59871378	0.59871294	0.59871294
	4.0	0.60369442	0.60290221	0.60290141	0.60290141
	6.0	0.60772381	0.60689043	0.60688968	0.60688968
	8.0	0.61155245	0.61069608	0.61069539	0.61069539

From Table 2.6 we observe that the local skin friction coefficient $f''(0)$ increases and the plate couple stress $\omega'(0)$ and the heat transfer coefficient $-\theta'(0)$ decrease as Ec increases.

Table 2.6: Comparison of the **bvp4c** results against the SLM approximate solutions with $N = 50$ and different values of Ec when $K = 15$, $Da = 2$, $Fr = 0.1$, $M = 0.5$, $Pr = 0.71$, $Q = 0.001$, $Gr = 0.01$, $Re = 0.1$.

	SLM results				bvp4c
	Ec	2nd order	4rd order	6th order	
$f''(0)$	0.02	-0.29407893	-0.29408064	-0.29408064	-0.29408064
	0.04	-0.29407416	-0.29407587	-0.29407587	-0.29407587
	0.06	-0.29406938	-0.29407110	-0.29407110	-0.29407110
	0.08	-0.29406461	-0.29406633	-0.29406633	-0.29406633
$\omega'(0)$	0.02	0.29836492	0.29836745	0.29836745	0.29836745
	0.04	0.29836051	0.29836305	0.29836305	0.29836305
	0.06	0.29835611	0.29835865	0.29835865	0.29835865
	0.08	0.29835170	0.29835425	0.29835425	0.29835425
$-\theta'(0)$	0.02	0.53454729	0.53477072	0.53477089	0.53477089
	0.04	0.48245265	0.48267803	0.48267819	0.48267819
	0.06	0.43035908	0.43058640	0.43058655	0.43058655
	0.08	0.37826657	0.37849582	0.37849597	0.37849597

From Table 2.7 we observe that the local skin friction coefficient $f''(0)$ and the heat transfer coefficient $-\theta'(0)$ decrease and the plate couple stress $\omega'(0)$ increases as Re increases.

Table 2.7: Comparison of the **bvp4c** results against the SLM approximate solutions with $N = 50$ and different values of Re when $K = 18$, $Da = 10$, $Fr = 1$, $M = 0.7$, $Pr = 0.71$, $Q = 0.001$, $Gr = 0.01$, $Ec = 0.01$.

	SLM results				bvp4c
	Re	2nd order	4rd order	6th order	
$f''(0)$	0.02	-0.12360153	-0.12633734	-0.12633764	-0.12633764
	0.04	-0.13759812	-0.13885433	-0.13885434	-0.13885434
	0.06	-0.15000900	-0.15064300	-0.15064300	-0.15064300
	0.08	-0.16146266	-0.16180679	-0.16180679	-0.16180679
$\omega'(0)$	0.02	0.15585890	0.15943367	0.15943405	0.15943405
	0.04	0.16944690	0.17109632	0.17109633	0.17109633
	0.06	0.18105770	0.18189429	0.18189429	0.18189429
	0.08	0.19149673	0.19195315	0.19195315	0.19195315
$-\theta'(0)$	0.02	0.62855441	0.62231291	0.62231136	0.62231136
	0.04	0.62160297	0.61762891	0.61762785	0.61762785
	0.06	0.61593239	0.61319868	0.61319761	0.61319761
	0.08	0.61097154	0.60899043	0.60898923	0.60898923

Table 2.8 shows that the skin friction coefficient $f''(0)$ decreases as the heat absorption parameter Q increases. The heat transfer coefficient $\theta'(0)$ increases highly as the heat absorption parameter Q increases. This finding is similar to the results obtained by Sharma et al. [50].

Table 2.8: Effects of heat absorption coefficient on the skin friction $f''(0)$ and the rate of heat transfer $-\theta'(0)$ with parameters $K = 1$, $Da = 1$, $M = 0.3$, $Fr = 0.5$, $Gr = 2.2$, $Pr = 0.71$, $Ec = 0.04$, $Re = 2$.

Q	$f''(0)$	$-\theta'(0)$
0.1	-0.90861632	0.67600217
0.3	-0.98526875	0.91063667
0.5	-1.03476577	1.08914019
1.0	-1.20061066	1.62471447
1.5	-2.03032583	3.83707505

The effect of the micropolar parameter K on the velocity, microrotation and temperature profiles is presented in Figures 2.1. We observed that the velocity decreases as the micropolar parameter K increases, whereas the temperature and angular velocity both increase as the micropolar parameter increases. These results are in agreement with the results obtained by Cheng [15], Salleh et al. [48] and Sharma et al. [50].

In addition to this, the velocity is a maximum when $K = 0$ (Newtonian fluid) implying that the presence of micro-elements decelerates the fluid flow.

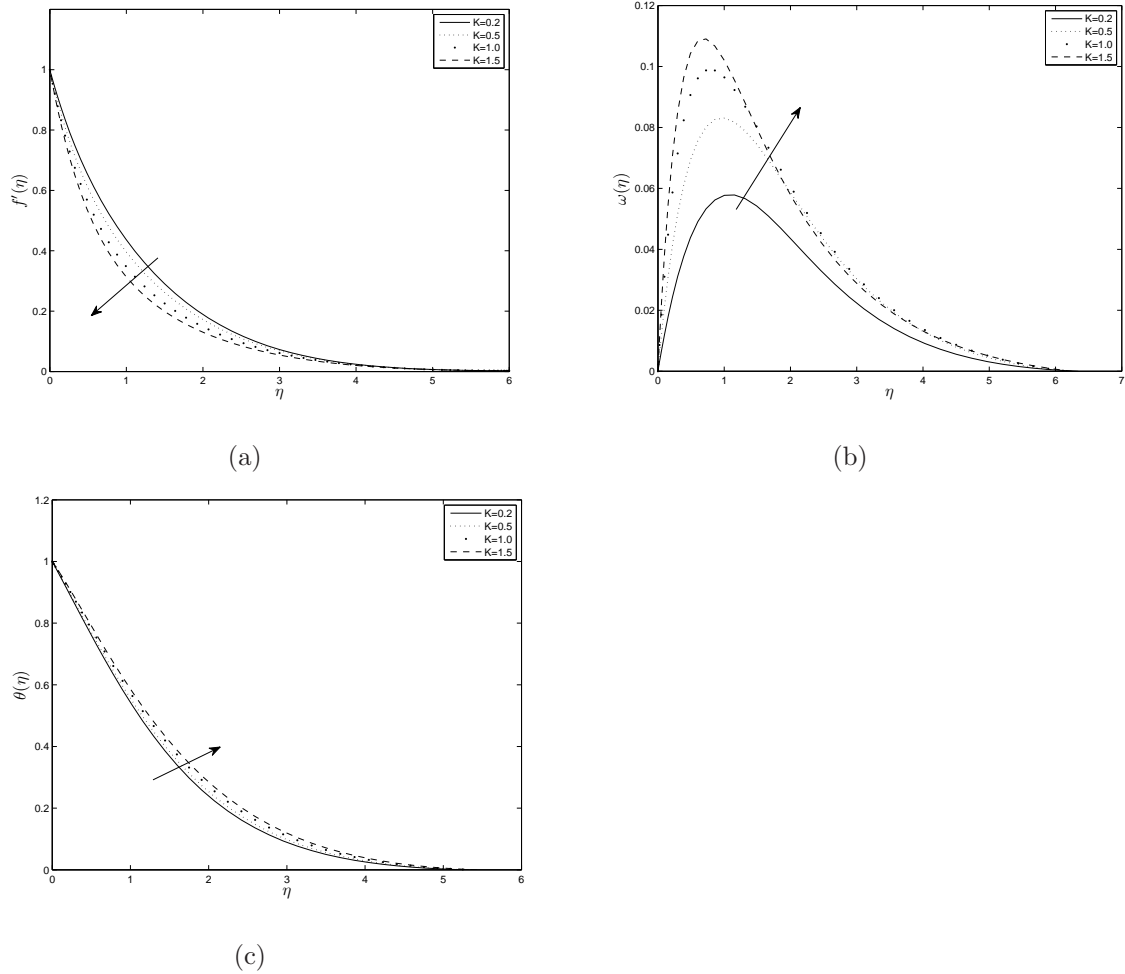


Figure 2.1: Velocity, micropolar and temperature plots with respect to K with parameters; $M = 0.3$, $Da = 1$, $Fr = 0.1$, $Gr = 1.2$, $Pr = 0.71$, $Q = 0.01$, $Ec = 0.04$, $Re = 2$.

Figure 2.3 shows the effect of the Forcheimmer (inertial porous drag) parameter on the velocity and temperature profiles. An increase in Forcheimmer numbers lowers the velocity and so raises the fluid temperature. We further observe that Fr enhances the microrotation and temperature profiles.

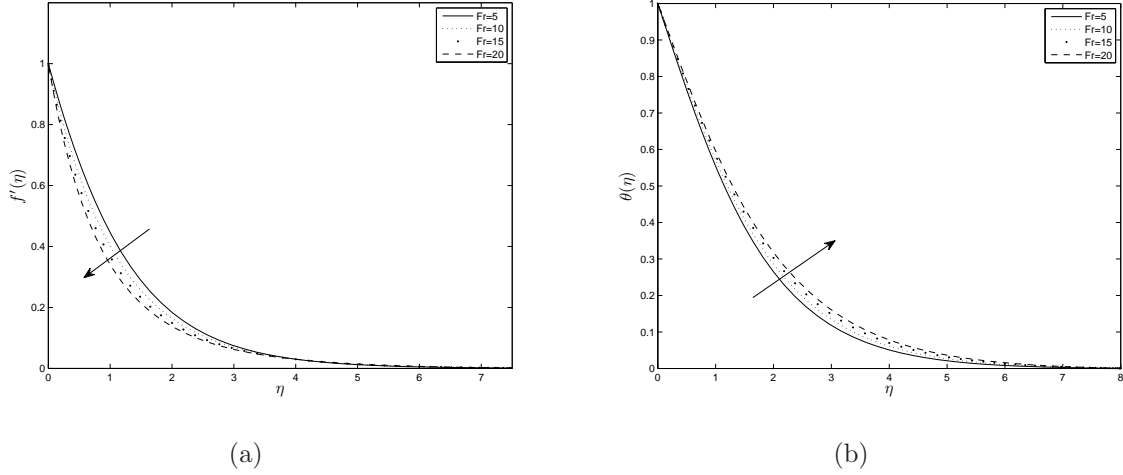


Figure 2.3: Velocity and temperature plots with respect to Fr with parameters; $K = 0.01$, $M = 0.3$, $Da = 2$, $Gr = 0.5$, $Pr = 0.71$, $Q = 0.08$, $Ec = 0.03$, $Re = 1$

Figure 2.4(a) shows the effect of the magnetic field the parameter on the velocity. The velocity decreases as the magnetic field increases from $M = 0$ to $M = 2$. The presence of a magnetic field in an electrically conducting flow creates a drag-like force called the Lorentz force which opposes the fluid motion, (see [50, 49]).

Figure 2.4(b) shows that as the magnetic field increases, the angular velocity field increases near the plate but decreases far from the wall of the plate. This result is in agreement with the results obtained by Eldabe et al. [18].

Figure 2.4(c) shows that as the magnetic field increases the temperature field also increases. The results are in agreement with the results obtained by Cheng [15] and Sharma et al. [50].

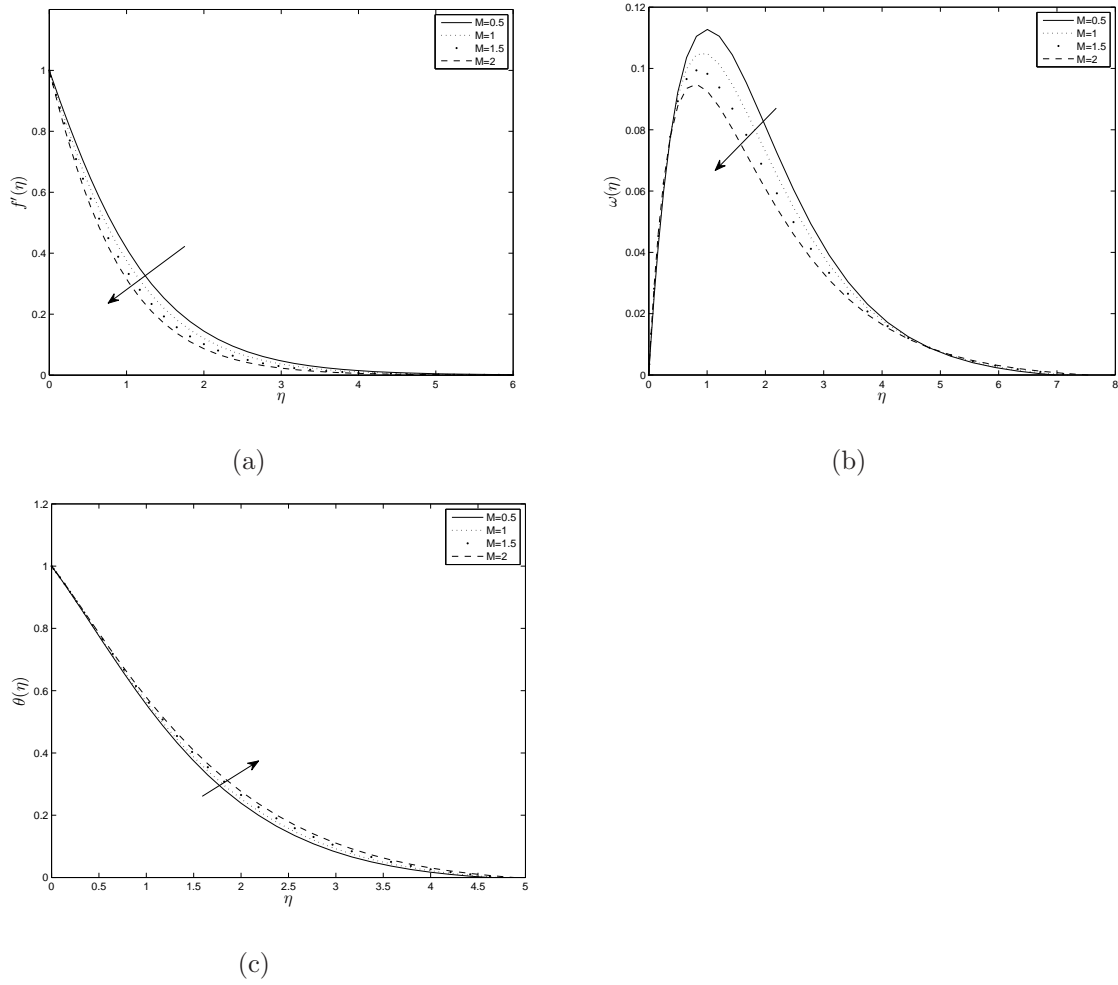


Figure 2.4: Velocity, microrotation and temperature plots with respect to M with parameters; $Pr = 0.71$, $K = 1$, $Da = 1$, $Fr = 0.5$, $Gr = 2.2$, $Q = 0.01$, $Ec = 0.04$, $Re = 2$

Figure 2.5(a) and Figure 2.5(b) show the effect of Grashof numbers on the velocity and temperature profiles. As the Grashof number increases the velocity profile also increases while on the other hand, the temperature profile decreases.

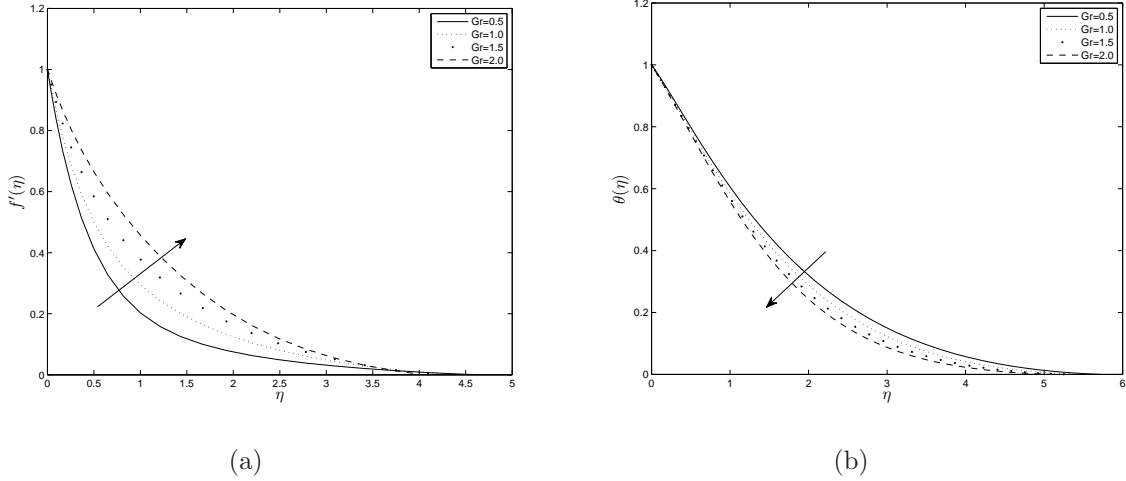


Figure 2.5: Effect of Grashof number (Gr) on velocity and temperature profiles; $K = 1$, $M = 0.3$, $Da = 1$, $Fr = 0.5$, $Pr = 0.71$, $Q = 0.01$, $Ec = 0.04$, $Re = 2$

Figures 2.6(a) and 2.6(b) show the effect of internal heat absorption parameter on the velocity and temperature profiles. As the heat absorption parameter increases it causes a considerable reduction in the velocity and temperature profiles. These results are in well agreement with the results obtained by Sharma et al. [49].

Figures 2.7(a) and 2.7(b) show the effect of local Reynolds number on velocity and temperature profiles. As the Reynolds number increases the velocity decreases whereas the temperature increases. This result is in agreement with the results obtained by Abdel [1] and Awad and Sibanda [8].

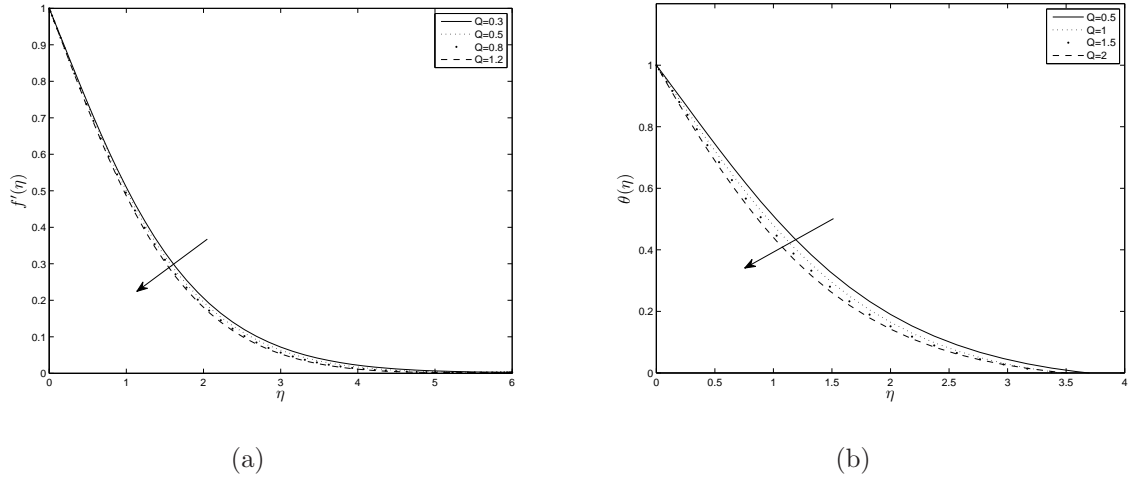


Figure 2.6: Effect of heat absorption on velocity and temperature profiles with parameters; $Pr = 0.71$, $M = 0.5$, $Re = 0.1$, $K = 0.1$, $Da = 1$, $Fr = 0.5$, $Gr = 2.4$, $Ec = 0.4$

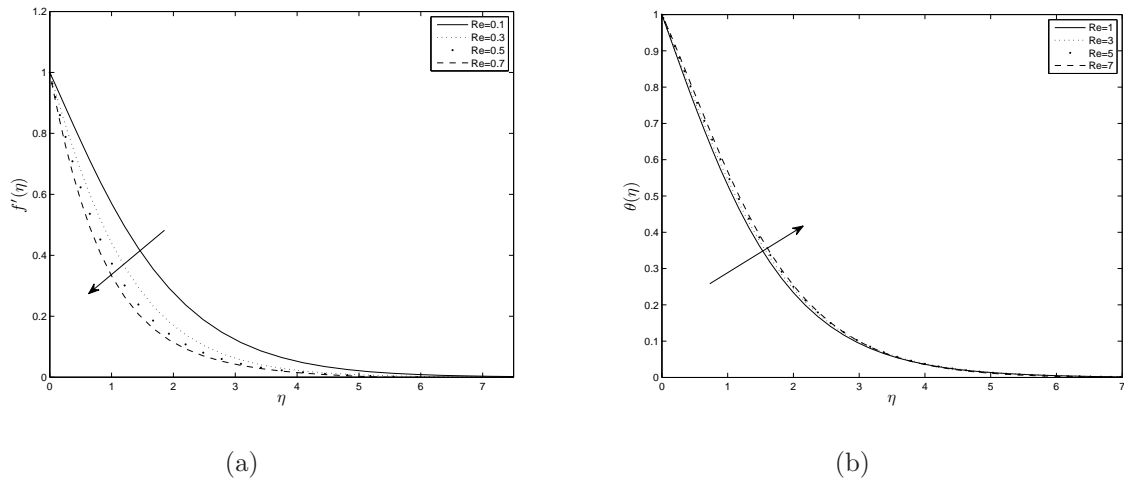


Figure 2.7: Effect of local Reynolds number (Re) on velocity and temperature profiles; $K = 6$, $M = 0.3$, $Da = 0.8$, $Fr = 0.5$, $Gr = 2.2$, $Pr = 0.71$, $Q = 0.01$, $Ec = 0.04$

Figure 2.8, shows the effect of Eckert numbers on temperature profiles. As the Eckert number increases the temperature also increases. These are agree with the results obtained by Bhargava et al. [12] and Eldabe et al. [18].

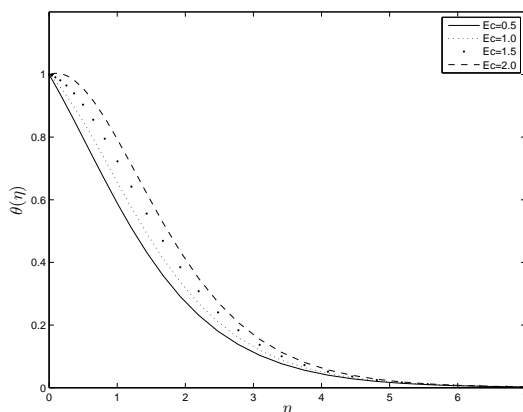


Figure 2.8: Effect of Eckert number on temperature profile; $K = 0.1$, $M = 0.5$, $Da = 1$, $Fr = 0.5$, $Pr = 0.71$, $Gr = 2.4$, $Q = 0.01$, $Re = 0.1$

2.6. Summary

In this chapter we have investigated steady boundary layer flow and heat transfer in an incompressible, electrically conducting micropolar fluid flow over an infinite vertical permeable plate in the presence of a transverse magnetic field and heat absorption. Using similarity transformations, the governing equations were transformed into non-linear ordinary differential equations and solved using the successive linearisation method (SLM). The validity of the solutions was confirmed by further solving the equations using the Matlab boundary layer solver, the **bvp4c**.

The effects of the micropolar parameter, the magnetic field parameter, the Darcy parameter, the Forcheimmer parameter, the Grashof number and the local Reynolds number

on the fluid properties and heat transfer characteristics has been investigated. The main finding may be summarized as follows;

- (i) The velocity decreases as the micropolar parameter increases, whereas the temperature and the angular velocity increase as the micropolar parameter K increases.
- (ii) The velocity and the angular velocity fields increase with an increase in the Darcy parameters whereas the temperature decreases with an increase in the Darcy parameters.
- (iii) An increase in Fr lowers the velocity but raises the fluid temperature.
- (iv) The velocity and the angular velocity decrease with an increase in the magnetic parameter but increases as the Grashof number increases.
- (v) The temperature increases with an increase in the magnetic parameter and the Grashof number.
- (vi) The angular velocity and the temperature profiles decrease with an increase in the heat absorption but the temperature increases as the Eckert number increases.
- (vii) The skin friction coefficient $f''(0)$ decreases with an increase in the magnetic field parameter and the heat absorption parameter.
- (viii) The skin friction coefficient $f''(0)$ and the rate of heat transfer $-\theta'(0)$ both decrease with increases in the micropolar parameter.
- (ix) The rate of heat transfer $-\theta'(0)$ increases with the increase in the heat absorption parameter, the Darcy parameters Da and the magnetic field M parameter.

3

Steady MHD convection in a micropolar fluid with Dufour and Soret effects

3.1. Introduction

Steady MHD flow and convection in micropolar fluids with Dufour and Soret effects has been investigated by different researchers. Srinivascharya and Reddy [54] investigated the flow of micropolar fluids in the presence of Soret and Dufour effects and solved the equations using a numerical method. Alam et al. [3] used a shooting method to determine the effects of Dufour and Soret parameters on the flow of a micropolar flow.

Bhargava et al. [12] studied steady MHD convection in a micropolar fluid with Dufour and Soret effects in the presence of mass and heat transfer using the element free Galerkin method (EFGM). The effect of Soret and Dufour parameters on free convection along a vertical wavy surface was also studied by Narayana and Sibanda [37] using a numerical method.

In this Chapter we re-visit the problem presented in Chapter 2 but now with the added complexity of Dufour and Soret effects. The present model is an extension of the earlier study by Sharma et al. [50] for steady magnetohydrodynamic convection in a micropolar fluid through a porous medium. We use the spectral homotopy analysis method (SHAM) to solve the governing nonlinear differential equations.

3.2. The governing equations

We consider the steady magnetohydrodynamic flow and convection in a micropolar fluid past on an infinite vertical plate in the presence of viscous dissipation and variable suction velocity in a porous medium. The x -axis is along the vertical plate and the y -axis is in the horizontal direction. A magnetic field of uniform strength B_0 is applied transversely to the direction of the flow.

The plate moves impulsively in its own plane with constant velocity u_0 and the ambient fluid temperature is T_∞ .

A heat source is placed within the flow to allow for possible heat absorption effect. With the usual boundary layer and Boussinesq approximations, the problem is governed by the following set of equations (see Srinivascharya et al. [54], Sharma et al. [49, 50]).

$$\frac{\partial u}{\partial x} + \frac{\partial v}{\partial y} = 0, \quad (3.1)$$

$$u \frac{\partial u}{\partial x} + v \frac{\partial u}{\partial y} = \frac{(\mu + k)}{\rho} \frac{\partial^2 u}{\partial y^2} + \frac{k}{\rho} \frac{\partial \mathbf{N}}{\partial y} - \left(\frac{\sigma B_0^2}{\rho} + \frac{(\mu + k)}{k_p \rho} \varepsilon + \frac{F \varepsilon^2}{k_p^{1/2}} u \right) u + g\beta(T - T_\infty) + g\beta^*(C - C_\infty), \quad (3.2)$$

$$u \frac{\partial \mathbf{N}}{\partial x} + v \frac{\partial \mathbf{N}}{\partial y} = \frac{\gamma}{\rho j} \frac{\partial^2 \mathbf{N}}{\partial y^2} - \frac{k}{\rho j} \left(2\mathbf{N} + \frac{\partial u}{\partial y} \right), \quad (3.3)$$

$$u \frac{\partial T}{\partial x} + v \frac{\partial T}{\partial y} = \frac{k_f}{\rho c_p} \frac{\partial^2 T}{\partial y^2} + \frac{1}{\rho c_p} \left(\frac{(\mu + k)\varepsilon}{k_p} u^2 + \frac{F \rho \varepsilon^2}{k_p^{1/2}} u^3 + (\mu + k) \left(\frac{\partial u}{\partial y} \right)^2 \right) - \frac{Q_0}{\rho c_p} (T - T_\infty) + \frac{D_m}{C_s C_p} k_T \frac{\partial^2 C}{\partial y^2}, \quad (3.4)$$

$$u \frac{\partial C}{\partial x} + v \frac{\partial C}{\partial y} = D_m \frac{\partial^2 C}{\partial y^2} + \frac{D_m k_T}{T_m} \frac{\partial^2 T}{\partial y^2}. \quad (3.5)$$

The plate is maintained at a uniform temperature T_w . The boundary conditions on the vertical surface and in the free stream can be defined as follows,

$$y = 0 : u = u_0, \quad v = 0, \quad \mathbf{N} = -n \frac{\partial u}{\partial y}, \quad T = T_w, \quad C = C_w,$$

$$y \rightarrow \infty : u \rightarrow 0, \quad \mathbf{N} \rightarrow 0, \quad T = T_\infty, \quad C = C_\infty,$$

where u and v are the velocity components along the x and y -axes, \mathbf{N} is the component of the microrotation vector normal to the x y - plane, T is the fluid temperature, C is concentration of the solute inside the boundary layer, g is the magnitude of the acceleration due to gravity, ρ is the fluid density, μ is the absolute viscosity, k is the vortex viscosity, γ is the spin-gradient viscosity, ν is the kinematic viscosity, j is the microinertia density, D_m is mass diffusivity, β and β^* are thermal and concentration expansion coefficients respectively, and n is defined in Chapter 2. The last two terms on the right-hand side of the energy equation (3.4) are the heat source term and the Dufour or diffusion-thermo effect and the middle terms other than the heat source term signify the viscous dissipation effect in the Darcy-Forchheimer media. The last term on the right-hand side of the concentration equation (3.5) is the Soret or thermal-diffusion effect, (see Sharma

et al. [49, 50], Awad and Sibanda [8]).

We introduce the following dimensionless variables:

$$\begin{aligned} \eta &= y\sqrt{\frac{U_0}{2\nu x}}, & \psi &= \sqrt{2\nu U_0 x}f(\eta), & \theta(\eta) &= \frac{T - T_\infty}{T_w - T_\infty}, \\ \phi(\eta) &= \frac{C - C_\infty}{C_w - C_\infty}, & \mathbf{N} &= \sqrt{\frac{U_0^3}{2\nu x}}\omega(\eta), & \gamma &= \left(\mu + \frac{k}{2}\right)j = \mu j\left(1 + \frac{K}{2}\right), & j &= \frac{2\nu x}{U_0}. \end{aligned}$$

Substituting the above variables into the governing equations (3.1)-(3.5), the equations reduce to the second order differential equations;

$$\kappa f''' + ff'' + K\omega' - 2Re \left(M + \frac{\kappa}{Da} + \frac{Fr}{Da}f' \right) f' + 2Re (Gr\theta + Gm\phi) = 0 \quad (3.6)$$

$$\left(1 + \frac{K}{2}\right)\omega'' - K(2\omega + f'') + f\omega' + f'\omega = 0, \quad (3.7)$$

$$\begin{aligned} \frac{1}{Pr}\theta'' + f\theta' + 2ReEc \left(\kappa \frac{1}{Da}(f')^2 + \frac{Fr}{Da}(f')^3 \right) \\ + \kappa Ec(f'')^2 - 2ReQ\theta + Du\phi'' = 0, \end{aligned} \quad (3.8)$$

$$\frac{1}{Sc}\phi'' + f\phi' + Sr\theta'' = 0, \quad (3.9)$$

with boundary conditions

$$f(0) = 0, \quad f'(0) = 1, \quad \omega(0) = -nf''(0) = 0, \quad \theta(0) = 1, \quad \phi(0) = 1, \quad (3.10)$$

$$f'(\infty) \rightarrow 0, \quad \omega(\infty) \rightarrow 0, \quad \theta(\infty) \rightarrow 0, \quad \phi(\infty) \rightarrow 0. \quad (3.11)$$

In the above equations, a prime denotes differentiation with respect to η . Note that the physical parameters appearing in equations (3.6)-(3.9) i.e., γ , K , Ec , Pr , M , Da , Fr , Gr , Gm , Q , ν and Re were defined in Chapter 2. Furthermore, Sc is the Schmidt number, Sr is the Soret number and Du is Dufour number defined as follows. These parameters are, $Sc = \frac{\nu}{D_m}$, $Sr = \frac{D_m k_T}{\nu T_m} \left(\frac{T_w - T_\infty}{C_w - C_\infty} \right)$, $Du = \frac{D_m k_T}{c_p c_s \nu} \left(\frac{C_w - C_\infty}{T_w - T_\infty} \right)$. The other variables which are mentioned in the above equations are defined on pages 93 and 94 in this dissertation.

3.3. The skin friction coefficient, the local Nusselt and the local sherwood numbers

The skin friction coefficient at the surface of plate is given by:

$$c_f = \frac{\tau_w}{\rho u_w^2} \quad \text{where} \quad \tau_w = -[(\mu + k)\frac{\partial u}{\partial y} + k\mathbf{N}]_{y=0}. \quad (3.12)$$

Hence, in dimensionless form:

$$c_f/\sqrt{Re} = -(1 + k)\frac{\partial U_0}{\partial Y}|_{Y=0}. \quad (3.13)$$

The heat transfer coefficient at the wall of the plate surface in term of local Nusselt number is calculated as follows:

$$N_u(x) = \frac{-x}{(T_W - T_\infty)} \frac{\partial T}{\partial y} \Big|_{y=0}. \quad (3.14)$$

Hence, in dimensionless form:

$$N_u(x) = -\sqrt{\frac{Re}{2}} \frac{\partial \theta}{\partial Y} \Big|_{Y=0}, \quad (3.15)$$

The local sherwood number is defined as:

$$S_h(x) = \frac{-x}{(C_W - C_\infty)} \frac{\partial C}{\partial y} \Big|_{y=0}. \quad (3.16)$$

Hence, in dimensionless form:

$$S_h(x) = -\sqrt{\frac{Re}{2}} \frac{\partial \phi}{\partial Y} \Big|_{Y=0}. \quad (3.17)$$

We use the Spectral-homotopy analysis method to find numerical solutions of equations (3.6)-(3.9).

3.4. The spectral-homotopy analysis method

The spectral homotopy analysis method (SHAM) is used to solve the non-linear ordinary differential equations (3.6)-(3.9). We begin by using the domain truncation method to approximate the domain of the problem from $[0, \infty)$ to $[0, L]$, where L is chosen to be sufficiently large. We then transform $[0, L]$ to the domain $[-1, 1]$ on which the Chebyshev spectral collocation method can be used by using the transformations;

$$x = \frac{2\eta}{L} - 1 \quad \text{where } x \in [-1, 1]. \quad (3.18)$$

Now introduce the transformations;

$$f(\eta) = F(x) + F_0(\eta), \quad \omega(\eta) = H(x) + H_0(\eta), \quad (3.19)$$

$$\theta(\eta) = G(x) + G_0(\eta), \quad \phi(\eta) = U(x) + U_0(\eta). \quad (3.20)$$

where

$$F_0(\eta) = 1 - e^{-\eta}, \quad H_0(\eta) = \eta e^{-\eta}, \quad (3.21)$$

$$G_0(\eta) = e^{-\eta}, \quad U_0(\eta) = e^{-\eta}. \quad (3.22)$$

Substituting equations (3.18)-(3.20) in the governing equations and the boundary conditions (3.6)-(3.11) gives

$$F''' + a_{11}F'' + a_{12}F' + a_{13}F + a_{14}H' + a_{15}G + a_{16}U + \frac{L}{2(\kappa)}F''F - \frac{LRe}{\kappa} \frac{Fr}{Da} F'F' = A_1(x), \quad (3.23)$$

$$H'' + a_{21}H' + a_{22}H + a_{23}F'' + a_{24}F' + a_{25}F - \frac{L}{K+2}FH' - \frac{L}{K+2}F'H = A_2(x), \quad (3.24)$$

$$G'' + a_{31}G' + a_{32}G + a_{33}F'' + a_{34}F' + a_{35}F + a_{36}U'' + \frac{4PrEc}{L^2}\kappa(F'')^2 + \frac{4RePrEcFr}{LDa}(F')^3 + L^2 \left(\frac{6RePrEcFr}{LDa}F'_0 + \frac{2RePr\kappa Ec}{Da} \right) (F')^2 + \frac{L}{2}PrFG' = A_3(x), \quad (3.25)$$

$$U'' + a_{41}U' + a_{42}G'' + a_{43}F' + \frac{L}{2}ScU'F = A_4(x), \quad (3.26)$$

where $K + 1 = \kappa$, subject to the boundary conditions in which the microelements close to the wall are unable to rotate in such a way that, the value of $n = 0$:

$$\begin{aligned} F(-1) = F'(-1) = F'(1) = H(-1) = H(1) = 0, \\ G(-1) = G(1) = U(-1) = U(1) = 0. \end{aligned} \quad (3.27)$$

Here

$$\left. \begin{aligned}
 a_{11} &= \frac{L}{2\kappa} F_0, & a_{12} &= -\frac{L^2}{2\kappa} \left(ReM + \frac{Re\kappa}{Da} + \frac{2ReFrF'_0}{Da} \right), \\
 a_{13} &= \frac{L^3}{8\kappa} F''_0, & a_{14} &= \frac{L^2 K}{4\kappa}, & a_{15} &= \frac{ReGrL^3}{4\kappa}, \\
 a_{16} &= \frac{ReGmL^3}{4\kappa}, & a_{21} &= \frac{-LF_0}{(K+2)}, & a_{22} &= -L^2 \frac{(F'_0 + 2k)}{2(K+1)}, \\
 a_{23} &= -\frac{2K}{(K+2)}, & a_{24} &= -\frac{LH_0}{(K+2)}, & a_{25} &= -\frac{H'_0}{2(K+1)} L^2, \\
 a_{31} &= \frac{L}{2} PrF_0, & a_{32} &= -\frac{L^2 Re}{2} PrQ, & a_{33} &= 2EcPr\kappa F''_0, \\
 a_{34} &= \frac{LRePrEc}{Da} (2\kappa + 3FrF'_0) F'_0, & a_{35} &= \frac{L^2}{4} PrU'_0, \\
 a_{36} &= PrDu, & a_{41} &= \frac{L}{2} ScF_0, & a_{42} &= ScSr, & a_{43} &= \frac{L^2}{4} ScU'_0.
 \end{aligned} \right\} \quad (3.28)$$

The primes in equations (3.23)-(3.53) denote differentiation with respect to x and

$$\left. \begin{aligned}
 A_1(x) &= \frac{L^3}{8\kappa} \left(\frac{2ReFr}{Da} (F'_0)^2 - \kappa F'''_0 - F_0 F''_0 + 2MReF'_0 - KH'_0 \right) \\
 &\quad - \frac{L^3}{4\kappa} \left(\frac{2ReK}{Da} F'_0 \right) - \frac{L^3}{4\kappa} (ReGrU_0 + ReGmU_0), \\
 A_2(x) &= -\frac{L^2}{4} G''_0 + \frac{L^2}{2(K+2)} (2KH_0 + KF''_0 + F_0 G'_0 + F'_0 G'_0), \\
 A_3(x) &= -\frac{L^2}{4} \left(U''_0 - PrF_0 U'_0 - \frac{2RePr\kappa Ec}{Da} (F'_0)^2 - \frac{2RePrEcFr}{Da} (F'_0)^3 \right) \\
 &\quad - \frac{L^2}{4} (Pr\kappa Ec (F''_0)^2 - 2RePrQU_0 + PrDuU''_0), \\
 A_4(x) &= -\frac{L^2}{4} (ScSrU''_0 + U''_0 + ScF_0 U'_0).
 \end{aligned} \right\} .$$

To apply the spectral-homotopy analysis method (SHAM) to this problem we may choose the following linear operators;

$$\mathcal{L}[F(x; q), H(x; q), G(x; q), U(x; q)] = \left[\begin{array}{l} \frac{\partial^3 F}{\partial x^3} + a_{11} \frac{\partial^2 F}{\partial x^2} + a_{12} \frac{\partial F}{\partial x} + a_{13} F + a_{14} \frac{\partial H}{\partial x} + a_{15} G + a_{16} U, \\ \frac{\partial^3 H}{\partial x^3} + a_{21} \frac{\partial H}{\partial x} + a_{22} H + a_{23} \frac{\partial^2 F}{\partial x^2} + a_{24} \frac{\partial F}{\partial x} + a_{25} F, \\ \frac{\partial^2 G}{\partial x^2} + a_{31} \frac{\partial G}{\partial x} + a_{32} G + a_{33} \frac{\partial^2 F}{\partial x^2} + a_{34} \frac{\partial F}{\partial x} + a_{35} F + a_{36} \frac{\partial^2 U}{\partial x^2}, \\ \frac{\partial^2 U}{\partial x^2} + a_{41} \frac{\partial U}{\partial x} + a_{42} \frac{\partial^2 G}{\partial x^2} + a_{43} F. \end{array} \right]$$

where $q \in (0, 1)$ is the embedding parameter. We also demand that the initial approximations be the solutions of the linear equations (see Motsa et al. [35])

$$F_0''' + a_{11} F_0'' + a_{12} F_0' + a_{13} F_0 + a_{14} H_0' + a_{15} G_0 + a_{16} U_0 = A_1(x), \quad (3.29)$$

$$H_0'' + a_{21} H_0' + a_{22} H_0 + a_{23} F_0'' + a_{24} F_0' + a_{25} F_0 = A_2(x), \quad (3.30)$$

$$G_0'' + a_{31} G_0' + a_{32} G_0 + a_{33} F_0'' + a_{34} F_0' + a_{35} F_0 + a_{36} U_0'' = A_3(x), \quad (3.31)$$

$$U_0'' + a_{41} U_0' + a_{42} G_0'' + a_{43} F_0 = A_4(x), \quad (3.32)$$

subject to the boundary conditions:

$$\begin{aligned} F_0(-1) = F_0'(-1) = F_0'(1) = H_0(-1) = 0, \\ G_0(1) = H_0(1) = U_0(-1) = U_0(1) = 0. \end{aligned} \quad (3.33)$$

The equations (3.29)-(3.32) are to be solved subject the the boundary conditions (3.33). If an exact solution cannot be found, we can use the Chebyshev pseudospectral method to solve the equations.

The derivatives of the functions $F_i(x)$, $H_i(x)$, $G_i(x)$ and $U_0(x)$ at the collocation points are given by

$$\begin{aligned}
 \frac{dF_i(x_j)}{dx} &= \sum_{k=0}^N \mathcal{D}_{kj} F_i(x_j), & \frac{d^2 F_i(x_j)}{dx^2} &= \sum_{k=0}^N \mathcal{D}_{kj}^2 F_i(x_j), & \frac{d^3 F_i(x_j)}{dx^3} &= \sum_{k=0}^N \mathcal{D}_{kj}^3 F_i(x_j), \\
 \frac{dH_i(x_j)}{dx} &= \sum_{k=0}^N \mathcal{D}_{kj} H_i(x_j), & \frac{d^2 H_i(x_j)}{dx^2} &= \sum_{k=0}^N \mathcal{D}_{kj}^2 H_i(x_j), \\
 \frac{dG_i(x_j)}{dx} &= \sum_{k=0}^N \mathcal{D}_{kj} G_i(x_j), & \frac{d^2 G_i(x_j)}{dx^2} &= \sum_{k=0}^N \mathcal{D}_{kj}^2 G_i(x_j), \\
 \frac{dU_i(x_j)}{dx} &= \sum_{k=0}^N \mathcal{D}_{kj} U_i(x_j), & \frac{d^2 U_i(x_j)}{dx^2} &= \sum_{k=0}^N \mathcal{D}_{kj}^2 U_i(x_j).
 \end{aligned} \tag{3.34}$$

The collocation points x_j are given by (see Canuto [13], Trefethen [55])

$$x_j = \cos \frac{\pi j}{N}, \quad j = 0, 1, 2, \dots, N. \tag{3.35}$$

and \mathcal{D} is the Chebyshev spectral differentiation matrix whose entries (see [13], [55]) are given by

$$\begin{aligned}
 \mathcal{D}_{kj} &= -\frac{1}{2} \frac{c_k}{c_j} \frac{(-1)^{k+j}}{\sin \frac{\pi}{2N}(j+k) \sin \frac{\pi}{2N}(j-k)}, \quad j \neq k, \\
 \mathcal{D}_{kj} &= -\frac{1}{2} \frac{\cos \frac{\pi k}{N}}{\sin^2 \frac{\pi k}{N}}, \quad k \neq 0, \\
 \mathcal{D}_{00} &= -\mathcal{D}_{NN} = \frac{2N^2+1}{6}, \\
 \mathcal{D}_{kj} &= -\mathcal{D}_{N-k, N-j}, \quad k = \frac{N}{2} + 1, \dots, N.
 \end{aligned} \tag{3.36}$$

Here $c_0 = c_N = 2$ and $c_j = 1$ with $1 \leq j \leq N-1$.

Substituting equations (3.34) and (3.35) in (3.29)-(3.32) we obtain a linear system of

equations of the form

$$\mathbf{A}\mathbf{Y} = \mathbf{B}, \quad (3.37)$$

where \mathbf{A} , \mathbf{B} and \mathbf{Y} are defined:

$$\mathbf{A} = \begin{bmatrix} A11 & a_{14}\mathcal{D} & \text{diag}[a_{15}] & \text{diag}[a_{16}] \\ A21 & A22 & \mathbf{0} & \mathbf{0} \\ A31 & \mathbf{0} & A33 & a_{36}\mathcal{D}^2 \\ \text{diag}[a_{43}] & \mathbf{0} & a_{42}\mathcal{D}^2 & A44 \end{bmatrix} \quad (3.38)$$

Here $A11 = \mathcal{D}^3 + a_{11}\mathcal{D}^2 + a_{12}\mathcal{D} + \text{diag}[a_{13}]$, $A21 = a_{23}\mathcal{D}^2 + a_{24}\mathcal{D} + \text{diag}[a_{25}]$,
 $A22 = \mathcal{D}^2 + a_{21}\mathcal{D} + \text{diag}[a_{22}]$, $A31 = a_{33}\mathcal{D}^2 + a_{34}\mathcal{D} + \text{diag}[a_{35}]$,
 $A33 = \mathcal{D}^2 + a_{31}\mathcal{D} + \text{diag}[a_{32}]$, $A44 = \mathcal{D}^2 + a_{41}\mathcal{D}$.

$$\mathbf{Y} = \begin{bmatrix} F_0(x_0) \\ F_0(x_1) \\ \vdots \\ F_0(x_N) \\ \hline H_0(x_0) \\ H_0(x_1) \\ \vdots \\ H_0(x_N) \\ \hline G_0(x_0) \\ G_0(x_1) \\ \vdots \\ G_0(x_N) \\ \hline U_0(x_0) \\ U_0(x_1) \\ \vdots \\ U_0(x_N) \end{bmatrix}, \quad \mathbf{B} = \begin{bmatrix} A_1(x_0) \\ A_1(x_1) \\ \vdots \\ A_1(x_N) \\ \hline A_2(x_0) \\ A_2(x_1) \\ \vdots \\ A_2(x_N) \\ \hline A_3(x_0) \\ A_3(x_1) \\ \vdots \\ A_3(x_N) \\ \hline A_4(x_0) \\ A_4(x_1) \\ \vdots \\ A_4(x_N) \end{bmatrix} \quad (3.39)$$

where $\text{diag}[\]$ is a diagonal matrix of size $(N + 1) \times (N + 1)$ and $\mathbf{0}$ is a zero matrix of size $(N + 1) \times (N + 1)$. The matrix \mathbf{A} has dimensions $4(N + 1) \times 4(N + 1)$ while matrices \mathbf{B} and \mathbf{Y} have dimensions $4(N + 1) \times 1$. To incorporate the boundary conditions (3.33), we delete the first, and the last rows of \mathbf{A} , \mathbf{Y} , \mathbf{B} . The first and the last columns of \mathbf{A} are also deleted. This reduces the dimensions of \mathbf{A} to $4(N - 1) \times 4(N - 1)$ and those of \mathbf{Y} and \mathbf{B} to $4(N - 1) \times 1$.

The zeroth deformation equation is given by:

$$\begin{aligned} (1 - q)\mathcal{L}\{[F(x; q), H(x; q), G(x; q), U(x; q)] - [F_0(x), H_0(x), G_0(x), U_0(x)]\} \\ = q\hbar\{\mathcal{N}[F(x; q), H(x; q), G(x; q), U(x; q)] - \mathbf{B}\} \end{aligned} \quad (3.40)$$

where \mathcal{N} is the nonlinear differential operator

$$\mathcal{N}[F(x; q), H(x; q), G(x; q), U(x; q)] = \begin{bmatrix} \mathcal{N}_1[F(x; q), H(x; q), G(x; q), U(x; q)] \\ \mathcal{N}_2[F(x; q), H(x; q), G(x; q), U(x; q)] \\ \mathcal{N}_3[F(x; q), H(x; q), G(x; q), U(x; q)] \\ \mathcal{N}_4[F(x; q), H(x; q), G(x; q), U(x; q)] \end{bmatrix} \quad (3.41)$$

with

$$\begin{aligned} \mathcal{N}_1[F(x; q), H(x; q), G(x; q), U(x; q)] &= \frac{\partial^3 F}{\partial x^3} + a_{11} \frac{\partial^2 F}{\partial x^2} + a_{12} \frac{\partial F}{\partial x} + a_{13} F + a_{14} \frac{\partial H}{\partial x} + a_{15} G \\ &+ a_{16} U + \frac{L}{2\kappa} F \frac{\partial^2 F}{\partial x^2} \\ &- \frac{ReLFr}{Da\kappa} \left(\frac{\partial F}{\partial x} \right)^2, \end{aligned} \quad (3.42)$$

$$\begin{aligned} \mathcal{N}_2[F(x; q), H(x; q), G(x; q), U(x; q)] &= \frac{\partial^2 H}{\partial x^2} + a_{12} \frac{\partial H}{\partial x} + a_{22} H + a_{23} \frac{\partial^2 F}{\partial x^2} + a_{24} \frac{\partial F}{\partial x} + a_{25} F \\ &+ \frac{L}{(K+2)} F \frac{\partial H}{\partial x} + \frac{L}{(K+2)} H \frac{\partial F}{\partial x}, \end{aligned} \quad (3.43)$$

$$\mathcal{N}_3[F(x; q), H(x; q), G(x; q), U(x; q)] = \frac{\partial^2 G}{\partial x^2} + a_{31} \frac{\partial G}{\partial x} + a_{32} G + a_{33} \frac{\partial^2 F}{\partial x^2} + a_{34} \frac{\partial F}{\partial x} + a_{35} F$$

$$\begin{aligned}
 & +a_{36} \frac{\partial^2 U}{\partial x^2} + \frac{4Pr\kappa Ec}{L^2} \left(\frac{\partial^2 F}{\partial x^2} \right)^2 \\
 & + \frac{4RePrEcFr}{LDa} \left(\frac{\partial F}{\partial x} \right)^3 \\
 & + \frac{2RePrEc}{LDa} (L\kappa + 3FrF'_0) \left(\frac{\partial F}{\partial x} \right)^2 \\
 & + \frac{LPrF}{2} \frac{\partial G}{\partial x}, \tag{3.44}
 \end{aligned}$$

$$\begin{aligned}
 \mathcal{N}_4[F(x; q), H(x; q), G(x; q), U(x; q)] & = \frac{\partial^2 U}{\partial x^2} + a_{41} \frac{\partial U}{\partial x} + a_{42} \frac{\partial^2 G}{\partial x^2} + a_{43} F \\
 & + \frac{LScF}{2} \frac{\partial G}{\partial x}. \tag{3.45}
 \end{aligned}$$

The m^{th} order deformation equations are given by:

$$\mathcal{L}\{[F_m(x), H_m(x), G_m(x), U_m(x)] - \chi[F_{m-1}(x), H_{m-1}(x), G_{m-1}(x), U_{m-1}(x)]\} = \hbar \mathbf{R}_m \tag{3.46}$$

where

$$\chi_m = \begin{cases} 0, & m \leq 1, \\ 1, & m > 1. \end{cases} \tag{3.47}$$

subject to boundary conditions:

$$\begin{aligned}
 F_m(-1) = F'_m(-1) = F'_m(1) = H_m(-1) = 0, \\
 H_m(1) = G_m(-1) = G_m(1) = U_m(-1) = U_m(1) = 0. \tag{3.48}
 \end{aligned}$$

where

$$\mathbf{R}_m = \begin{bmatrix} R_{m,1}(x) \\ R_{m,2}(x) \\ R_{m,3}(x) \\ R_{m,4}(x) \end{bmatrix}, \quad (3.49)$$

with

$$\begin{aligned} R_{m,1}(x) &= F_{m-1}''' + a_{11}F_{m-1}'' + a_{12}F_{m-1}' + a_{13}F_{m-1} + a_{14}H_{m-1}' + a_{15}G_{m-1} + a_{16}U_{m-1} \\ &\quad - A_1(x)(1 - \chi_m) + \frac{L}{2\kappa} \sum_{n=0}^{m-1} F_n'' F_{m-1-n} \\ &\quad - \frac{ReLFr}{Da\kappa} \sum_{n=0}^{m-1} (F_n' F_{m-1-n}'), \end{aligned} \quad (3.50)$$

$$\begin{aligned} R_{m,2}(x) &= H_{m-1}'' + a_{21}H_{m-1}' + a_{22}H_{m-1} + a_{23}F_{m-1}'' + a_{24}F_{m-1}' + a_{25}F_{m-1} \\ &\quad - A_2(x)(1 - \chi_m) + \frac{L}{(K+2)} \sum_{n=0}^{m-1} F_n H_{m-1-n}' \\ &\quad + \frac{L}{(K+2)} \sum_{n=0}^{m-1} F_n' H_{m-1-n}, \end{aligned} \quad (3.51)$$

$$\begin{aligned} R_{m,3}(x) &= G_{m-1}'' + a_{31}G_{m-1}' + a_{32}G_{m-1} + a_{33}F_{m-1}'' + a_{34}F_{m-1}' + a_{35}F_{m-1} + a_{36}U_{m-1}'' \\ &\quad - A_3(x)(1 - \chi_m) + \frac{4Pr\kappa Ec}{L^2} \sum_{n=0}^{m-1} F_n'' F_{m-1-n}'' \\ &\quad + \frac{4RePrEcFr}{LDa} \sum_{n=0}^{m-1} F_{m-1-n}' \sum_{i=0}^n F_i' F_{n-i}' \\ &\quad + \left(\frac{6RePrEcFr}{LDa} F_0' + \frac{2RePr\kappa Ec}{Da} \right) \sum_{n=0}^{m-1} F_n' F_{m-1-n}' \\ &\quad + \frac{LPr}{2} \sum_{n=0}^{m-1} F_n G_{m-1-n}', \end{aligned} \quad (3.52)$$

$$R_{m,4}(x) = U''_{m-1} + a_{41}U'_{m-1} + a_{42}G''_{m-1} + a_{43}F_{m-1} - A_4(x)(1 - \chi_m) + \frac{LSc}{2} \sum_{n=0}^{m-1} U'_n f_{m-1-n}. \quad (3.53)$$

Now we use the Chebyshev pseudospectral transformation on equations (3.46)-(3.53) to get:

$$\mathbf{A}\mathbf{Y}_m = (\chi + \hbar)\mathbf{A}\mathbf{Y}_{m-1} - \hbar(1 - \chi_m)\mathbf{B} + \hbar\mathbf{C}_{m-1}, \quad (3.54)$$

subject to the boundary conditions (3.48) and

$$\mathbf{Y}_m = \begin{bmatrix} F_m \\ h_m \\ g_m \\ U_m \end{bmatrix}, \quad \mathbf{C}_{m-1} = \begin{bmatrix} P_{m-1} \\ Q_{m-1} \\ S_{m-1} \\ W_{m-1} \end{bmatrix}, \quad (3.55)$$

and

$$P_{m-1} = \frac{L}{2\kappa} \sum_{n=0}^{m-1} (\mathcal{D}^2 F_n) F_{m-1-n} - \frac{ReLFr}{Da\kappa} \sum_{n=0}^{m-1} (\mathcal{D}F_n)(\mathcal{D}F_{m-1-n}), \quad (3.56)$$

$$Q_{m-1} = \frac{L}{(K+2)} \sum_{n=0}^{m-1} F_n (\mathcal{D}H_{m-1-n}) + \frac{L}{(K+2)} \sum_{n=0}^{m-1} (\mathcal{D}F_n) H_{m-1-n}, \quad (3.57)$$

$$\begin{aligned} S_{m-1} &= \frac{4EcPr\kappa}{L^2} \sum_{n=0}^{m-1} (\mathcal{D}^2 F_n)(\mathcal{D}^2 F_{m-1-n}) \\ &+ \frac{4RePrEcFr}{LDa} \sum_{n=0}^{m-1} (\mathcal{D}F_{m-1-n}) \sum_{i=0}^n (\mathcal{D}F_i)(\mathcal{D}F_{n-i}) \\ &+ \left(\frac{6RePrEcFr}{LDa} F'_0 + \frac{2RePr\kappa Ec}{Da} \right) \sum_{n=0}^{m-1} (\mathcal{D}F_n)(\mathcal{D}F_{m-1-n}) \\ &+ \frac{LPr}{2} \sum_{n=0}^{m-1} F_n (\mathcal{D}G_{m-1-n}), \end{aligned} \quad (3.58)$$

$$W_{m-1} = \frac{LSc}{2} \sum_{n=0}^{m-1} (\mathcal{D}U_n) F_{m-1-n}. \quad (3.59)$$

The value of $\mathbf{Y}_m (m \geq 1)$ are then determined from the following recursive formula;

$$\mathbf{Y}_m = (\chi_m + \hbar)\mathbf{Y}_{m-1} + \hbar\mathbf{A}^{-1}[\mathbf{C}_{m-1} - (1 - \chi_m)\mathbf{B}]. \quad (3.60)$$

Starting from initial approximation obtained from (3.37) we can calculate the m^{th} order approximations using the iteration formula (3.60).

3.5. Results and Discussions

In this section, we discuss the convergence of the spectral homotopy analysis solution for $N = 80$ and $L = 15$. As in the case of the standard homotopy-analysis method the convergence of the spectral homotopy analysis method also depends on the careful selection of the auxiliary parameter \hbar which controls the convergence of the series solution, Motsa and Sibanda [35]. The valid values of \hbar for which convergence is guaranteed are obtained from the horizontal segment of the so called \hbar -curves.

Figures 3.1 show examples of \hbar curves from which we can select the appropriate values of \hbar . We took $L = 15$, and selected the values $\hbar = -1.25$ for the velocity and $\hbar = -1$ for microrotation, temperature and concentration profiles.

We use the value of the Prandtl number for air as $Pr = 0.71$ and the values of Duofur and Soret numbers are chosen in such a way that the product of the two is constant, in particular, $Du \times Sr = 0.06$, provided that the mean temperature is kept constant as well (see Alam et al. [3], Srinivasacharya and Reddy [54]). This is consistent with earlier studies by Awad and Sibanda [8], Alam et al. [3] and Srinivasacharya and Reddy [54].

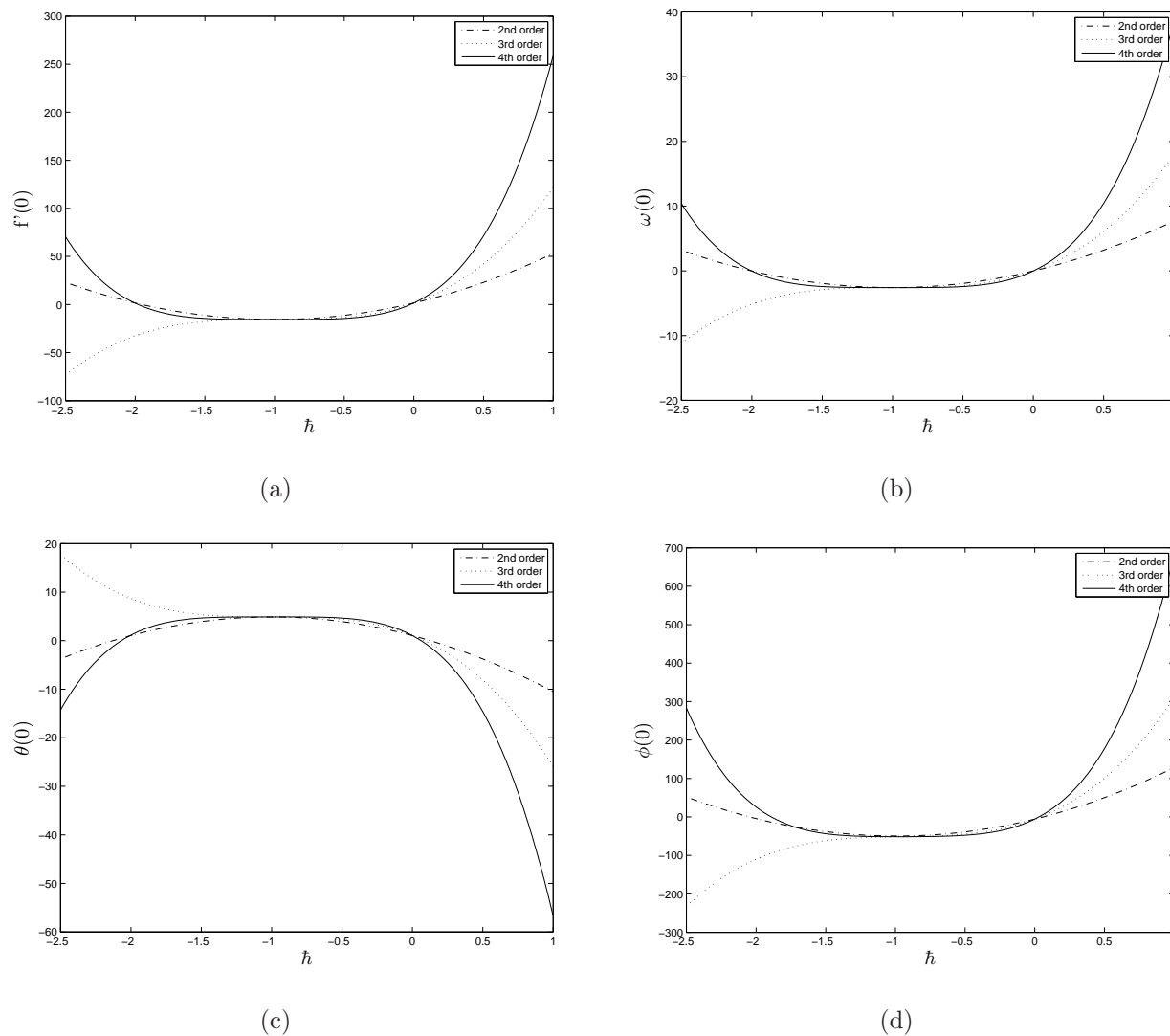


Figure 3.1: The h -curves for $f'(0)$, $\omega(0)$, $\theta(0)$ and $\phi(0)$ when; $K = 10$, $M = 0.3$, $Da = 3$, $Fr = 2$, $Gr = 0.85$, $Pr = 0.71$, $Q = 0.35$, $Ec = 0.03$, $Du = 0.75$, $Sc = 0.75$, $Sr = 0.2$, $Gm = 0.2$, $Re = 2$, $L = 15$

To validate the SHAM solutions, the system of governing equations were further solved using the Matlab **bvp4c** numerical solver. The comparison between the SHAM and the numerical solutions is shown in Tables 3.1-3.6 up to the 6th decimal place numbers. These results show us that the SHAM solutions converges to the numerical solution but that convergence requires more than six iterations as compared with the successive linearisation method.

The functions $f''(0)$, $\omega'(0)$, $-\theta'(0)$ and $-\phi'(0)$ are respectively proportional to the local skin friction coefficient, the plate couple stress, the heat transfer coefficient and the mass transfer coefficient. These functions have been obtained in Tables 3.1-3.6. In this study we have used $Pr = 0.71$ which corresponds to air (see Awad et al. [7], Alam et al. [3]).

A comparison of the SLM, **bvp4c** and the spectral homotopy analysis solutions is also presented in Tables 3.1-3.6. It is clear that the SLM results are in fact much more accurate compared to the SHAM results. We note in passing that the SLM has much in common with the quasi linearization method of Bellman and Kalaba [11] which is known to converge quadratically.

From Table 3.1 we observed that the local skin friction coefficient $f''(0)$, the heat transfer coefficient $-\theta'(0)$ and the mass transfer coefficient $-\phi'(0)$ increase and the plate couple stress $\omega'(0)$ decreases as K increases. These results are in agreement with Awad and Sibanda [8], Eldabe et al. [18], Sharma et al. [50], El- Arabawy [17] and Bachok and Ishak [9]. From Table 3.2 we observe that the local skin friction coefficient $f''(0)$, the heat transfer coefficient $-\theta'(0)$ and the mass transfer coefficient $-\phi'(0)$ decrease and the plate couple stress $\omega'(0)$ increases as M increases. These results are agreement with Sharma et al. [50], El- Arabawy [17].

Table 3.1: Comparison of the **bvp4c** results against the **SHAM** and **SLM** approximate solutions with $N = 100$ and different values of K with parameters; $M = 0.4$, $Da = 2$, $Fr = 1$, $Gr = 0.001$, $Pr = 0.71$, $Q = 0.0001$, $Ec = 0.001$, $Du = 0.6$, $Sc = 0.1$, $Sr = 0.1$, $Gm = 0.1$, $Re = 0.1$.

	SHAM results					SLM
	K	2nd order	4rd order	6th order	bvp4c	2nd order
$f''(0)$	12.0	-0.307220	-0.307588	-0.307589	-0.307589	-0.307589
	14.0	-0.299814	-0.300160	-0.300161	-0.300161	-0.300161
	16.0	-0.294113	-0.294437	-0.294438	-0.294438	-0.294438
	18.0	-0.289590	-0.289893	-0.289894	-0.289894	-0.289894
$\omega'(0)$	12.0	0.304481	0.304631	0.304630	0.304629	0.304630
	14.0	0.301173	0.301336	0.301335	0.301335	0.301335
	16.0	0.298466	0.298632	0.298632	0.298632	0.298632
	18.0	0.296218	0.296383	0.296383	0.296383	0.296383
$-\theta'(0)$	12.0	0.557354	0.554991	0.554218	0.552937	0.552937
	14.0	0.559139	0.556870	0.556151	0.554751	0.554751
	16.0	0.560454	0.558264	0.557601	0.556099	0.556099
	18.0	0.561443	0.559317	0.558708	0.557120	0.557119
$-\phi'(0)$	12.0	0.156781	0.157774	0.157844	0.157854	0.157854
	14.0	0.158108	0.159303	0.159368	0.159379	0.159379
	16.0	0.159161	0.160533	0.160591	0.160603	0.160603
	18.0	0.160016	0.161544	0.161594	0.161607	0.161607

Table 3.2: Comparison of the **bvp4c** results against the **SHAM** and **SLM** approximate solutions with $N = 120$ and different values of M with parameters; $K = 20$, $Da = 2$, $Fr = 1$, $Gr = 0.001$, $Pr = 0.71$, $Q = 0.0001$, $Ec = 0.001$, $Du = 0.6$, $Sc = 0.1$, $Sr = 0.1$, $Gm = 0.01$, $Re = 0.1$.

	SHAM results					SLM
	M	2nd order	4rd order	6th order	bvp4c	2nd order
$f''(0)$	2.0	-0.304360	-0.304607	-0.304608	-0.304608	-0.304608
	4.0	-0.326211	-0.326419	-0.326421	-0.326421	-0.326421
	6.0	-0.346927	-0.347105	-0.347106	-0.347106	-0.347106
	8.0	-0.366678	-0.366831	-0.366833	-0.366833	-0.366833
$\omega'(0)$	2.0	0.308221	0.308341	0.308341	0.308341	0.308341
	4.0	0.324257	0.324335	0.324335	0.324335	0.324335
	6.0	0.339056	0.339102	0.339102	0.339102	0.339102
	8.0	0.352818	0.352840	0.352840	0.352839	0.352839
$-\theta'(0)$	2.0	0.557626	0.555159	0.554279	0.553076	0.553076
	4.0	0.551967	0.549151	0.548209	0.547395	0.547395
	6.0	0.546461	0.543486	0.542652	0.542043	0.542043
	8.0	0.541135	0.538158	0.537483	0.536973	0.536973
$-\phi'(0)$	2.0	0.157270	0.159227	0.159230	0.159242	0.159242
	4.0	0.153540	0.155675	0.155655	0.155665	0.155665
	6.0	0.150311	0.152499	0.152472	0.152480	0.152480
	8.0	0.147473	0.149638	0.149612	0.149618	0.149618

From Table 3.3 we observe that the local skin friction coefficient $f''(0)$, the heat transfer coefficient $-\theta'(0)$ and the mass transfer coefficient $-\phi'(0)$ increase and the plate couple stress $\omega'(0)$ decreases as Da increases. These results are in agreement with Awad and Sibanda [8], Eldabe et al. [18], Sharma et al. [50],

From Table 3.4 we observe that the local skin friction coefficient $f''(0)$, the heat transfer coefficient $-\theta'(0)$ and the mass transfer coefficient $-\phi'(0)$ decrease and the plate couple stress $\omega'(0)$ increases as Fr increases. The results are in well agreement with Sharma et al. [50]. From Table 3.5 we observe that the local skin friction coefficient $f''(0)$, the heat transfer coefficient $-\theta'(0)$ and the mass transfer coefficient $-\phi'(0)$ increase and the plate couple stress $\omega'(0)$ decreases as Gr increases. The results are in well agreement with Sharma et al. [49]. From Table 3.6 we observe that the local skin friction coefficient $f''(0)$, the heat transfer coefficient $-\theta'(0)$ and the mass transfer coefficient $-\phi'(0)$ decrease and the plate couple stress $\omega'(0)$ increases as Re increases.

Table 3.3: Comparison of the **bvp4c** results against the **SHAM** and **SLM** approximate solutions with $N = 120$ and different values of Da with parameters; $K = 20$, $M = 0.3$, $Fr = 1$, $Gr = 0.001$, $Pr = 0.71$, $Q = 0.0001$, $Ec = 0.001$, $Du = 0.6$, $Sc = 0.1$, $Sr = 0.1$, $Gm = 0.01$, $Re = 0.1$.

	SHAM results				bvp4c	SLM
	Da	2nd order	4rd order	6th order		2nd order
$f''(0)$	0.2	-0.916293	-0.916289	-0.916289	-0.916289	-0.916289
	0.4	-0.634144	-0.634181	-0.634182	-0.634182	-0.634182
	0.6	-0.513242	-0.513318	-0.513318	-0.513318	-0.513318
	0.8	-0.442997	-0.443108	-0.443109	-0.443109	-0.443109
$\omega'(0)$	0.2	0.640934	0.640942	0.640942	0.640941	0.640942
	0.4	0.511320	0.511283	0.511283	0.511282	0.511283
	0.6	0.444961	0.444928	0.444927	0.444927	0.444927
	0.8	0.402509	0.402494	0.402494	0.402494	0.402494
$-\theta'(0)$	0.2	0.409112	0.407560	0.407509	0.406351	0.406350
	0.4	0.469504	0.469833	0.469835	0.469085	0.469085
	0.6	0.500234	0.499242	0.499218	0.498637	0.498636
	0.8	0.519293	0.517134	0.516949	0.516459	0.516458
$-\phi'(0)$	0.2	0.109223	0.108819	0.108816	0.108828	0.108828
	0.4	0.122846	0.123325	0.123330	0.123337	0.123337
	0.6	0.131779	0.133009	0.133012	0.133017	0.133017
	0.8	0.138474	0.140204	0.140195	0.140200	0.140200

Table 3.4: Comparison of the **bvp4c** results against the **SHAM** and **SLM** approximate solutions with $N = 100$ and different values of Fr with parameters; $K = 20$, $Da = 2$, $M = 0.3$, $Gr = 0.01$, $Pr = 0.71$, $Q = 0.0001$, $Ec = 0.001$, $Du = 0.6$, $Sc = 0.1$, $Sr = 0.1$, $Gm = 0.01$, $Re = 1$.

	SHAM results				bvp4c	SLM
	Fr	2nd order	4rd order	6th order		2nd order
$f''(0)$	0.1	-0.281056	-0.281326	-0.281328	-0.281328	-0.281328
	0.4	-0.282284	-0.282560	-0.282562	-0.282562	-0.282562
	0.6	-0.283100	-0.283380	-0.283382	-0.283382	-0.283382
	0.8	-0.283916	-0.284199	-0.284200	-0.284200	-0.284200
$\omega'(0)$	0.1	0.291115	0.291270	0.291270	0.291270	0.291270
	0.4	0.291887	0.292046	0.292046	0.292046	0.292046
	0.6	0.292400	0.292561	0.292561	0.292561	0.292561
	0.8	0.292911	0.293074	0.293075	0.293074	0.293074
$-\theta'(0)$	0.1	0.563250	0.561215	0.560707	0.558986	0.558986
	0.4	0.562994	0.560955	0.560442	0.558727	0.558726
	0.6	0.562823	0.560782	0.560266	0.558554	0.558554
	0.8	0.562653	0.560610	0.560090	0.558383	0.558383
$-\phi'(0)$	0.1	0.161261	0.162998	0.163038	0.163053	0.163053
	0.4	0.161159	0.162864	0.162905	0.162920	0.162920
	0.6	0.161092	0.162774	0.162818	0.162832	0.162832
	0.8	0.161024	0.162685	0.162730	0.162745	0.162745

Table 3.5: Comparison of the **bvp4c** results against the **SHAM** and **SLM** approximate solutions with $N = 100$ and different values of Gr with parameters; $K = 20$, $M = 0.3$, $Da = 2$, $Fr = 1$, $Pr = 0.71$, $Q = 0.0001$, $Ec = 0.001$, $Du = 0.6$, $Sc = 0.1$, $Sr = 0.1$, $Gm = 0.01$, $Re = 0.1$.

	SHAM results					SLM
	Gr	2nd order	4rd order	6th order	bvp4c	2nd order
$f''(0)$	0.01	-0.284653	-0.284939	-0.284940	-0.284939	-0.284939
	0.04	-0.284398	-0.284683	-0.284683	-0.284681	-0.284681
	0.06	-0.284228	-0.284512	-0.284513	-0.284509	-0.284509
	0.08	-0.284058	-0.284341	-0.284342	-0.284337	-0.284337
$\omega'(0)$	0.01	0.293372	0.293537	0.293536	0.293536	0.293536
	0.04	0.293208	0.293371	0.293370	0.293367	0.293367
	0.06	0.293098	0.293261	0.293260	0.293255	0.293255
	0.08	0.292988	0.293150	0.293149	0.293143	0.293143
$-\theta'(0)$	0.01	0.562498	0.560454	0.559933	0.558228	0.558228
	0.04	0.562546	0.560507	0.559992	0.558283	0.558283
	0.06	0.562578	0.560543	0.560031	0.558319	0.558319
	0.08	0.562610	0.560578	0.560071	0.558355	0.558355
$-\phi'(0)$	0.01	0.160968	0.162607	0.162653	0.162667	0.162667
	0.04	0.161005	0.162639	0.162687	0.162700	0.162700
	0.06	0.161030	0.162661	0.162709	0.162722	0.162722
	0.08	0.161054	0.162683	0.162732	0.162743	0.162743

Table 3.6: Comparison of the **bvp4c** results against the **SHAM** and **SLM** approximate solutions with $N = 60$ and different values of Re with parameters; $K = 20$, $Da = 2$, $M = 0.3$, $Fr = 1$, $Gr = 0.01$, $Pr = 0.71$, $Q = 0.0001$, $Ec = 0.001$, $Du = 0.6$, $Sc = 0.1$, $Sr = 0.1$, $Gm = 0.01$.

	SHAM results				bvp4c	SLM
	Re	2nd order	4rd order	6th order		2nd order
$f''(0)$	0.1	-0.284729	-0.285015	-0.285017	-0.285017	-0.285017
	0.2	-0.398653	-0.398794	-0.398795	-0.398795	-0.398795
	0.3	-0.490474	-0.490560	-0.490560	-0.490560	-0.490560
	0.4	-0.569904	-0.569959	-0.569960	-0.569960	-0.569960
$\omega'(0)$	0.1	0.293421	0.293586	0.293586	0.293586	0.293586
	0.2	0.373972	0.373981	0.373981	0.373981	0.373981
	0.3	0.431516	0.431487	0.431487	0.431486	0.431487
	0.4	0.476988	0.476950	0.476950	0.476949	0.476950
$-\theta'(0)$	0.1	0.562484	0.560439	0.559915	0.558212	0.558212
	0.2	0.531887	0.529171	0.528743	0.527993	0.527993
	0.3	0.507187	0.505881	0.505831	0.504472	0.504471
	0.4	0.487101	0.486919	0.486921	0.484771	0.484771
$-\phi'(0)$	0.1	0.160957	0.162597	0.162643	0.162658	0.162658
	0.2	0.143530	0.145531	0.145511	0.145519	0.145519
	0.3	0.133827	0.135217	0.135217	0.135230	0.135230
	0.4	0.127285	0.128135	0.128141	0.128162	0.128162

Table 3.7 shows the effects of the Dufour and Soret numbers on the skin friction coefficient, the rate of heat transfer and the rate of mass transfer at the surface. The skin friction coefficient $f''(0)$ decreases as the Soret number increases and the Dufour number decreases simultaneously. However, the heat transfer coefficient $-\theta'(0)$ increases with the Soret numbers. The mass transfer coefficient $-\phi'(0)$ increases as the Dufour parameters increase and the Soret number decreases. This result is similar to the results obtained by Alam et al. [3], Awad and Sibanda [8], Sharma et al. [49].

Table 3.7: Effects of Soret and Dufour parameters on the skin friction $f''(0)$, the rate of heat transfer $-\theta'(0)$ and the rate of mass transfer $-\phi'(0)$ with parameters; $K = 1$, $Da = 1$, $Fr = 0.5$, $M = 0.3$, $Pr = 0.71$, $Gr = 2.2$, $Ec = 0.03$, $Q = 0.5$, $Sc = 0.2$, $Gm = 0.4$, $Re = 2$.

Sr	Du	$f''(0)$	$-\theta'(0)$	$-\phi(0)$
0.1	0.60	0.50139750	0.43634696	0.15576580
0.2	0.30	0.49525875	0.44718774	0.15278269
0.3	0.20	0.49412866	0.45002648	0.15077433
0.4	0.15	0.49421974	0.45090710	0.14901267
0.5	0.12	0.49479344	0.45100868	0.14735570
0.6	0.10	0.49560614	0.45072027	0.14575661

Table 3.8 shows the effect of the heat absorption parameter on the skin friction coefficient, the rate of heat transfer and the rate of mass transfer at the surface. The skin friction coefficient $f''(0)$ decreases as the heat absorption parameter increases whereas heat transfer coefficient $-\theta'(0)$ at the wall of the plate increases as heat absorption parameter increases. The mass transfer coefficient $-\phi'(0)$ decreases as the the heat absorption parameter increases. These results are similar with the results obtained by Awad and Sibanda [8], Sharma et al. [49].

Table 3.8: Effects of heat absorbtion coefficient on skin friction $f''(0)$, the rate of heat transfer $-\theta'(0)$ and the rate of mass transfer $-\phi'(0)$ with parameters; $K = 5$, $M = 0.3$, $Da = 2$, $Fr = 2$, $Gr = 5$, $Pr = 0.71$, $Ec = 0.03$, $Du = 0.6$, $Sr = 0.1$, $Sc = 0.05$, $Gm = 3$, $Re = 1$.

Q	$f''(0)$	$-\theta'(0)$	$-\phi(0)$
0.1	0.50139750	0.43634696	0.15576580
0.3	0.40128563	0.69523677	0.14454457
0.4	0.37100550	0.78992323	0.14197975
0.5	0.34602669	0.87419187	0.14007613
0.6	0.32461854	0.95105651	0.13856492
0.8	0.28906729	1.08889347	0.13624184

The effect of the micropolar parameter on the velocity, microrotation, temperature and concentration profiles is presented in Figures 3.2. As the micropolar parameter increases the velocity profile decreases, whereas the angular velocity, the concentration and temperature profiles increase as the micropolar parameter increases. These results are in agreement with the results obtained by Cheng [15], Salleh et al. [48] and Sharma et al.

[50].

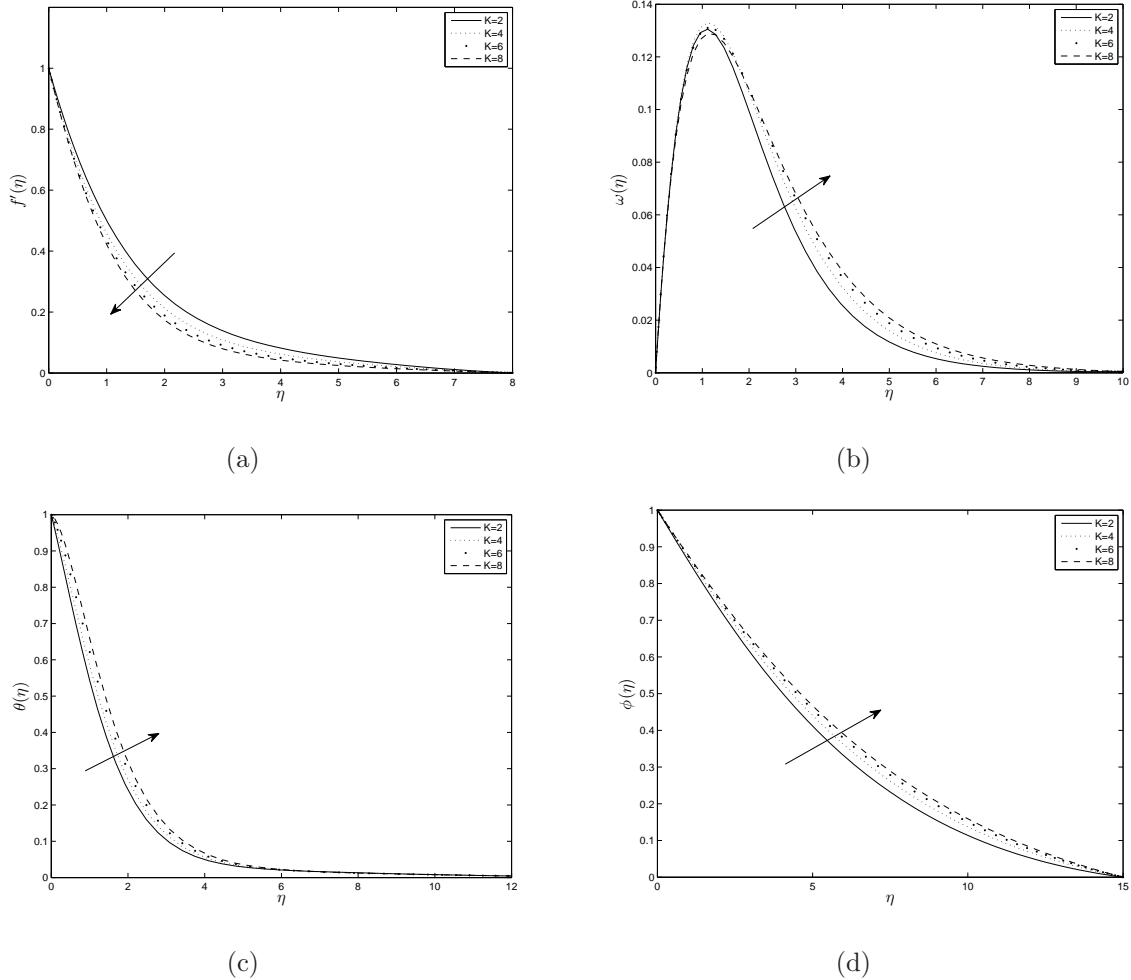


Figure 3.2: Velocity, microrotation, temperature and concentration plots with respect to K with parameters; $M = 0.3$, $Da = 3$, $Fr = 1$, $Gr = 1$, $Pr = 0.71$, $Q = 0.01$, $Ec = 0.1$, $Du = 0.6$; $Sc = 0.1$, $Sr = 0.1$, $Gm = 0.3$, $Re = 1$.

Figure 3.3 shows the effect of the Darcy parameters on the velocity field, we observed that the velocity field increases with the increase of the Darcy parameters where as the temperature profile decreases as the Darcy parameter increases. So on the velocity field, since the Darcy number denotes the porous bulk matrix resistance and is directly proportional to permeability, so an increase in the Darcy number corresponds to a rise in

permeability. This result is in well agreement with the results obtained by Cheng [15], Beg et al. [10] and Sharma et al. [50].

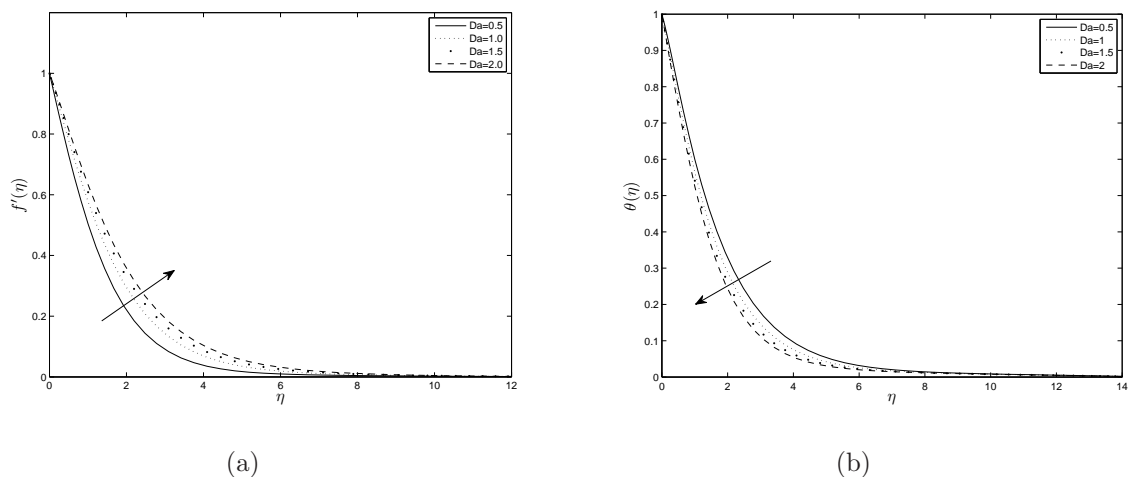


Figure 3.3: Velocity and Temperature plots with respect to Da with parameters; $K = 15$, $Da = 2$, $M = 0.3$, $Fr = 1$, $Gr = 1$, $Pr = 0.71$, $Q = 0.1$, $Ec = 0.01$, $Du = 0.6$, $Sc = 0.1$, $Sr = 0.1$, $Gm = 0.5$, $Re = 1$.

Figures 3.4 show the effects of the Forcheimmer (inertial porous drag) parameter on the velocity and temperature profiles. The velocity profile considerably decreases while the temperature profile increases as the Forcheimmer parameter increases.

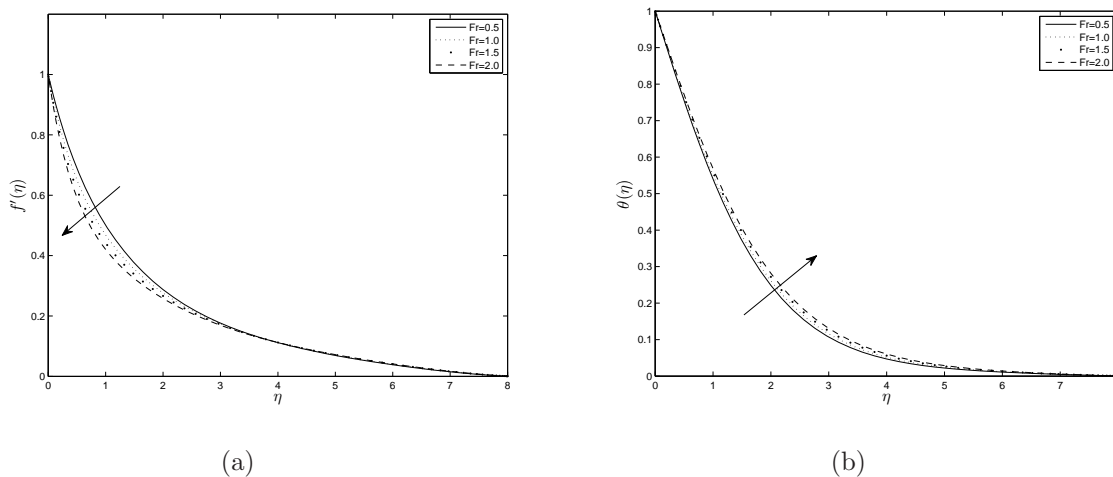


Figure 3.4: Velocity and temperature plots with respect to Fr with parameters; $K = 1$, $M = 0.3$, $Da = 1.5$, $Gr = 2$, $Pr = 0.71$, $Q = 0.01$, $Ec = 0.03$, $Du = 0.6$, $Sc = 0.5$, $Sr = 0.1$, $Gm = 3$, $Re = 2$.

Figure 3.5 shows the effect of magnetic field parameter M on the fluid properties. The velocity and temperature profiles decrease as the magnetic field parameter increases from non-electrically conducting case $M = 0$ to the maximum magnetic field strength corresponding to $M = 2$. The presence of a magnetic field in an electrically conducting flow creates a drag force called the Lorentz force ([50], [49]) which slows down the motion of fluid.

Figure 3.6 shows the effects of the Grashof number on the velocity and temperature profiles. As the Grashof number increases the velocity increases but the temperature profile decreases. The velocity increases significantly near the surface of the fluid.

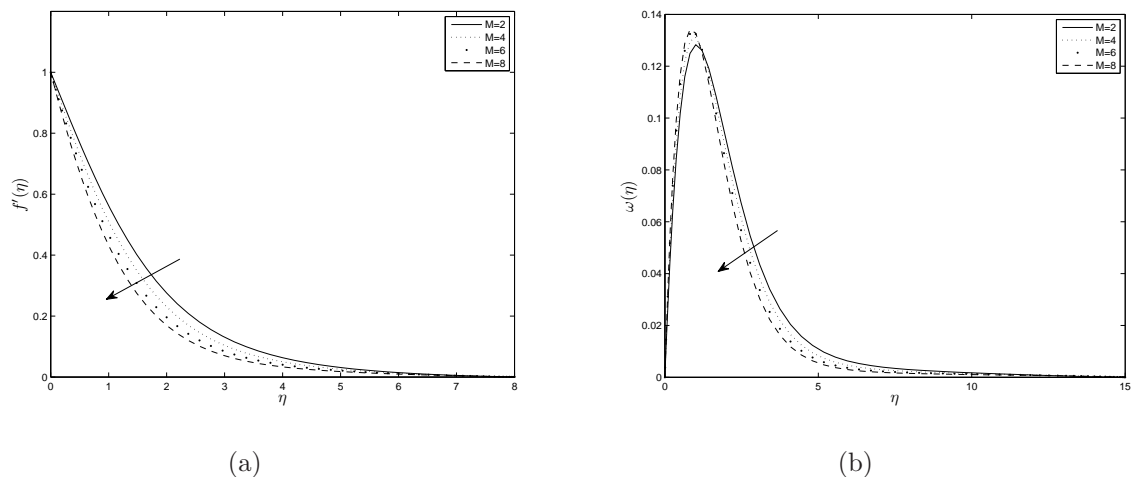


Figure 3.5: Velocity plot with respect to M with parameters; $K = 2$, $Da = 2$, $Fr = 1$, $Gr = 1$, $Pr = 0.71$, $Q = 0.01$, $Ec = 0.01$, $Du = 0.6$, $Sc = 0.1$, $Sr = 0.1$, $Gm = 0.5$, $Re = 0.1$.

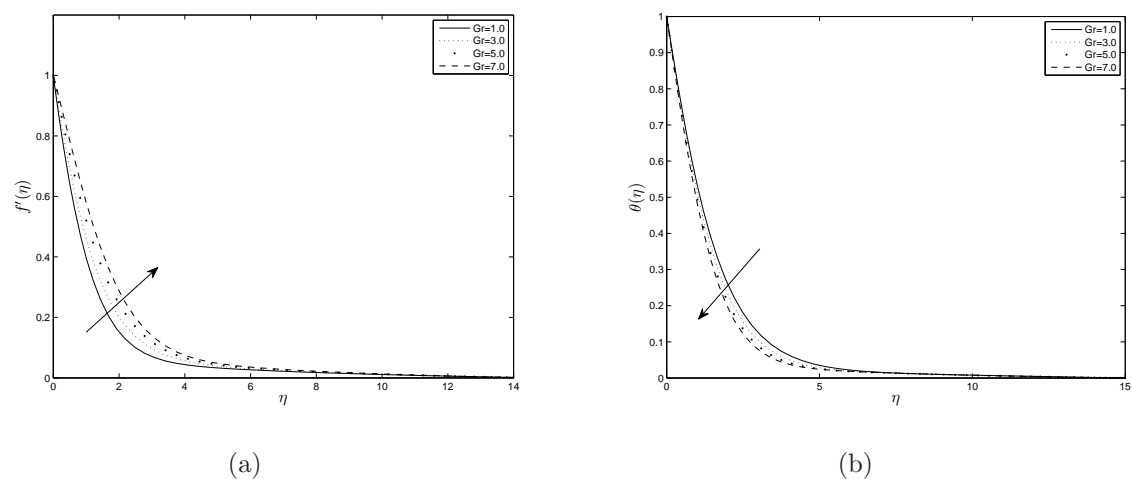


Figure 3.6: Effect of Grashof number on velocity and temperature profiles with parameters; $K = 18$, $M = 0.3$, $Da = 1$, $Fr = 1$, $Pr = 0.71$, $Q = 0.1$, $Ec = 0.01$, $Du = 0.6$, $Sc = 0.1$, $Sr = 0.1$, $Gm = 0.5$, $Re = 1$.

Figure 3.7 shows the effect of the heat absorption parameter on the fluid velocity and temperature profiles. As the heat absorption parameter increases both the velocity and temperature profiles decrease. This is also consistent with the earlier finding by Sharma et al. [49] and Sharma et al. [50].

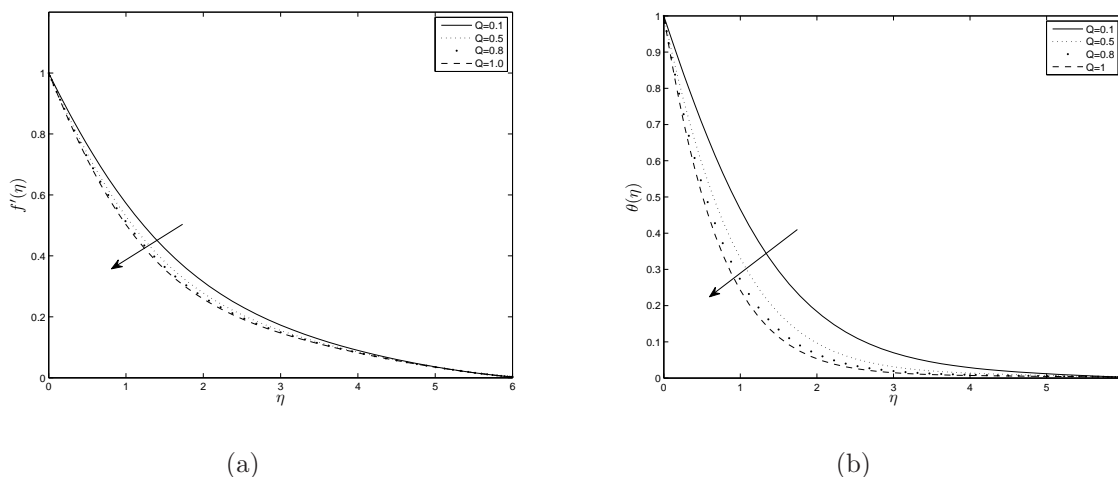


Figure 3.7: Effect of heat absorption on the velocity and temperature profiles with parameters; $K = 1$, $Da = 2$, $M = 0.3$, $Fr = 1$, $Gr = 1$, $Pr = 0.71$, $Q = 0.1$, $Ec = 0.01$, $Du = 0.6$, $Sc = 0.1$, $Sr = 0.1$, $Gm = 0.5$, $Re = 1$.

Figure 3.8 shows the effects of the Dufour and Soret numbers on the fluid temperature and concentration profiles. As the Soret number decrease and the Dufour number increases simultaneously the temperature profile is increase because the fluid in the porous medium is heated. In contrast, as the Soret number decrease and the Dufour number increases simultaneously decreases the concentration profile. These results agree with the past studies such as, Awad and Sibanda [8] and Sharma et al. [49].

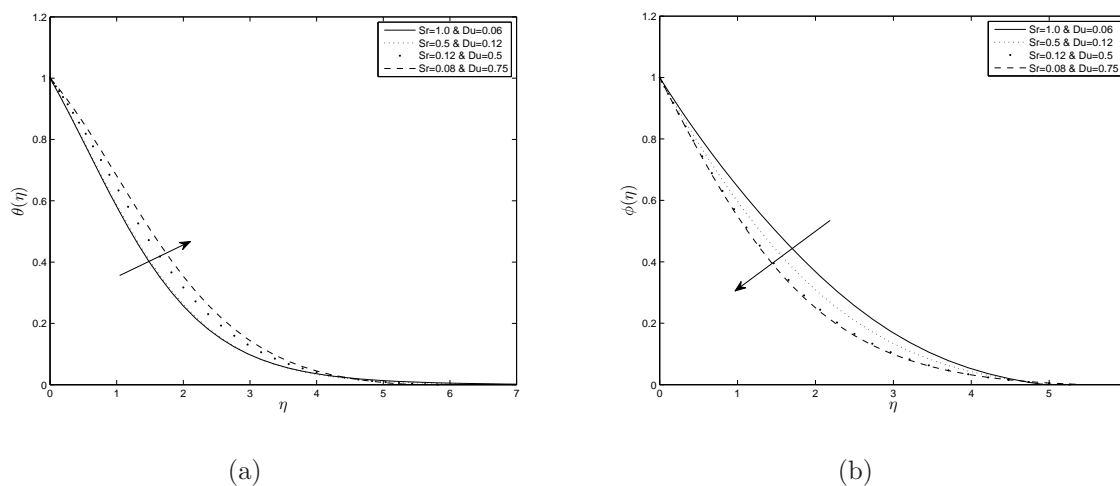


Figure 3.8: The effect of Dufour and Sorer numbers on temperature and concentration profiles with parameters; $K = 1$, $M = 0.3$, $Da = 1$, $Fr = 2$, $Gr = 5$, $Pr = 0.71$, $Q = 0.1$, $Ec = 0.3$, $Sc = 0.5$, $Gm = 3$, $Re = 0.1$.

3.6. Summary

This study presented steady magneto-hydrodynamic boundary layer flow, heat and mass transfer in an incompressible micropolar fluid flow over an infinite vertical permeable plate. The flow was subject to a transverse magnetic field, heat absorption, Dufour and Soret effects and viscous dissipation. Using similarity transformations the governing equations have been transformed into non-linear ordinary differential equations, and solved, using the spectral homotopy analysis methods (SHAM). Moreover, we have considered the effects of the micropolar parameter, the magnetic field parameter, Darcy parameter, Forcheimmer parameter, Grashof number and the Soret and Dufour number on the fluid properties and on heat and mass transfer characteristics. The spectral homotopy analysis methods (SHAM) solutions were further solved using the Matlab **bvp4c** numerical solver and the successive linearisation method to validate the method. The main findings can

be summarized as;

- (i) The velocity profile decreases whereas the angular velocity, the temperature and the concentration profiles increase as the micropolar parameter increases.
- (ii) The velocity increases with increasing in plate velocity or the Darcy number and decreases as each of the magnetic parameter, the Forcheimmer number and the micropolar parameter increases.
- (iii) An increase in the Forcheimmer parameter causes a significant increase in the temperature profile but in contrary reduces in the velocity profile.
- (iv) The velocity profile decreases as the Grashof number increases whereas the temperature profile increases as the Grashof number increases.
- (v) The skin friction coefficient $f''(0)$ decreases as the Soret number increases (the Dufour number decreases) but in contrast the heat transfer coefficient $-\theta'(0)$ and the mass transfer coefficient $-\phi'(0)$ are increase.
- (vi) The skin friction coefficient $f''(0)$ and the mass transfer coefficient $-\phi'(0)$ decrease as the magnetic field parameter increases whereas the heat transfer coefficient $-\theta'(0)$ increases as the magnetic field parameter increases.
- (vii) The skin friction coefficient $f''(0)$ and the mass transfer coefficient $-\phi'(0)$ decrease as the heat absorption parameter increases whereas the heat transfer coefficient $-\theta'(0)$ increases as the heat absorption parameter increases.

4

Conclusion

We have investigated the steady free convective heat and mass transfer flow in micropolar fluid flow past a moving semi-infinite vertical porous plate in the presence of a magnetic field Dufour and Soret effects and viscous dissipation. The aim of this study was to use the successive linearisation method (SLM) and spectral homotopy analysis method to study the effects of different fluid and surface parameters on the fluid properties and heat and mass transfer characteristics. Similarity transformations were used to reduce the governing partial differential equations to ordinary differential equations. The influence of fluid parameters such as the micropolar parameter, the Darcy number, Prandtl number, Schmidt number, magnetic parameter, heat absorption parameter, Soret and Dufour numbers and thermal Grashof numbers on the velocity, microrotation, temperature and concentration fields was studied.

In Chapter 1 we presented the research background, a review of mass and heat transfer in micropolar fluids, free and mixed convection, the homotopy analysis and spectral homotopy analysis methods. In Chapter 2 we presented the successive linearisation method (SLM) for solving systems of highly nonlinear differential equations. The effects of dif-

ferent fluid and surface parameters on steady free convection and heat transfer flow in micropolar fluids was determined. The SLM solutions were compared with the **bvp4c** solutions in terms of accuracy.

In Chapter 3 we investigated steady free convection, heat and mass transfer in a micropolar fluid flow subject to the Soret and Dufour effects. Similarity transformations were used to reduce the governing partial differential equations to ordinary differential equations. These equations were solved using the spectral homotopy analysis method (SHAM). A comparison of the SLM and spectral-homotopy analysis results is also presented. From this we can see that the successive linearisation method (SLM) has been found to be more useful to obtaining accurate results than the spectral homotopy analysis method (SHAM).

The main findings in this work may be summarised as follows;

- The velocity decreases whereas the angular velocity, the temperature and the concentration profiles increase as the micropolar parameter increases.
- The velocity increases with the increase of plate velocity or Darcy number and decreases as each of magnetic parameter increases, Forchhimer number and the micropolar parameter increases.
- The temperature increases as the micropolar parameter increases.
- An increase in Forcheimmer parameter is seen to cause a considerable reduction in the velocity and temperature profiles.
- The Soret number enhances the temperature profile but reduces the concentration profiles. The Dufour number has the opposite effect.

- The skin friction coefficient decreases as the Soret number increases (the Dufour number decreases) but the heat transfer coefficient and the mass transfer coefficient are increase..
- The skin friction and the mass transfer coefficients decrease as the magnetic field parameter increases whereas heat transfer coefficient increases as the magnetic field parameter increases.
- The skin friction and the mass transfer coefficients decrease as the heat absorption parameter increases whereas heat transfer coefficient increases as heat absorption parameter increases.

Nomenclature

B_0	strength of magnetic field
Q_0	heat absorption coefficient
u, v	velocity components along and perpendicular to plate respectively
C	specific concentration of the fluid
c_p	specific heat at constant pressure
c_s	concentration susceptibility
n	frequency of oscillations
U_0	dimensionless velocity,
V_0	suction velocity at the plate
Gr	Grashof number
Gm	solatal Grashof number
Fr	Forcheimmer parameter
Pr	Prandtl number
g	gravitational acceleration medium
T	temperature in boundary layer
x, y	co-ordinate system
F	empirical constant
N	angular velocity
M	magnetic field parameter
j	micro-inertia per unit mass
K	Eringen micropolar parameter
Re	local Reynolds number
T_w	surface temperature

T_∞	free stream temperature
Da	Darcy parameter
Sc	Schmidt number
Ec	Eckert number
D_m	mass diffusivity
D_u	Dufour number
Sr	Soret number
C_w	Specific concentration at the surface
C_∞	concentration of the fluid far away from the surface.
T_m	mean fluid temperature
k_T	the thermal diffusion ratio
C_s	the Concentration susceptibility

Greek symbols

ρ	fluid density
γ	spin-gradient viscosity
κ_f	thermal conductivity
β, β^*	thermal and concentration expansion coefficients
ε	porosity
σ	electrical conductivity
κ	vortex viscosity
ϕ	dimensionless concentration
κ_p	permeability of the porous
ω, θ	microrotation, temperature
μ	fluid dynamic viscosity

Bibliography

- [1] G. M. Abdel-Rahman, Effect of a magnetic field on a micropolar fluid flow in the vicinity of an axisymmetric stagnation point on a circular cylinder, *Chem. Eng. Technol.* **32** (2009), 1252 - 1258.
- [2] G. Ahmadi, Self-similar solution of incompressible micropolar boundary layer flow over a semi-infinite plate, *Int. J. Eng. Sci.* **14** (1976), 639 - 646.
- [3] M. S. Alam, M. Ferdows, M. Ota and M. A. Maleque, Dufour and Soret effects on steady free convection and mass transfer flow past a semi-infinite vertical porous plate in a porous medium, *Int. J. Appl. Mech. Eng.* **3** (2003), 535 - 545.
- [4] M. Aouadi, Numerical study for micropolar flow over a stretching sheet, *Comput. Mater. Sci.* **38** (2007), 774 - 780.
- [5] T. Ariman, M. A. Turk and N. D. Sylvester, Microcontinuum fluid mechanics - A review, *Int. J. Eng. Sci.* **11** (1973), 905 - 930.
- [6] T. Ariman, M. A. Turk and N. D. Sylvester, Applications of microcontinuum fluid mechanics, *Int. J. Eng. Sci.* **12** (1974), 273 - 293.

-
- [7] F.G. Awad, P. Sibanda, S.S. Motsa, O.D. Makinde, Convection from an inverted cone in a porous medium with cross-diffusion effects, *Computers and Mathematics with Applications* **61** (2011), 1431-1441.
- [8] F.G. Awad and P. Sibanda, Dufour and Soret effects on heat and mass transfer in a micropolar fluid in a horizontal channel, *WSEAS Transactions on Heat and Mass Transfer* **5** (2010), 165-177.
- [9] N. Bachok and A. Ishak, MHD stagnation-point flow of a micropolar fluid with prescribed wall heat flux, *European Journal of Scientific Research* **35** (2009), 436-443.
- [10] O. A. Beg, J. Zueco, R. Bhargava and H. S. Takhar, Magnetohydrodynamic convection flow from a sphere to a non-darcian porous medium with heat generation or absorption effects: network simulation, *Int. J. Therm. Sci.* **48** (2009), 913 - 921.
- [11] R. Bellman and R. Kalaba, Quasilinearization and nonlinear boundary value problems, *Elsevier, New York*, 1965.
- [12] R. Bhargava, R. Sharma and O. A. Beg, Oscillatory chemically-reacting MHD free convection heat and mass transfer in a porous medium with soret and dufour effect: Finite element modeling, *Int. J. Appl. Math. Mech.* **5** (2009), 15 - 37.
- [13] C. Canuto, M. Y. Hussaini, A. Quarteroni and T. A. Zang, Spectral methods in fluid dynamics, *Springer-Verlag, Berlin*, 1988.
- [14] A. J. Chamkha and A. B. Nakhi, MHD mixed convection radiation interaction along a permeable surface immersed in a porous medium in the presence of soret and dufours effects, *Heat Mass Transfer* **44** (2008), 845 - 856.

-
- [15] C. Y. Cheng, Fully developed natural convection heat and mass transfer of a micropolar fluid in a vertical channel with asymmetric wall temperatures and concentrations, *Int. Commun. Heat Mass Transfer* **33** (2006), 627 - 635.
- [16] W. S. Don and A. Solomonoff, Accuracy and speed in computing the chebyshev collocation derivative, *SIAM J. Sci. Comput.* **16** (1995), 1253 - 1268.
- [17] H. A. M. El-Arabawy, Effect of suction or injection on the flow of a micropolar fluid past a continuously moving plate in the presence of radiation, *Int. J. Heat Mass Transfer* **46** (2003), 1471 - 1477.
- [18] N. T. Eldabe and M. E.M. Ouaf, Chebyshev finite difference method for heat and mass transfer in a hydromagnetic flow of a micropolar fluid past a stretching surface with ohmic heating and viscous dissipation, *Appl. Math. Comput.* **177** (2006), 561 - 571.
- [19] A. C. Eringen, Simple micro fluids, *Int. J. Eng. Sci.* **2** (1964), 205 - 217.
- [20] A. C. Eringen, Theory of micropolar fluids, *J. Math. Mech.* **16** (1966), 1 - 16.
- [21] A. C. Eringen, Theory of thermomicrofluids, *J. Math. Anal. Appl.* **38** (1972), 480-496.
- [22] R. S. R. Gorla, Mixed convection in a micropolar fluid from a vertical surface with uniform heat flux, *Int. J. Engi. Sci.* **30** (1992), 349 - 358.
- [23] I. A. Hassanien, A. H. Essawy and N. M. Moursy, Natural convection flow of micropolar fluid from a permeable uniform heat flux surface in porous medium, *Appl. Math. Comput.* **152** (2004), 323 - 335.
- [24] F. P. Incropera and D. P. DeWitt, Fundamentals of heat and mass transfer, *Purdue Univesity*, 1990.
-

-
- [25] A. Ishak, R. Nazar and I. POP, Flow of a micropolar fluid on a continuous moving surface, *Arch. Mech.* **58** (2006), 529 - 541.
- [26] M. A. Kamal, M. Ashraf and K. S. Syed, Numerical solution of steady viscous flow of a micropolar fluid driven by injection between two porous disks, *Appl. Math. Comput.* **179** (2006), 1 - 10.
- [27] M. E. M. Khedr, A. J. Chamkha and M. Bayomi, MHD flow of a micropolar fluid past a stretched permeable surface with heat generation or absorption, *Nonlinear Anal. Modell. Control* **14** (2009), 27- 40.
- [28] Y. J. Kim and K. S. Kim, Boundary layer flow of micropolar fluids past an impulsively started infinite vertical plate, *Phys. Scr.* **75** (2007), 132 - 137.
- [29] S. J. Liao, The proposed homotopy analysis technique for the solution of non-linear problems, *Ph.D. Thesis, Shanghai Jiao Tong University*, 1992.
- [30] Z. Makukula, P. Sibanda and S. Motsa, A novel numerical technique for two-dimensional laminar flow between two moving porous walls, *Mathematical Problems in Engineering*, **2010** (2010), Article ID 528956, 1 - 15. doi:10.1155/2010/528956
- [31] Z. Makukula, S. S. Motsa and P. Sibanda, On a new solution for the viscoelastic squeezing flow between two parallel plates, *J. Adv. Res. Appl. Math.* **2** (2010), 31-38.
- [32] R. A. Mohamed and S. M. Abo-Dahab, Influence of chemical reaction and thermal radiation on the heat and mass transfer in mhd micropolar flow over a vertical moving porous plate in a porous medium with heat generation, *Int. J. Therm. Sci.* **48** (2009), 1800 - 1813.

-
- [33] S. S. Motsa, S. Shateyi and P. Sibanda, A model of steady viscous flow of a micropolar fluid driven by injection or suction between a porous disk and a non-porous disk using a novel numerical technique, *Can. J. Chem. Eng.* **88** (2010), 991 - 1002.
- [34] S. S. Motsa, P. Sibanda, F. G. Awad and S. Shateyi, A new spectral-homotopy analysis method for the MHD Jeffery-Hamel problem, *Comput. Fluids* **39** (2010), 1219 - 1225.
- [35] S. S. Motsa, P. Sibanda and S. Shateyi, A new spectral-homotopy analysis method for solving a nonlinear second order BVP, *Commun. Nonlinear Sci. Numer. Simul.* **15** (2010), 2293 - 2302.
- [36] S. S. Motsa, P. Sibanda and S. Shateyi, On a new quasi-linearization method for systems of nonlinear boundary value problems, *Math. Meth. Appl. Sci.* **34**, (2011), 1406 - 1413.
- [37] P. A. L. Narayana and P. Sibanda, Soret and Dufour effects on free convection along a vertical wavy surface in a fluid saturated darcy porous medium, *Int. J. Heat Mass Transfer* **53** (2010), 3030 - 3034.
- [38] R. Nazar, A. Ishak, and I. pop, Unsteady boundary layer flow over a stretching sheet in a micropolar fluid, *World Academy of Science, Engineering and Technology* **38** (2008), 118 - 122.
- [39] D. Pal and S. Chatterjee, Mixed convection magnetohydrodynamic heat and mass transfer past a stretching surface in a micropolar fluid-saturated porous medium under the influence of ohmic heating, soret and dufour effects, *Commun. Nonlinear Sci. Numer. Simul.* **16** (2011), 1329 - 1346.

-
- [40] J. Peddieson and R. P. McNitt, Boundary layer theory for a micropolar fluid, *Recent Adv. Eng. Sci.* **5** (1970), 405 - 426.
- [41] I. Pažanin, Effective flow of micropolar fluid through a thin or long pipe, *Mathematical Problems in Engineering* **2011**, Article ID 127070 (2011), 1 - 18.
- [42] M. M. Rahman, I. A. Eltayeb and S. M. M. Rahman, Thermo-micropolar fluid flow along a vertical permeable plate with uniform surface heat flux in the presence of heat generation, *Therm. Sci.* **13** (2009), 23 - 36.
- [43] M. M. Rahman and T. Sultana, Radiative heat transfer flow of micropolar fluid with variable heat flux in a porous medium, *Nonlinear Anal. Modell. Control* **13** (2008), 71 - 87.
- [44] A. Raptis, Flow of a micropolar fluid past a continuously moving plate by the presence of radiation, *Int. J. Heat Mass Transfer* **41** (1998), 2865 - 2866.
- [45] S. Rawat, R. Bhargava and O. A. Beg, A finite element study of the transport phenomena in MHD micropolar flow in a Darcy-forchheimer porous medium, *Proceedings of the World Congress on Engineering and Computer Science, San Francisco, USA* (2007) 1-6.
- [46] D. A. S. Rees and I. Pop, Free convection boundary layer flow of micropolar fluid from a vertical flat plate, *IMA J. Appl. Math.* **61** (1998), 179 - 197.
- [47] M. Sajid, Z. Abbas and T. Hayat, Homotopy analysis for boundary layer flow of a micropolar fluid through a porous channel, *Appl. Math. Modelling* **33** (2009), 4120-4125.
- [48] M. Z. Salleh, R. Nazar and I. Pop, Mixed convection boundary layer flow from a solid sphere with newtonian heating in a micropolar fluid, *SRX Physics* **2010** (2010), 1-9.

-
- [49] R. Sharma, R. Bhargava and P. Bhargava, A numerical solution of unsteady MHD convection heat and mass transfer past a semi-infinite vertical porous moving plate using element free galerkin method, *Comput. Mater. Sci.* **48** (2010), 537 - 543.
- [50] R. Sharma, R. Bhargava and I. V. Singh, Combined effect of magnetic field and heat absorption on unsteady free convection and heat transfer flow in a micropolar fluid past a semi-infinite moving plate with viscous dissipation using element free galerkin method, *Appl. Math. Comput.* **217** (2010), 308 - 321.
- [51] J. J. Shu and J. S. Lee, Fundamental solutions for micropolar fluids, *J. Eng. Math.* **61** (2008), 69 - 79.
- [52] P. Sibanda and F. Awad, Flow of a micropolar fluid in channel with heat and mass transfer, *World Scientific and Engineering Academy and Society (WSEAS)* (2010), 112 - 120.
- [53] V. M. Soundalgekar and H. S. Takhar, Flow of a micropolar fluid on a continuous moving plate, *Int.J. Eng. Sci.* **21** (1983), 961 - 965.
- [54] D. Srinivasacharya and Ch. RamReddy, Soret and Dufour effects on mixed convection in a non-darcy porous medium saturated with micropolar fluid nonlinear analysis, *Modell. Control* **16** (2011), 100 - 115.
- [55] L. N. Trefethen, Spectral methods in Matlab, *SIAM* (2000).
- [56] Z. Ziabakhsh and G. Domairry, Homotopy analysis solution of micropolar flow in a porous channel with heat and mass transfer, *Adv. Theor. Appl. Mech.* **1** (2008), 79-94